FIELD MONITORING OF DEFORMATION EFFECTS CAUSED BY LANDSLIDES WITH FIBER OPTIC METHODS

HEYELANLARIN YARATMIŞ OLDUĞU DEFORMASYON ETKİLERİNİN FİBER OPTİK YÖNTEMLERLE SAHADA İZLENMESİ

YUNUS EMRE KAYA

ASSOC. PROF. DR. MUSTAFA KEREM KOÇKAR

Supervisor

Submitted to

Graduate School of Science and Engineering of Hacettepe University

as a Partial Fulfillment to the Requirements

for the Award of the Degree of Master of Science

in Civil Engineering

2024

ABSTRACT

FIELD MONITORING OF DEFORMATION EFFECTS CAUSED BY LANDSLIDES WITH FIBER OPTIC METHODS

Yunus Emre KAYA

Master of Science, Department of Civil Engineering

Supervisor: Assoc. Prof. Dr. Mustafa Kerem Koçkar

January 2024, 158 pages

Landslides are among the most dangerous natural disasters that occur frequently worldwide, often triggered by intense rainfall, earthquakes, snowmelt, or human activities. Beyond their direct impact on human life, landslides are significant for their potential to damage structural and lifeline systems (residential buildings, hospitals, railways, pipelines, etc.) and their adverse effects on ecological balance. Since the beginning of the 21st century, extreme meteorological events related to climate change have increased the frequency and intensity of landslides worldwide. In Türkiye, the fact that seismic events significantly contribute to initiating landslides apart from climatic conditions has raised the importance of landslide risk assessment and management processes, necessitating the development of effective prevention and action strategies. Among the most crucial strategies are the adoption of effective landslide monitoring methods and the consequent development of early warning systems. In landslide monitoring, numerous methodologies have been defined, encompassing extensometers, inclinometers, geodetic approaches, and remote sensing or satellite images. However, these methods face limitations in real-time data flow and short response time in data transmission. Fiber optic technologies, in contrast, offer significant advantages over other methods, including high accuracy, long-distance measurement capabilities, and resilience to adverse environmental conditions. These systems enable real-time detection of ground movements and deformations through integration of early warning mechanisms for landslide risks. This thesis examines the potential of fiber optic systems, a light-based technology, in landslide monitoring through a pilot landslide site in Yalova, Türkiye. The region was chosen due to its intense rainfall, active fault lines, and the continuously observed mass movement. The susceptibility of the region to landslides has been substantiated through the application of Limit Equilibrium Methods (LEM) conducted in the context of this thesis. In analyzing data obtained from fiber optic cables, instead of the traditional Optical Time Domain Reflectometer (OTDR) method, which is the point sensing method, the Brillouin Optical Time Domain Analyzer (BOTDA) technology, which is Distributed Strain and Temperature Sensing (DSTS) method, was preferred, enabling continuous measurements along the cable length. In the case study, fiber optic cables with diameters of 3 mm and 4.5 mm were integrated into the BOTDA system, and a monitoring section, about 50 m in length, was installed through a planned configuration in the Yalova region. The deformations (strains) experienced by these cables due to seismic activity and precipitation were monitored over 50 days. In the most active point of the monitoring area, strain values exhibited considerable variations, ranging between -2000 to 7000 με for the 3-mm fiber cable and -500 to 2000 με for the 4.5-mm fiber cable. With its limited global precedents, this research is expected to lead the way in establishing advanced monitoring and early warning systems in Türkiye.

Keywords: Mass movement, Fiber Optic Methods, Light-based Solutions, BOTDA, Landslide Monitoring, Early Warning

ÖZET

HEYELANLARIN YARATMIŞ OLDUĞU DEFORMASYON ETKİLERİNİN FİBER OPTİK YÖNTEMLERLE SAHADA İZLENMESİ

Yunus Emre KAYA

Yüksek Lisans, İnşaat Mühendisliği Bölümü

Tez Danışmanı: Doç. Dr. Mustafa Kerem Koçkar

Ocak 2024, 158 sayfa

Heyelanlar, dünya genelinde sıklıkla meydana gelen en tehlikeli doğal afetler arasındadır ve genellikle yoğun yağış, depremler, kar erimesi veya insan faaliyetleri tarafından tetiklenirler. İnsan yaşamı üzerindeki doğrudan etkilerinin ötesinde, heyelanlar, yapısal ve altyapı sistemleri (konutlar, hastaneler, tren yolları, boru hatları, vb.), ve ekolojik denge üzerindeki olumsuz etkileriyle önem taşırlar. 21. yüzyılın başından bu yana, iklim değişikliğiyle ilişkili aşırı meteorolojik olaylar, dünya genelinde heyelanların sıklığını ve şiddetini artırmıştır. Türkiye'de, iklimsel koşullara ek olarak, sismik olaylar heyelanların tetiklenmesine önemli ölçüde katkıda bulunmaları heyelan risk değerlendirme ve yönetim süreçlerinin önemini artırmış ve etkili önleme ve eylem stratejilerinin geliştirilmesini zorunlu kılmıştır. En önemli stratejiler arasında etkili heyelan izleme yöntemlerinin benimsenmesi ve bunun sonucunda erken uyarı sistemlerinin geliştirilmesi yer alır. Heyelan izlemede, ekstensometreler, inklinometreler, jeodezik yaklaşımlar, fotogrametrik modeller, ve uzaktan algılama veya uydu teknikleri dahil olmak üzere sayısız metodoloji tanımlanmıştır. Ancak, bu yöntemler gerçek zamanlı veri akışı ve veri iletiminde kısa tepki süresi konusunda sınırlamalara sahiptirler. Fiber optik teknolojiler ise, diğer yöntemlere göre, yüksek doğruluk, uzun mesafe ölçüm kapasitesi ve zorlu çevresel koşullarına dayanıklılık gibi önemli avantajlara sahiptir. Bu sistemler, yer hareketlerini ve deformasyonları gerçek zamanlı olarak tespit etmeyi sağlar ve heyelan riskleri için erken uyarı mekanizmalarına entegre edilir. Bu tez çalışmasında, ışık temelli teknolojilerden biri olan fiber optik sistemlerin heyelan izleme alanındaki potansiyeli, Türkiye'nin Yalova ilinde bir pilot heyelan sahasında incelenmiştir. Bölgenin tercih edilmesinde, mevcut yoğun yağışlar ile aktif fay hatları ve bu etkiler ile bölgede gözlemlenen sürekli kütle hareketinin varlığı etkili olmuştur. Bu tez kapsamında yapılan Limit Denge Yöntemleri (LEM) analizi ile bölgenin heyelanlara karşı hassasiyeti kanıtlanmıştır. Fiber optik kablolarından elde edilen verilerin analizinde, noktasal algılama metodu olan geleneksel Optik Zaman Alanı Reflektometre (OTDR) yöntemi yerine, kablo boyunca sürekli ölçüm sağlayan Dağıtılmış Gerinim ve Sıcaklık Algılama (DSTS) metotlarından olan Brillouin Optik Zaman Alanı Analizcisi (BOTDA) teknolojisi tercih edilmiştir. Yalovadaki pilot çalışmada, çapları 3 mm ve 4.5 mm olan fiber optik kablolar BOTDA sistemine entegre edilmiş ve yaklaşık 50 m'lik bir izleme alanı planlı bir konfigürasyonla kurulmuştur. Bu çalışmada, kablolarda sismik aktivite ve yağış sonucu meydana gelen deformasyonlar (gerilmeler) 50 gün boyunca izlenmiştir. İzleme alanının en aktif noktasında, gerilme değerleri, 3 mm'lik fiber kablo için -2000'den 7000 με'ye ve 4.5 mm'lik fiber kablo için -500'den 2000 με'ye kadar önemli değişiklikler göstermiştir. Küresel örnekleri sınırlı sayıda olan bu çalışmanın, Türkiye'de gelişmiş izleme ve erken uyarı sistemlerinin kurulmasında öncülük etmesi beklenmektedir.

Anahtar Kelimeler: Kütle Hareketi, Fiber Optik Metotlar, Işık-tabanlı Çözümler, BOTDA, Heyelan İzleme, Erken Uyarı

ACKNOWLEDGMENTS

I express my deepest gratitude to Associate Professor Dr. Mustafa Kerem Koçkar, my thesis supervisor, for his outstanding mentorship and unwavering support throughout this thesis journey. His remarkable patience and invaluable constructive criticism have played a crucial role in guiding and shaping the course of my academic endeavor.

My family played an indispensable role in my academic life, and I extend my heartfelt thanks to them for their unwavering support, motivation, and guidance. Their love, patience, and understanding were my most significant source of motivation.

The support from my love, Tuğçe Baştürk, was invaluable. She was a constant source of encouragement, motivation, and unwavering assistance. Her presence has made this journey even more meaningful and successful, and I am deeply indebted.

I am also deeply thankful to the dedicated and diligent project team, including Dr. Arzu Arslan Kelam, Mr. Gökhan Şahin, Mr. Cem Demir, Mr. Ahmet Kaan Karabulut, Mr. Barış Ural, Mr. Abdullah Enes Özşimşir, Ms. Nur Sena Yıldırım and Mr. Mustafa Hatipoğlu, without whom this journey would not have been possible.

I would like to express my sincere appreciation to Professor Dr. Haluk Akgün for sharing his extensive knowledge during the project and for his invaluable presence and insightful feedback at my thesis defense.

I am deeply grateful to Professor Dr. Mustafa Şahmaran for his generous sharing of expertise, invaluable input, and constructive critique during my thesis defense.

I profoundly appreciate the members of my thesis defense committee, namely, Professor Dr. Berna Unutmaz and Associate Professor Dr. Abdullah Sandıkkaya, for dedicating their valuable time to review and provide invaluable comments on my study.

I would like to thank my mentors Mr. A. Baki Mert, Mr. Metin Özer, Ms. Feray Korkmaz and Dr. Turgay Karakaş, for their support and inspiring advice.

I would like to express my sincere thanks to my dear friends, Mr. İbrahim Demirhan, Mr. Mehmet Çalıkoğlu, Mr. Ertuğrul Albamya, Mr. Oğulcan Akgül, Mr. Veysel Torun, Mr. Mehmet Yüksel and Mr. Ayberk Vural for their kind support and motivation.

I would like to extend my sincere thanks to my dear friends Mr. Yiğit Biçer, Mr. Serkan Hünerli, Mr. Mehmet Emrah Kubat, Mr. Mert Ulaş, Mr. İlker Kılınçarslan and Mr. Sefa Yıldırım for their valuable support and motivation.

I would like thank to The Scientific and Technological Research Council of Türkiye (TÜBİTAK) for funding this study performed in the scope of the ARDEB-1001, Grant No: 121M761 research project and I would like to thank the BİDEB department of TÜBİTAK for their support under the BİDEB-2210 program.

I would like to thank The Disaster and Emergency Management Authority (AFAD) for its support and the General Directorate of Meteorology (MGM) for providing us with access to technical data and reports.

Finally, I would like to express my gratitude to Yalova University, especially Rector Professor Dr. Mehmet Bahçekapılı and Vice Rector Professor Dr. Cahit Külekçi, for providing the work permit and the logistics possibilities.

TABLE OF CONTENTS

LIST OF TABLES

LIST OF FIGURES

SYMBOLS AND ABBREVIATIONS

Symbols

με	Microstrain

ABBREVIATIONS

AFAD	The Disaster and Emergency Management Authority
BH	Borehole
BOTDA	Brillouin Optical Time Domain Analyzer
DAS	Distributed Acoustic Sensing
DEM	Digital Elevation Model
DSTS	Distributed Strain and Temperature Sensing
FBG	Fiber Bragg Grating
FS	Factor of Safety
InSAR	Interferometric Synthetic Aperture Radar
IPCC	Intergovernmental Panel on Climate Change
LEM	Limit Equilibrium Method
LiDAR	Light Detection and Ranging
LVDT	Linear Variable Differential Transformers
MGM	General Directorate of Meteorology
MTA	Mineral Research and Exploration
NAFZ	North Anatolian Fault Zone
OTDR	Optical Time Domain Reflectometer
S_{DS}	Short-period design spectral acceleration
SP	Sensitive Point

1. INTRODUCTION

1.1. Introduction

In Türkiye and the rest of the world, landslides are among the most damaging natural disasters. They unquestionably pose a severe risk, on par with earthquakes and floods (Akgün and Bulut, 2007; Gökçe et al., 2008). Landslides are typically considered natural disasters caused by typhoons, earthquakes, floods, or volcanic eruptions. Additionally, at the beginning of the 21st century, there has been a significant increase in both the frequency and intensity of extreme meteorological events globally, often categorized within the top or bottom 10% in terms of severity (IPCC, 2012), a trend primarily attributed to ongoing climate changes and irregularities. This issue increases the occurrence and severity of landslides. Landslides are often sudden and unpredictable, making them difficult to control and manage. Since landslides could be catastrophic, they typically have more significant socioeconomic impacts than are recognized. In many nations worldwide, landslides result in substantial economic losses, and these losses appear to rise as the population grows and more unstable slope sites are used to accommodate the growing demand for residential places. The socioeconomic impacts of landslides are profound and varied, affecting both individual livelihoods and broader economic systems.

Furthermore, landslides also destroy residences, companies, farms, forests, and the water quality of streams, all of which result in significant financial losses (Schuster, 1996). Historically, the costs associated with landslides in the U.S. have been substantial. In the late 1950s, landslides were estimated to cost hundreds of millions of dollars annually in the U.S. (Schuster and Highland, 2001). The same is true for Türkiye, but Türkiye is one of the countries most affected by natural disasters due to its geographical location. Both landslides and earthquakes have a significant impact on Türkiye's socio-economic development level. The Disaster and Emergency Management Authority (AFAD) of the Republic of Türkiye has carried out a study on the number of impacted locations, incidents, and events that resulted in evacuations, as well as the number of individuals who were evacuated due to various hazards in Türkiye between 1950 and 2008 (Table 1). According to the study, landslides are the most common type of disaster, considering the number of impacted communities, occurrences, and evacuation events.

Table 1. Experienced hazards and their effects in Türkiye between 1950 and 2008 (Gökçe et al., 2008)

Hazards	**Number of Affected Residential Areas**	**Number of Occurrence**	**Number of Events That Have Led to Evacuation**	**Number of People Evacuated**
Landslide	4161 (%34.18)	12794 (%42.63)	6347	63969 (%25.40)
Rock Fall	899 (%7.38)	2769 (%9.23)	1367	20836 (%8.26)
Flood	1861 (%15.23)	3873 (%12.91)	2249	26081 (%10.36)
Earthquake	2952 (%24.25)	5267 (%17.55)	4807	106838 (%42.42)
Others	665 (%5.46)	1076 (%3.59)	658	8200 (%3.25)
Snow Avalanches	207 (%1.7)	670 (%2.23)	292	4112 (%1.63)
Multiple Hazards	1427 (%11.73)	2967 (%6.89)	1058	19102 (%7.57)
Unclassified		1491 (%4.97)	704	2723 (%1.1)
Total	12172	30007	17482	251861

The relationship between the quantity of landslides and negatively affected structures has made studies on landslides more significant. These factors have increased the importance of risk assessment and knowledge of landslides, leading to a greater focus on early warning systems (Li et al., 2012; Liu et al., 2010; Pei et al., 2011). Numerous methods are available today for pinpointing possible slope instabilities and landslides, each with benefits and disadvantages.

Techniques for monitoring landslides include inclinometers, tiltmeters, extensometers, satellite pictures, air photography, ground-based LIDAR, and others (Savvaidis, 2003; Pei et al., 2011). These techniques are used to identify future deformation rather than early warning.

Optical fiber systems are increasingly recognized as superior for various applications due to their advanced features and capabilities. These features and capabilities can be listed as follows (Wang et al., 2008; Gupta, 2018; Measures, 2001).

- User-friendly
- High-speed data transmission
- Compactness and portability
- Sensitivity to temperature changes and strain
- Expansive transmission capacity
- Resilient to Electromagnetic Disturbances
- Resistant to Environmental Challenges
- Economic Efficiency
- Capability for real-time Monitoring

Although optical fibers have been around since the 1800s, using them in landslide early warning systems is relatively recent (Al-Azzawi, 2007).

1.2 Aim of the Study

According to Disaster and Emergency Management Authority (AFAD) and Mineral Research and Exploration (MTA) databases, Yalova Province is at the forefront of the landslide inventory reported between 1960 and 2018, considering the frequency of landslide recurrence. For this reason, Yalova province has been identified as one of the priority areas for landslide hazard and risk by AFAD, and it has been emphasized that this region should be prioritized in landslide hazard and risk studies to be conducted in our country. In addition, precipitation earthquakes and other triggering mechanisms heavily affect landslides within Yalova provincial borders (Gökçe et al., 2008). The 1999 Kocaeli Earthquake records showed that the reactivated landslides in this region greatly impacted the damage distribution. In addition to the shallow landslides that occurred during the earthquake, the mobilization of existing landslides significantly affected the damage distribution (Duman et al., 2006). Along the residential areas between the center of Yalova and Çınarcık, it was observed that many housing estates and buildings near the coast have slid towards the sea with lateral spreading and deformations due to landslides triggered by the earthquake. It was also recorded that these buildings were damaged and utterly uninhabitable, and there were casualties. Some of these landslide areas have been declared disaster-prone areas and closed to housing. All these emphasize the importance of monitoring landslides and developing early warning systems.

Fiber optic methods are light-based techniques (UNESCO, 2015). Light-based fiber optic methods are known to provide fast and environmentally friendly results. The fiber optic cables required to implement these technologies are made of thin materials, mainly silica glass or special plastics, to transmit light signals. These materials consist of a central core surrounded by a cladding layer. The core and cladding are distinguished by their respective refractive indices, where the core has a higher index that allows light to be trapped and guided within the core based on the principles of Snell's law (Shirley, 1951). In addition, an external protective coating is applied over these layers to protect the cable from physical damage (Powers, 1997).

In this regard, the sensitivity characteristics of the alternative fiber optic cables were simulated at a laboratory scale and identified in detail. As a result of these sensitivity analyses, the cable to be used in the field was determined (Demir, 2023). Real-time monitoring studies have started in an active landslide area within the borders of Yalova province, which might have been triggered by earthquakes and precipitation, to make real-time projections of the results obtained here in the field. During the studies performed, the cable itself was used as a sensor by taking advantage of the ability of the system to take measurements along the cable with the Brillouin Optical Time Domain Analyzer (BOTDA) based fiber optic sensing method. First, geotechnical characterization and numerical modeling were conducted in the landslide area. A monitoring system was prepared on the susceptible slope parts, and two different single-mode fiber optic cables monitored the landslide: one was more sensitive (3 mm), and the other one was more resistant to external effects (4.5 mm). Monitoring deformations caused by landslides with fiber optic methods has started in Yalova with the mentioned techniques for the aforementioned reasons.

1.3 Overview of Thesis Structure and Content

Chapter One introduces the thesis, outlining its aims and objectives. Chapter Two contains a literature summary on mass movement, monitoring methods, and landslide monitoring with fiber optic methods.

Chapter Three delves into the working theories and principles of fiber optic systems, elucidating them in detail. This chapter also explains the advantages and applications of these systems, supported by references and citations from existing literature.

Chapter Four focuses on prior research and presents the outcomes of artificial landslide monitoring using fiber optic systems established in the project within a laboratory setting. Additionally, this chapter includes a simple field study conducted at Hacettepe University, which served as a preliminary study to the pilot study in Yalova.

Chapter Five addresses the general characteristics of Yalova province and the location of the pilot study area, emphasizing its susceptibility to earthquakes and precipitation. Furthermore, this chapter comprehensively examines the area designated for monitoring, integrating insights from geotechnical reports. It also encompasses the appropriate site selection studies in the study area with Limit Equilibrium Method (LEM) analyses using the Geostudio 2012 Slope/W program.

Chapter Six, the Methodology chapter, elucidates the monitoring system in detail. It describes the setup of the monitoring area, including the preparation of the channel and installation of fiber optic cable within the inclinometer pipes. This process is clearly illustrated with the aid of figures. This chapter further discusses how the data received by the BOTDA device is processed and analyzed.

Chapter Seven thoroughly examines the data obtained from the study. Initially, it explains the state of the monitoring area during the 15-day Pre-Monitoring Testing Phase before the actual monitoring began. Then, it identifies the five most sensitive points within the monitoring area, focusing on how precipitation affects the slope at these points. The analysis also includes an evaluation of the impact of precipitation along the entire fiber cable. Furthermore, the chapter analyzes the strain in the fiber cables, considering the time-history data from four earthquakes that occurred during the monitoring period. The chapter concludes by comparing the field results with those obtained in laboratory settings.

Chapter Eight presents a comprehensive synthesis of the thesis and concludes with a summation of the findings. It evaluates the relative properties of the two types of cables used in the study. Chapter Nine outlines prospective research to be conducted within the scope of the project and proposes recommendations for future studies.

2. LITERATURE REVIEW

2.1. Introduction

Landslides represent one of the most destructive natural disasters globally. They manifest as a catastrophe with equal significance as earthquake or flood hazards in Türkiye. (Gökçe et al., 2008; Dağ and Bulut, 2012; Okalp and Akgün, 2016). Slope stability analysis ensures the safe and cost-effective design of engineering structures like excavations, embankments, and dams. It involves identifying geological, material, environmental, and economic factors and comprehending the potential risks' characteristics, extent, and frequency. With slope stability analysis, under what conditions can the masses move, drained and undrained stability analysis, landslide probability, and redesign suggestions are provided with back analysis.

Modes of Failure

Varnes (1978) categorizes landslides based on their movement patterns and the characteristics of the materials involved. A simplified version of Varnes' classification can be found in Table 2. According to this table, it is possible to identify any landslide by considering two criteria: the first criterion relates to the characteristics of the material, while the second criterion describes the type of movement exhibited by the landslide.

Table 2. Slope Failure Modes (Varnes, 1978)

Type of Movement		Type of Material		
		Bedrock	Engineering Soils	
			Coarse	Fine
Fall		Rock Fall	Debris Fall	Earth Fall
Topple		Rock Topple	Debris Topple	Earth Topple
Slide	Rotational	Rockslide	Debris Slide	Earth Slide
	Translational			
Spread		Rock Spread	Debris Spread	Earth Spread
Flow		Rock Flow	Debris Flow	Earth Flow
Complex		Combination of two or more principal types of movement		

Limit Equilibrium Methods (LEM)

Slope stability analysis is critical in geotechnical engineering and environmental science, focusing on assessing potential instability in natural and artificial slopes (Morgenstern and Price 1967). It is vital in preventing landslides and other geotechnical failures, which can lead to significant economic loss and human casualties. The analysis involves understanding the balance of forces within a slope, including the influence of gravity, soil properties, water pressure, and external loads (Bishop 1955).

The earliest studies on slope stability analysis were primarily concerned with simple, homogeneous slopes and used limit equilibrium methods. These methods, such as the Bishop Simplified and the Fellenius methods, are based on the balance of forces and moments on a potential failure surface (Bishop

1955, Fellenius 1936). These approaches, while simplistic, provided a foundation for understanding the basic principles of slope stability. As shown in Table 3, some Limit Equilibrium Methods (LEM) consider moment balance, some force balance, and both in their calculations.

Over time, more complex methods have been developed to account for the heterogeneous nature of slopes. These include the Morgenstern-Price method, which allows for variable shear strength along the slip surface (Morgenstern and Price 1965).

Table 3. Static Equilibrium Conditions Satisfied by Limit Equilibrium Method (Pami et al., 2021)

Method	Force Equilibrium		Moment Equilibrium
	x	y	
Ordinary Method of Slices	No	No	Yes
Bishop's Simplified	Yes	No	Yes
Janbu's Simplified	Yes	Yes	No
Lowe and Karafiath's	Yes	Yes	No
Corps of Engineers	Yes	Yes	No
Spencer Method	Yes	Yes	Yes
Bishop's Rigorous	Yes	Yes	Yes
Janbu's Generalized	Yes	Yes	No
Sarma’s	Yes	Yes	Yes
Morgenstern-Price	Yes	Yes	Yes

LEM used in slope stability analysis has been extensively explored, revealing various aspects crucial to geotechnical engineering. The LEM is widely recognized in landslide analysis for its reliability and effectiveness, which have been established through extensive application. This method is characterized by its relative simplicity and accessibility, making it a preferred choice in engineering practices. Comprehensive analyses, encompassing potential sliding surface identification, the evaluation of water pressure impacts, and diverse stability condition assessments, are facilitated by this method. Using LEM was considered appropriate upon examining the geometry, geological composition, and water pressure dynamics of the monitoring area in Yalova.

A comparative study by Liu et al. (2015) juxtaposed the LEM with finite element methods, focusing on two-dimensional slope examples. It was found that the LEM tends to yield a slightly lower factor of safety compared to finite element methods, highlighting the conservative nature of LEM in ensuring safety in geotechnical design (Liu et al., 2015). In an insightful study by Shamsher Sadiq et al. (2018), the LEM was applied to explore the Birham landslide in Murree, Pakistan. The SLOPE/W program that was used in this thesis delved into the stability of slopes under static and dynamic loading conditions.

2.2. Common Methods for Monitoring and Assessing Landslides

Landslides create significant infrastructure, ecosystem, and human safety issues, especially in geologically active regions. Monitoring these movements enables understanding their dynamics, predicting potential failures, and implementing appropriate mitigation measures. Landslide monitoring involves various methods to assess slope stability and identify potential hazards. In recent years, there has been a growing awareness of the hazards posed by landslides and the significance of risk management (Arslan Kelam et al., 2015). To achieve more effective landslide risk management, optimization of the utilization of extensive datasets, employment of monitoring resources strategically, and enhancement of communication with residents in regions prone to landslides are being performed (Casagli et al., 2023).

The importance of landslide monitoring cannot be overstated due to the unexpected nature of large-scale landslides. Early detection and warning are of great importance in mitigating the impact of these natural hazards (Qu et al., 2016).

Numerous factors, including changes in moisture content, can trigger landslides. Seismic refraction tomography, a method that provides images of the elastic properties of subsurface materials in landslide settings, is sensitive to these changes (Whiteley et al., 2020). However, achieving accurate and reliable displacement prediction, essential for landslide mitigation, remains a challenge due to the complex nonlinear characteristics of landslide monitoring data (Niu et al., 2021).

In landslide monitoring, numerous methodologies have been defined, encompassing geotechnical methods, geodetic approaches, photogrammetric modalities, and remote sensing or satellite techniques (Savvaidis, 2003). Geotechnical methods play a crucial role in landslide monitoring. After a large landslide event, several exploration methods were evaluated for their applicability to investigate and monitor landslide areas. In geotechnical landslide monitoring, inclinometers have emerged as indispensable instruments for assessing and monitoring landslides. These instruments, which measure subsurface deformations, offer precise insights into the movement and behavior of slopes, enabling professionals to detect even small shifts that might precede a major landslide event (Trofymchuk et al., 2017). Furthermore, inclinometers remain an essential method in the field of landslide monitoring. Their ability to detect subsurface deformations provides invaluable insights into the internal dynamics of landslides.

Using inclinometer data is vital for understanding landslides, including their causes, movements, and how to mitigate them. Nevertheless, care must be taken during inclinometer installation, regular monitoring, and precise data acquisition to ensure the accuracy and reliability of the processed information. This emphasis on the importance of methodological steps is exemplified in the research of Stark and Choi (2008), wherein they provided comprehensive guidelines for understanding, installing, and interpreting inclinometers within their study. However, in their research, they have been noted that inaccurate information and results were obtained due to the difficulties encountered in the above-mentioned methodological stages. Figure 1 shows a detailed schematic of the inclinometer.

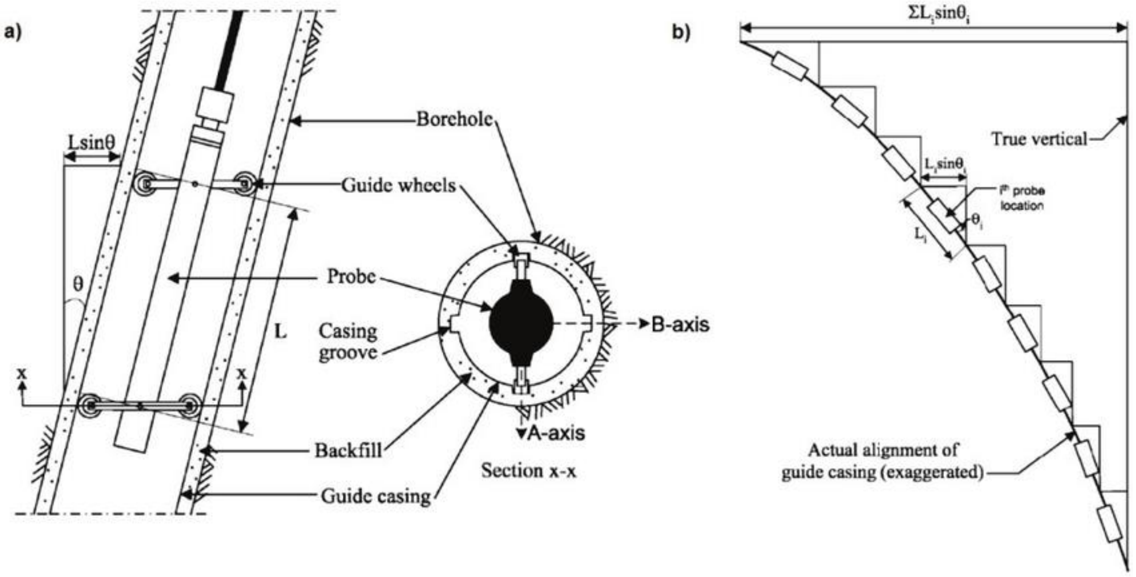

Figure 1. Schematic of the slope inclinometer: (a) inclinometer device, (b) illustration of operation (Dunnicliff, 1993; Stark and Choi, 2008; Cala et al., 2016)

Extensometers emerge as significant tools in monitoring landslide movements across various terrains. These instruments provide precise measurements of ground displacements, offering invaluable insights into landslides' dynamics and triggering factors. With the capability to detect both surface and subsurface movements, extensometers provide a comprehensive understanding of the complex behaviors exhibited by landslides. Their straightforward installation and high reliability make them indispensable in designing and implementing early warning systems. Furthermore, using extensometers contribute to a deeper comprehension of landslides, facilitating the mitigation of potential risks and hazards. (Corominas et al., 1999; Corominas et al., 2005; Intrieri et al., 2012).

In addition to the critical role played by inclinometers and extensometers, piezometers are another indispensable technique for landslide monitoring. These devices are instrumental in assessing the influence of slope saturation, primarily induced by heavy rainfall, which frequently serves as a triggering mechanism for landslides. A critical component of slope stability analysis is established by precisely measuring pore water pressures and piezometric levels, allowing the detection of threshold levels. These defined thresholds serve as crucial early warning indicators, offering insights into conditions potentially resulting in catastrophic slope failure (Savvaidis, 2003).

Light Detection and Ranging (LiDAR) enables the precise identification of areas at risk of landslides by creating high-resolution three-dimensional maps. This technology uses laser beams to measure the topographic features of the earth's surface with millimetric precision. This property allows for a detailed examination of land changes before and after landslides. Especially in challenging and hard-to-reach areas, LiDAR facilitates the rapid and effective scanning of large expanses. This technology is used in early warning systems for landslides and is critical in preventing or minimizing potential disasters. Mora et al. (2018) demonstrated a methodology using multi-temporal LiDAR-derived Digital Elevation Models (DEMs) for landslide change detection. This method effectively maps surface changes indicating landslide activity, highlighting the precision of LiDAR in detecting sub-meter surface features crucial for landslide mapping. Xu et al. (2021) further emphasized the effectiveness of integrating LiDAR with Interferometric Synthetic Aperture Radar (InSAR) technology for landslide identification and deformation monitoring. This integration enhances the accuracy of landslide detection, especially in areas with complex terrains and dense vegetation.

2.3. Advanced Landslide Monitoring Using Fiber Optical Systems

Fiber optic cables offer a continuous and highly responsive means of monitoring strain and temperature variations, serving diverse objectives. The utilization of fiber optic cables for the monitoring of landslides stands as a significant and pioneering advancement within the academic domain. The integration of optical fiber sensors has significantly enriched the domain of landslide monitoring. Research has highlighted the potential of these sensors, emphasizing their precise measurement capabilities and extensive monitoring range. The following sections will explain the technical specifications and details of fiber optic cables. While the extent of investigations and applications concerning monitoring through fiber optic cables remains limited, there are considerable studies.

In regions prone to landslides, deploying fiber optic cables within boreholes drilled at strategically determined locations is becoming increasingly prevalent for monitoring ground displacements. These cables, functioning similarly to inclinometers, enable continuous and detailed assessment of ground movements. There are studies in the literature that have demonstrated the effectiveness of the fiber optic in landslide monitoring approach in various geotechnical applications by using different methods (i.e., point distributed sensors such as OTDR; distributed sensors such as BOTDA and DAS) and provided valuable information on landslide dynamics (Zeni et al., 2015; Pei H. et al., 2011; Kogure and Okuda, 2018; Liu et al., 2010; Marzuki et al., 2015; Minardo et al., 2021; Lebang et al., 2021; Zhao et al., 2021; Zheng et al., 2017; Zhu et al., 2012).

Apart from the other sensors, the high resolution and successful monitoring capacity of the Brillouin optical time-domain analysis (BOTDA) technique have been highlighted, pinpointing its applicability in diverse terrains and conditions. Concurrently, introducing a state-of-the-art high-resolution distributed strain sensing system has emphasized the precision and accuracy achievable in landslide monitoring. These advancements underscore the evolution and capabilities of monitoring systems in the context of landslide detection (Zeni et al., 2015; Yu et al., 2018).

The Pei et al. (2011) study focuses on using Fiber Bragg Grating (FBG)-based technology for landslide and debris flow monitoring. The research introduces two innovative optical fiber sensor systems: an FBG-based in-place inclinometer for landslide monitoring and an FBG-based column-net system for detecting debris flows. They conducted laboratory calibrations and installed these systems at a Weijiagou Valley, Sichuan Province, China site. Their work demonstrated that these FBG-based systems offer advantages in monitoring geohazards, showing promising results in accuracy, reliability, and real-time monitoring capabilities in the field.

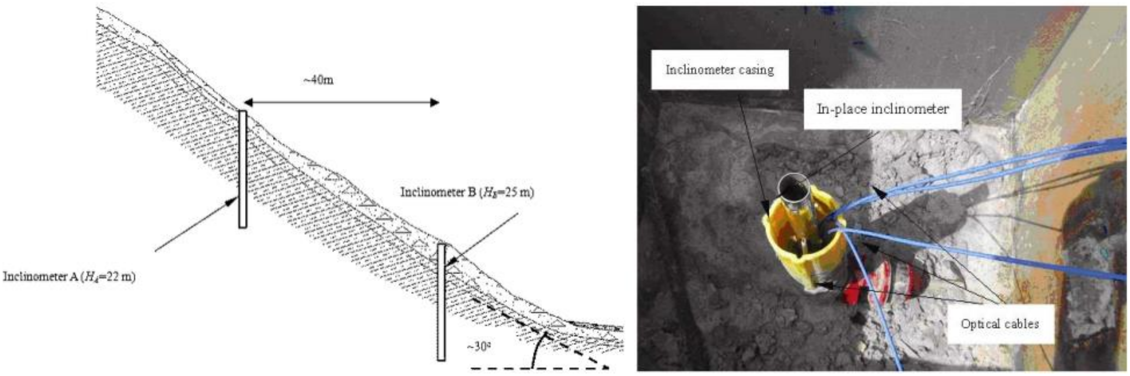

Figure 2. Application of Fiber optic landslide monitoring in the field (Pei et al., 2011)

Some studies propose effective deployment strategies for FBG sensors in real-world scenarios, highlighting their potential for early landslide detection (Liu et al., 2010; Marzuki et al., 2015).

The continuous monitoring of optical fiber sensor technology has led to the development of diverse configurations and methodologies, each tailored to address specific challenges in landslide monitoring. A study by Lebang et al. (2021) focused on detecting displacement using optical fiber sensors. The adaptability of optical fiber sensors in capturing precise displacement data was demonstrated through experimentation with various configurations. The potential of these sensors in diverse geotechnical scenarios was emphasized, displaying their versatility in real-case applications.

Minardo et al. (2021) employed a distributed optical fiber strain sensor based on stimulated Brillouin scattering to monitor the deformations of a tunnel located in a landslide-prone area in the southern Italian Apennines. This tunnel, which is part of the national railway system, had been significantly damaged by landslide movements and was rebuilt in 1992. The study has been observing the internal deformations of the tunnel using this sensor since 2016. The elongation of the fiber cables crossing these joints aligns with data from other measurement systems. The study also reveals an increase in the rate of fiber deformation during the initial and final parts of the monitoring period, corresponding to the acceleration in landslide movements as recorded by the area's inclinometers.

Zhao et al. (2021) extensively explored the Precise Point Positioning - Brillouin Optical Time Domain Analysis (PPP-BOTDA) Distributed Optical Fiber Sensing Technology and its application in the Baishuihe Landslide. The research emphasized the advanced capabilities of the PPP-BOTDA technology, highlighting its precision, reliability, and extensive monitoring capacity. The study further solidified the significance of distributed optical fiber sensing techniques in complex landslide scenarios.

Kogure and Okuda (2018) monitored rainfall-induced strain changes in a landslide using distributed fiber optic sensing with Rayleigh backscattering Distributed Acoustic Sensing (DAS). Measurements revealed two types of deformation within the landslide mass: sliding at the boundary between tuff and mudstone and creep in mudstone layers. The study highlighted the effectiveness of distributed fiber optic sensing in detecting strain changes and deformations in landslide areas, particularly in deeper sections activated by heavy rainfall.

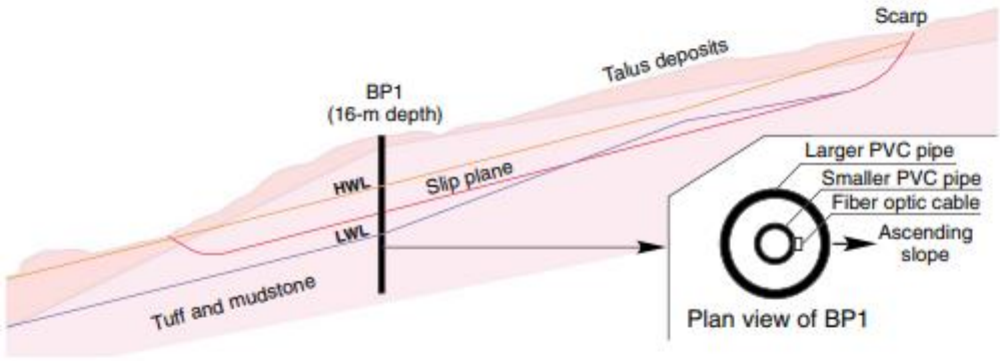

Figure 3. Application of Fiber optic landslide monitoring in the field (Kogure and Okuda, 2018)

Rørstadbotnen et al. (2023) developed an early warning system in Rissa, Norway. The research from July 2021 to February 2022 utilized distributed acoustic sensing data during road construction over quick clay deposits. The study tested various analysis methods, including Rayleigh wave dispersion from active sledgehammer shots and ambient noise cross-correlation, to estimate shear-wave velocity profiles up to a depth of 15 meters. This study mentioned that the variation in shear-wave velocity observed during the monitoring period was relatively small, with a maximum change of about 23 m/s.

Zheng et al. (2017) explored the potential of a combined optical fiber transducer for slope deformation monitoring, elucidating the basic mechanics and capabilities of optical fiber transducers (Zheng et al., 2017). Continuing from this initial research, a study conducted in 2019 explored the effectiveness and efficiency of an optical fiber sensor that utilizes Optical Time-Domain Reflectometry (OTDR) to detect and monitor different geotechnical movements (Zheng et al., 2019). In 2020, the research centered on applying fiber optic sensors in landslide monitoring. The sensor demonstrated a response over a wide range of 212.1 mm in shrinkage and 87.9 mm in elongation. The sensor's predicted displacements were nearly identical to the measured crack opening displacement, with relative errors primarily within 10% (Zheng et al., 2020).

Zhu et al. (2012) investigated the application of fiber optic sensing technology in monitoring a roadside slope in Hong Kong and demonstrated its effectiveness in geotechnical instrumentation. The sliding mass, equipped with various stabilization measures such as soil nails and soldier piles, was subjected to detailed strain measurements following heavy rainfall. After the rainfall event on June 19, 2008, a significant strain increase exceeding 800 με (με) was observed in one of the soil nails, indicating that the effect of water seepage and increased groundwater pressure on the stability of the slope was monitored with a fiber optic system (Zhu et al., 2012).

As shown in Figure 4, in the Bahçecik region of Kocaeli, Türkiye, the research conducted by Arslan Kelam et al. (2016 and 2022) demonstrates the effectiveness of optical fiber-based monitoring systems in the detection and analysis of mass movements. The study employed a BOTDA along with optical fiber cables for long-term monitoring, detecting subtle movements indicative of mass movements such as landslides (Arslan Kelam et al., 2016). The subsequent research builds upon this, marking a significant advancement in applying this technology for mass movement assessment in Türkiye. This study correlates strain data, ranging from 0 με to 4600 με, with an estimated cumulative displacement of approximately 0.283 meters, showcasing significant ground movement over the monitoring period (Arslan Kelam et al., 2022). Both pieces of research underscore the validation of the collected data through periodic surface topography measurements, which strongly agree with the displacements estimated by the optical fiber system (Arslan Kelam et al., 2016 and 2022). This validation not only reinforces the system's reliability and the suitability of the cable used for monitoring mass movements but also highlights the system's potential to be transformed into an early warning system. By setting threshold strain values, such as the observed peak of 4600 με, and considering the effects of triggering factors, the system could be employed to alert authorities, significantly contributing to the hazard and risk assessments of mass movements and potentially serving as a pioneering model for similar studies in regions with analogous geotechnical challenges. Figure 5 shows a με-Distance graph, which is the output of these studies.

Figure 4. Fiber Optic Cable configuration at the landslide site in Bahçecik, Kocaeli (Arslan Kelam et al., 2022)

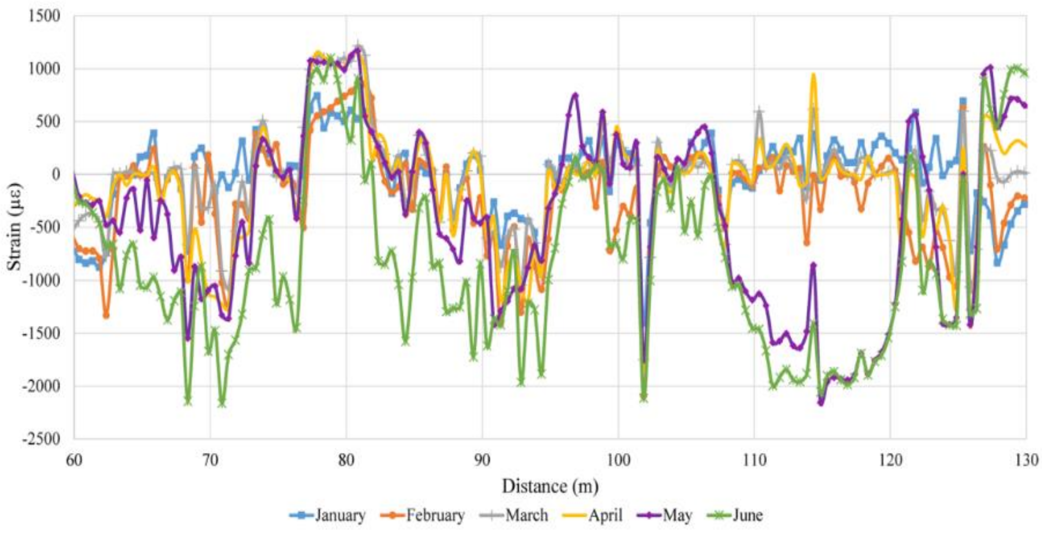

Figure 5. Strain data obtained with BOTDA for the six months measured in the field (Arslan Kelam et al., 2022)

In a detailed investigation conducted by Han et al. (2023), the precision and sources of error in optical fiber inclinometer technology, as used in geotechnical monitoring, were examined using Optical Frequency Domain Reflectometry (OFDR). It was found that the error magnitude in measurements taken with a 20-meter-long, 65 mm diameter inclinometer increased quadratically with the length of monitoring. The importance of keeping the inclinometer angle below 30 degrees for accurate readings was also highlighted. Additionally, the impact of boundary conditions on measurement accuracy was emphasized, leading to the proposal of a comprehensive error equation. This study provides essential contributions to enhancing the accuracy and reliability of optical fiber inclinometers in geotechnical engineering.

2.4. Why was the distributed sensor (BOTDA) used?

When selecting a device, understanding its operational principles and intended applications is essential. In the field of fiber optic sensing, the distinctions between point sensing, quasi-distributed sensing, and distributed sensing are critical for understanding their respective applications and capabilities. Each approach offers unique advantages depending on the specific requirements of the sensing application.

Zhu et al. (2023) enhanced point sensing using a FBG sensor system with microwave-photonic interferometry and the Vernier effect. This method offers precise, localized measurements, ideal for structural health monitoring and detecting specific physical changes like strain or temperature at discrete locations.

OTDR, a point sensing technique, tests the integrity and performance of fiber optic cables. OTDR measures the backscattering and reflections within the fiber. This technique sends short light pulses into the fiber and detects light losses caused by any breaks, bends, or other abnormalities in the fiber. OTDR is used to identify cable faults and connection points, especially during the installation and maintenance of fiber optic networks (Agrawal, 2012).

Zhong et al. (2022) study utilized Quasi-Distributed Sensing, combining the precision of point sensing with the broad reach of distributed sensing. They employed series-integrated FBGs for high-resolution temperature measurements, demonstrating their potential in industrial temperature profiling and moderate-area environmental monitoring applications.

BOTDA, a technique incorporated in distributed fiber optic sensors, detects temperature and strain changes by measuring Brillouin scattering within the fiber. This method leverages the distributed sensing capability to map temperature and strain variations along the fiber's entire length, utilizing the interaction between light and acoustic waves that varies with the fiber's physical property changes. Predominantly used in structural health monitoring and geotechnical applications, BOTDA excels in long-distance fiber optic sensor systems, offering comprehensive coverage and detailed insights (Zhang et al., 2018).

DAS, a distributed sensing method using fiber optic cables, detects acoustic events over extensive distances by analyzing Rayleigh scattering within the fiber. This technique that focuses on the scattering of light caused by minute particles or the fiber material itself, allows for monitoring sound waves and vibrations along the entire fiber length. Employed in various applications, including pipeline monitoring, seismic research, and border security, DAS leverages its distributed nature to provide comprehensive acoustic monitoring across vast areas (Hartog, 2017; NJ Lindsey, 2017). The BOTDA has several significant advantages over other methods for landslide monitoring:

- High Sensitivity and Long Range: BOTDA, with high sensitivity, can measure temperature and strain changes along fiber optic cables. This method can detect slight changes over kilometers of fiber length, making it ideal for covering large areas, such as landslide-prone regions (Zhang et al., 2018).

- Data Versatility: BOTDA can simultaneously measure both temperature and strain changes. This feature helps better understand the changes caused by landslides and allows for more accurate risk assessments.
- More Durability to External Factors: BOTDA is less sensitive to external factors than other methods. For example, the DAS method may be affected by environmental noise, while BOTDA is less impacted by such external factors, providing more reliable data (Hartog, 2017).

These advantages are the main reasons for choosing BOTDA over other methods in landslide monitoring and early warning systems. The high sensitivity, continuous monitoring capability, and resistance to environmental conditions provided by BOTDA play a crucial role in enhancing security in landslide-prone areas.

3. BACKGROUND AND THEORY

3.1. Introduction

Fiber optic cables (Figure 6) were first developed for endoscopes in the 1950s by Basil Hirschowitz, C. Wilbur Peters, and Lawrence E. Curtiss. However, fiber optic cables, a revolutionary technology in telecommunications, were first developed in the 1970s by Corning Glass Works. These cables were designed to overcome the limitations of traditional copper wires in terms of bandwidth and transmission distance (Hirschowitz et al., 1954; Maurer et al., 1970; Thyagarajan and Ghatak, 2007). Fiber optic measurement systems have gained significant importance in various industrial applications due to their exceptional customizability, heat resistance, and deformation resistance. These systems are extensively utilized for tasks such as detecting leaks and identifying corrosion in pipelines, providing early warning systems for fire detection, and assessing deviation and structural health in diverse structures. In these systems, light transmitted through the fiber is modulated by the expansion or contraction of the sensor, generating a signal that is subsequently converted into quantitative measurements by a device. These quantitative measurements represent the strain values associated with the respective engineering structures (Kwon and Choi, 2012; Wu et al., 2020).

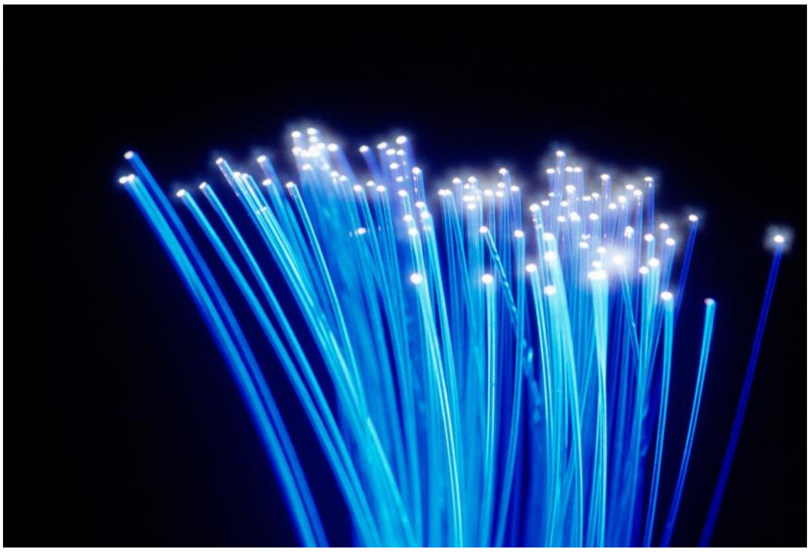

Figure 6. Fiber optical cable

The working principle of fiber optic cables is based on transmitting light signals. When a light signal enters the fiber, it bounces off the boundary between the core and the cladding. This bounce is due to the difference in refractive indices between these two layers, which causes the light to undergo total internal reflection. As a result, the light signal can travel great distances with minimal loss (Thyagarajan and Ghatak, 2007).

The nature of light as electromagnetic radiation, comprising discrete units of energy called photons, is widely acknowledged. Fiber optic cables share similarities with electrical cables, except that they facilitate light transmission instead of electrons. To comprehend the mechanism by which fiber optic cables transmit light, it becomes imperative to gain an understanding of light propagation through various media. Snell's law, also recognized as the law of refraction, elucidates photons' behavior as they transmit between two transparent dielectric media (Shirley, 1951).

As shown in Figure 7, fiber optic cables consist of two distinct components: the core and the cladding. Notably, the core possesses a higher refractive index than the cladding. Upon generation of the light signal from the source, a continuous phenomenon of total internal reflection takes place within the interface of the fiber optic cable core and cladding (Figure 8).

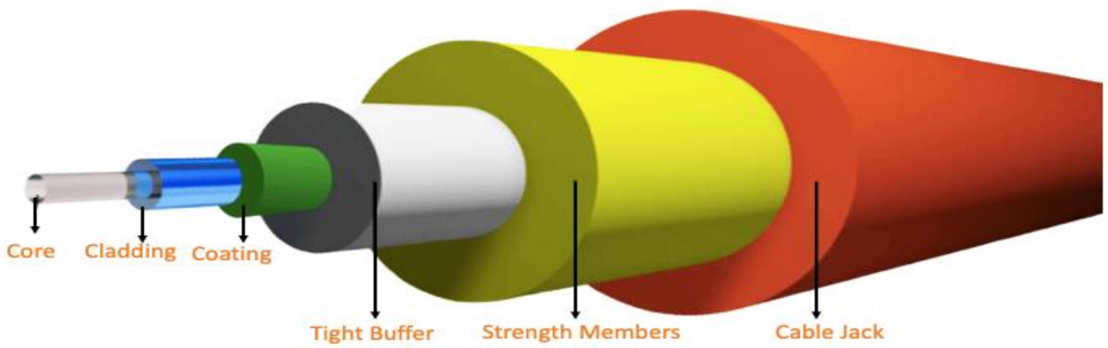

Figure 7. Structure of fiber optical cable

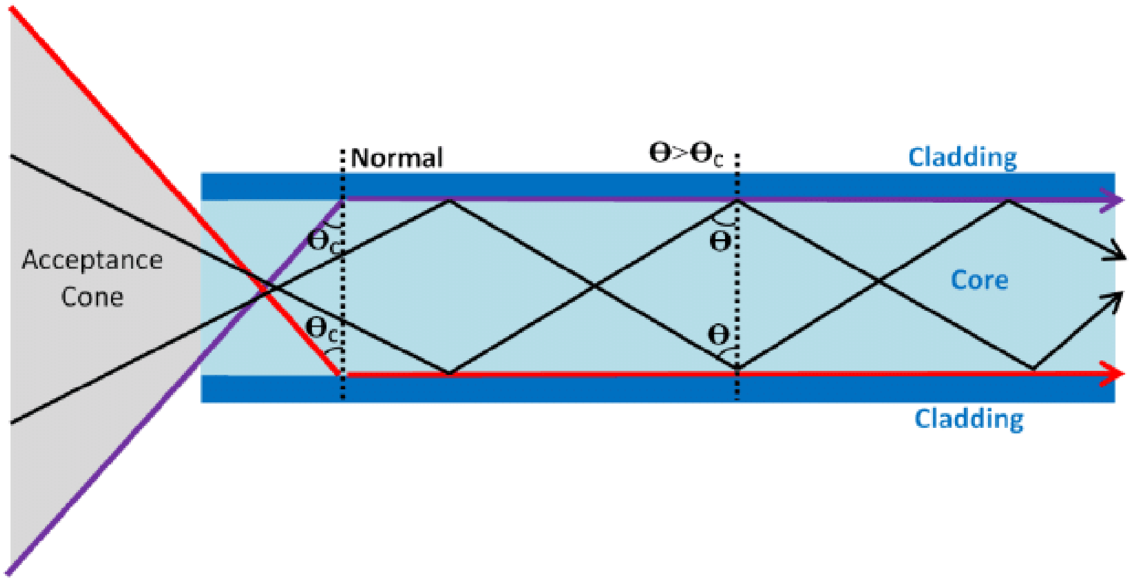

Figure 8. Total internal reflection in fiber optical cable

$$n_1 sin\theta_1 = n_2 sin\theta_2 \qquad (Eq. 1)$$

Figure 9 shows the mechanism of light reflection in a fiber optic cable. Fiber optic cables employ the optical phenomenon known as "Total Internal Reflection" to facilitate light transmission. Total internal reflection occurs when a photon transmits from a medium with a high refractive index to a medium with a lower refractive index. This situation leads to its complete reflection within the initial medium. The angle between the reflected light and the boundary is called the critical angle (Eq. 2).

$$\sin\theta_c = \frac{n_2}{n_1} \qquad (Eq. 2)$$

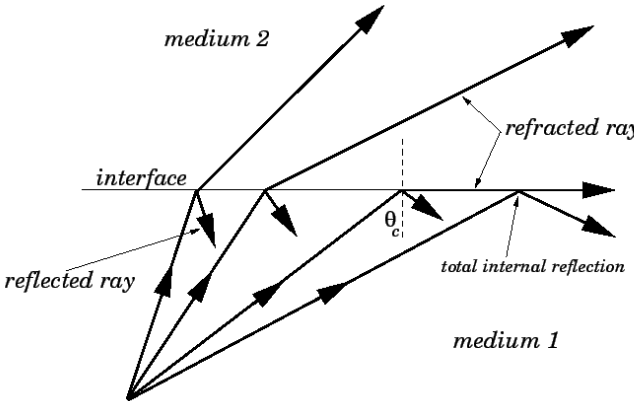

Figure 9. The process by which light reflects within a fiber optic cable

Fiber optic cables come in two primary types: single-mode and multi-mode. Single-mode fiber optic cables utilize a single light path, or mode, through the core of the cable, allowing for data transmission over long distances with minimal signal loss (Agrawal, 2012). This issue is achieved using a narrow core diameter that prevents light from bouncing around, thus reducing signal degradation. On the other hand, multi-mode fiber optic cables have a larger core diameter, allowing multiple light paths or modes to propagate simultaneously (Tripathi et al., 2010). While this results in a higher data capacity, it also leads to more signal loss over distance due to modal dispersion, making multi-mode cables more suitable for short-distance, high-data-rate applications such as within data centers. Both types of cables play crucial roles in different scenarios, depending on the specific requirements of data rate and transmission distance. Furthermore, these fiber optic cables have found applications in various fields, such as remote sensing techniques using standard single-mode fibers for monitoring high-voltage cable joints (Tia et al., 2005) and temperature monitoring in high-risk volcanic areas using multi-fiber cables containing single-mode optical fibers (Carlino et al., 2016).

This investigation focuses on three distinctive types of scattering phenomena in fiber optics, which are linear and non-linear scattering. Specifically, the types of scattering under consideration are Brillouin, Raman, and Rayleigh scattering. In this study, the emphasis has been placed on utilizing systems developed based on nonlinear Brillouin scattering theory principles. As observed in fiber optic cables, Brillouin scattering involves the reflection of light traveling within the fiber in the reverse path, resulting from spontaneous interaction with an acoustic wave. As acoustic waves also propagate through the medium, the reflected light undergoes a frequency shift known as the Brillouin Frequency. The magnitude of this frequency shift in the reflected light can be utilized to derive the velocity of the acoustic wave. Figure 10 illustrates the spectrum of different types of scattering.

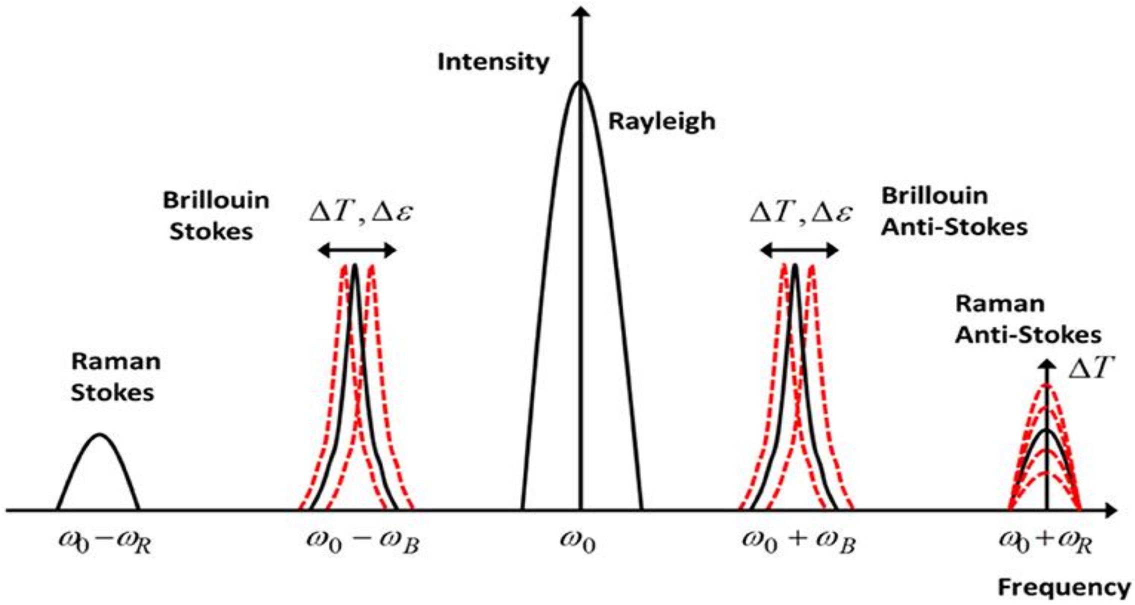

Figure 10. The spectrum of Rayleigh, Brillouin, and Raman scattering in fibers (Muanenda et al., 2019)

One key advantage of Brillouin scattering-based sensors lies in their capability to function at any segment along the length of the optical fiber, effectively transforming any part of the fiber into a viable sensor.

3.2. Benefits of using optical Fibers

Several features set optical fibers apart from conventional methods: they are small in diameter, light in weight, sensitive to temperature changes and strain, have a wide band range, are resistant to electromagnetic and environmental effects, and are inexpensive (Wang et al., 2008; Gupta, 2012; Measures, 2001).

Powers (1997) lists the benefits of fiber optics as having a large bandwidth, being tiny and light, being immune to electromagnetic interference, not sparking, not having crosstalk between channels, being compatible with solid-state sources, and being inexpensive.

A medium's bandwidth, dependent on car frequency, measures its frequency range breadth. A fiber cable's bandwidth can reach multiple THz, enabling data transport via numerous sources in various sectors. Fiber optics are compact and light because of their small dimensions and low density. This feature is helpful in field applications, mainly when a lengthy section has been considered. Because of these physical qualities, the wire may be installed in smaller spaces, which makes transportation easier. In electricity-related features and applications, electromagnetic interference is nearly hard to prevent and poses a challenge to data transmission. Because the technology of optical fibers is impervious to electromagnetic interference, it may be used where electromagnetic fields are present. In addition, optical fiber cables may be used in hazardous and flammable gas environments because they do not spark. As a sum, because of their composition and size, optical fibers are suitable for modern technology (Powers, 1997).

3.3. The Utilized Optical Fiber System

Fiber optic cables monitor and detect changes in various parameters (i.e., velocity, position, strain) in multiple structures (i.e., tunnels, pipelines) (Altuğ, 2007). In addition to fiber cables, a fiber optic system may also have sensors and a device that transmits light into the cable and gathers the backscattered light. A fiber optic system is utilized in combination with a variety of device types. In the context of this thesis, a Brillouin Time Domain Analyzer was used as a long-term source and receiver, as well as an Optical Time Domain Reflectometer (OTDR) to examine momentary damages and the condition of the cables for short periods.

3.2.1. Optical fiber system utilized with OTDR

Time domain reflectometry is a phenomenon that relies on ground motion in the event of a landslide and strain on a cable caused by any action. The backscattering duration of the pulsed light is monitored to determine the motion (Yan et al., 2010). Its goal is to find, identify, and quantify events at every point along a fiber array. Light is sent to a cable by an OTDR, which then gathers backscattered light. The return time of backscattered light may be calculated using amplitude (Fang et al., 2012). OTDR provides the decibel (dB) reflection location corresponding to a cable change caused by any effect.

The ratio of the input optical power to the output optical power (measured) for a specific wavelength can be expressed as a decibel, a unit of measurement used for power unit comparisons. Equation 3 defines the number of decibels (Mohammed & Fatth, 2013).

$$dB = 10\log_{10}\frac{P_i}{P_o} \qquad (Eq. 3)$$

3.2.2. Optical fiber system utilized with BOTDA

Although it uses a distributed optical fiber, BOTDA operates based on Brillouin scattering. Because these systems utilize the time difference between the light that is initially sent and the light that is reflected, similar to the principles of the OTDR, they are categorized as time domain systems. (Ohno et al., 2001). The primary distinction between the BOTDA and the OTDR is the scattering principle used; specifically, the BOTDA employs Brillouin scattering, whereas the OTDR utilizes Rayleigh scattering. The difference between the launched and backscattered light causes a frequency shift measured by Brillouin scattering (Halley, 1987). According to Thyagarajan and Ghatak (2007), the BOTDA detects variations in frequency, whereas the OTDR measures changes in energy loss (measured in decibels).

Determining temperature and strain through Brillouin scattering relies on analyzing the frequency change observed in the scattered light. This velocity shift associated with Brillouin scattering is mathematically represented, as demonstrated by Equation 4.

$$V_B = \frac{2nV_a}{\lambda_p} \qquad (Eq. 4)$$

Where;

V_A = Acoustic wave velocity

n = Index of refraction

λ_p = Initial light wavelength

The acoustic wave and refractive index are affected by variations in temperature and strain. The representation of strain in the fiber cable is expressed as shown in Equation 5.

$$\varepsilon = \frac{\Delta L}{L} \qquad (Eq. 5)$$

$K_{B\varepsilon}$ represents the Brillouin Scattering stimulation caused by strain in the fiber cable (Eq. 6).

$$K_{B,\varepsilon} = \frac{dV_B}{d_\varepsilon} = \frac{2}{\lambda_p}\left(V_A \frac{dn}{d_\varepsilon} + n\frac{dV_A}{d_\varepsilon}\right) \qquad (Eq. 6)$$

$K_{B,\,T}$ represents the Brillouin Scattering stimulation caused by temperature in the fiber cable (Eq. 7).

$$K_{B,T} = \frac{dV_B}{dT} = \frac{2}{\lambda_p}\left(V_A \frac{dn}{dT} + n\frac{dV_A}{dT}\right) \qquad (Eq.7)$$

The alteration in wave velocity within the fiber optic cable gives rise to the Brillouin frequency shift, which is influenced by the parameters mentioned previously. This phenomenon can be elucidated by the equation provided below as Eq. 8.

$$the \qquad V_A = \sqrt{\frac{E(1-k)}{(1+k)(1-2k)p}} \qquad (Eq.8)$$

where, E = Young's modulus

ρ = Fiber density

k = Poisson's ratio

The acoustic wave velocity and, thus, the Brillouin frequency depend on strain, as the equations suggest (Figure 11).

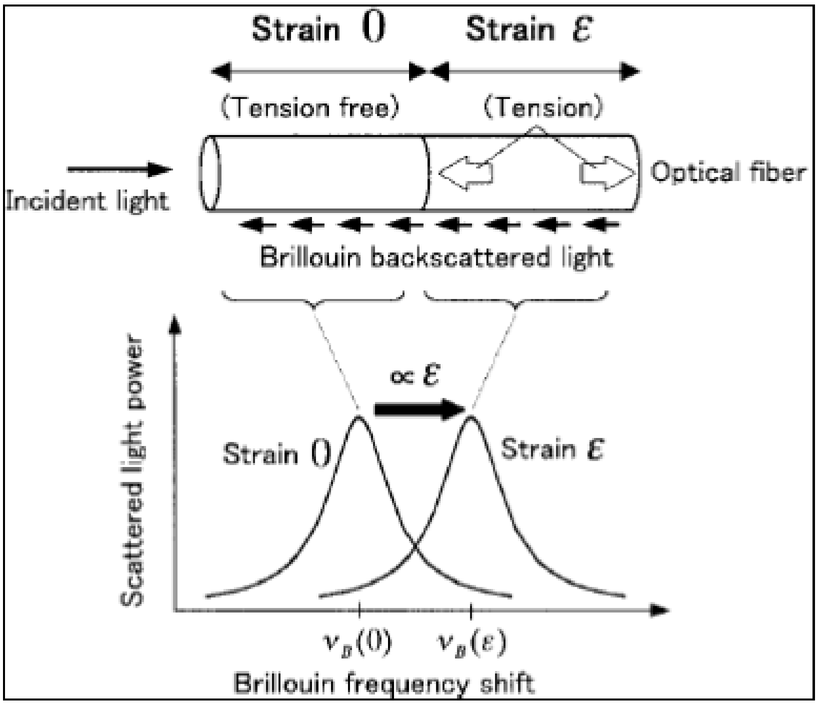

Figure 11. Brillouin frequency shift due to strain (Ohno et al., 2001)

Brillouin frequency shift in an optical fiber is correlated with longitudinal strain or ε by Equation 9:

$$\nu_B(\varepsilon) = \nu_B(0) + \frac{d\nu_B(\varepsilon)}{d\varepsilon}\varepsilon \qquad (Eq. 9)$$

Therefore, the Brillouin frequency shift can be used to determine the change in strain (Ohno et al., 2001).

Similar to the OTDR approach, the BOTDA employs time domain analysis by observing backscattered light. Therefore, the connection provided in Equation 10 can be used to estimate any Z distance where dispersed light is formed.

$$Z = \frac{cT}{2n} \qquad (Eq. 10)$$

where, c = light velocity

T = time elapsed between launching and backscatter

BOTDA uses this equation to locate the strain change. Spatial resolution is a crucial concept for precisely determining the place of change. Equation 11 may be used to formulate spatial resolution, which measures the precision of locations.

$$Z = \frac{c\tau}{2n} \qquad (Eq. 11)$$

where, τ = pulse width. As the equation shows, greater spatial resolution increases precision (Ohno et al., 2001).

Brillouin Optical Time Domain Analysis (BOTDA), the technical details and schematic diagram given in Figure 13, is a specific technique used to perform distributed temperature and strain measurements in optical fibers. It is based on the principle of Brillouin scattering. The BOTDA system employs two light source pumps and a probe that delivers a continuous wave into the fiber cable. These two sources propagate in opposite directions along the sensing optical fiber, allowing the scanning of optical frequency differences to detect the frequency shift phenomenon (Fenta et al., 2021). Furthermore, The BOTDA system boasts a 1 m spatial resolution and can detect strain changes with a precision of 0.1 με along a 3 km cable (Arslan Kelam et al., 2016).

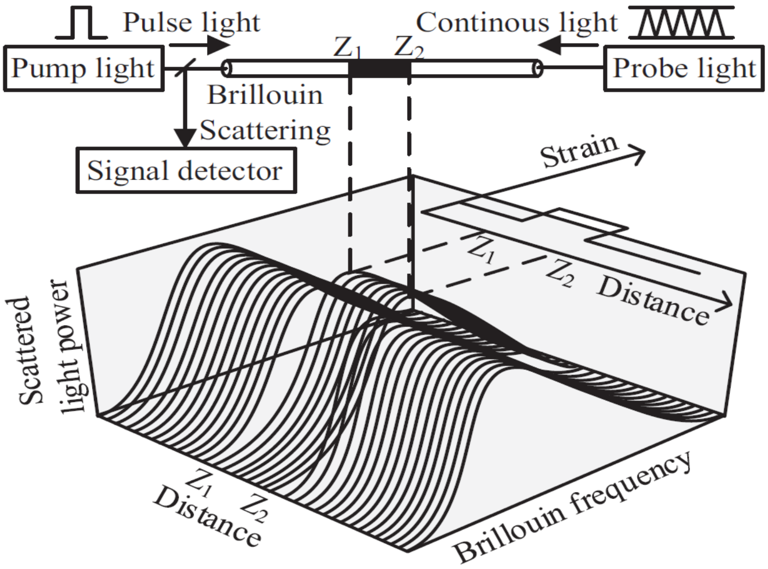

Figure 12. Schematization of the BOTDA (Liu et al.,2017)

4. PRELIMINARY STUDIES FOR FIELD STUDIES

4.1. Introduction

The small-scale laboratory testing studies performed before field application are critical for real-case applications in the field. The fundamental logic for this approach is to enable the identification and selection of appropriate materials (i.e., fiber cable), equipment tailored to field conditions, and sensitivity analysis for the deformation capability of the sensors while proactively addressing potential challenges. In this regard, the laboratory studies were conducted before the studies regarding the main objective of the thesis, which was to monitor a real case landslide site with a light-based fiber optic method (UNESCO, 2015), leading the way in determining the sensitivity of the fiber cables. With the help of these laboratory experiments, cables that could be used in field studies were tested, and an optimum cable was identified.

4.2. Laboratory Studies

The laboratory model was designed by considering the dimensions of the landslide container to be installed on the shaking table and considering factors such as maximum velocity, maximum deformation, damping motions, and plane strain conditions (Figure 13). Plexiglass plates were placed on the bottom of the container to minimize boundary effects along the vibration direction. The dimensions of the shaking table were determined according to the size effect and the capacity of the table.

Figure 13. Landslide Container and Shake Table

As mentioned in Section 3, fiber optic cables are categorized based on the mode of light propagation. Single-mode fiber optic cables transmit light flux at a single angle, whereas multi-mode cables do so at multiple diffused angles. The efficiency of fiber optic cables increases as their diameter decreases, making single-mode cables more capable of transmitting data than multi-mode cables.

Linear Variable Differential Transformers (LVDT) have been used to compare the data during laboratory studies and are employed to measure deformations, which are crucial for understanding deformation-strain relationships. LVDT is an electromechanical position transmitter sensor that offers precise and smooth positional information regarding an external force. LVDT operates on the principle of a transformer, converting motion information into an electrical signal. It consists of a winding assembly and a moveable core, with the core movements resulting in changes in electrical signals. The absence of mechanical contact between the core and windings in LVDTs prevents friction, leading to extended mechanical endurance and lower noise signal development. In addition to LVDTs, three-axis accelerometers with IP65 protection were used during the experiments to assess dynamic soil behavior characteristics in the landslide simulator and to control the dynamic acceleration.

Unlike the field study, one more data logger was used in addition to the BOTDA during the laboratory studies. This system was a 16-channel, 24-bit capacity data collection system, which operated with the shaking table, transmitting LVDT and triaxial accelerometer measurements to computers.

Artificial slopes with specific geometry were created in the landslide simulator. The relationship between LVDT data and fiber cable data was monitored. Experiments began with sand material, representing conditions similar to the application field.

During the laboratory studies, a manual deformation input code was written for the shake table motion with the help of Python, and a more realistic landslide motion was achieved. The manual deformation tests have been designed to simulate natural unidirectional sliding conditions, such as those that might occur during a landslide. This issue has been achieved by defining the motion as instantaneous velocity expressions in a text file, which are then applied to the shaking table. This approach differed from the sinusoidal wave method in preliminary tests, allowing for a more realistic simulation of landslide-triggering mechanisms. The landslide pool was divided into sensor zones, as shown in Figure 14. This division ensured testing, processing, analysis, and evaluation of the measurements to be more professional. Table 4 and Table **5** display strain measurements from the fiber optic system, physical deformations from LVDTs for nine consecutive tests, and test velocities and amplitudes for Sensor Zone 1 and 3.

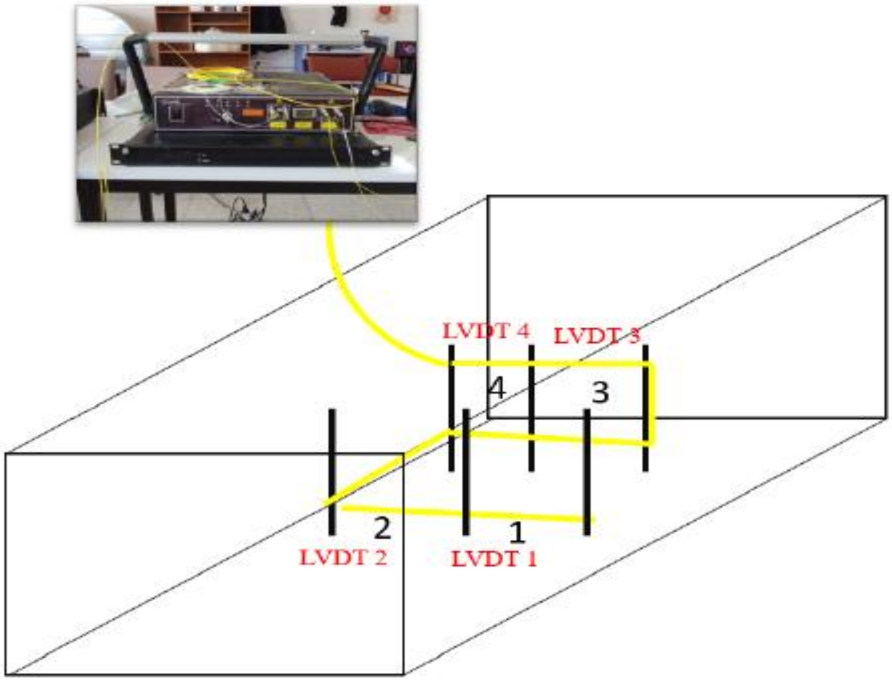

Figure 14. Schematic diagram of sensor zones.

Table 4. Variation of με and deformation in the toe (Sensor Zone 1) of the model slope (Sensor Zone 3)

Test No	Velocity (mm/s)	Amplitude (mm)	The toe of the slope Strain (με)	Deformation (mm)
1	150	50	669.0	0.25
2	150	90	1999.1	0.37
3	150	130	4626.7	0.62
4	150	150	4930.0	0.70
5	200	170	8125.9	1.20
6	200	90	13403.9	2.50
7	200	120	16696.6	2.66
8	200	150	19940.9	2.69
9	200	170	23524.2	2.75

Table 5. Variation of με and deformation in the crown of the model slope (Sensor Zone 3)

Test No	Velocity (mm/s)	Amplitude (mm)	Crown of the slope Strain (με)	Deformation (mm)
1	150	50	5035.9	0.20
2	150	90	6779.1	0.32
3	150	130	10265.5	0.42
4	150	150	13508.5	0.50
5	200	170	16494.2	0.60
6	200	90	17405.9	0.70
7	200	120	18623.1	0.74
8	200	150	20753.7	0.78
9	200	170	24887.1	0.82

The findings presented in Table 4 and Table 5 highlight a noteworthy correlation between the data collected through LVDT and the fiber optic system. Additionally, these measurements align with the observable slope failure, indicating agreement between the two measurement methods.

4.3. Preliminary Trials

Laboratory studies have provided an understanding of the sensitivity of fiber cable in small-scale operations. However, preliminary tests regarding the methods applied in the field studies also needed to be conducted. For these trials, a hand auger and inclinometer pipes have been used (Figure 15).

Figure 15. Hand auger and inclinometer pipes

Within the scope of these trials, a 1-meter deep borehole was drilled using a handauger, and an inclinometer pipe instrumented with fiber optic cables was installed in the borehole put down in the back yard of the Civil Engineering Department of Hacettepe University (Figure 16).

Figure 16. Inclinometer pipe and fiber cables in the hole drilled with a hand auger

First, the inclinometer pipe was used by directly taping the fiber cables on the inclinometer pipe without any treatment. However, the expected efficiency of the fiber cables could not be obtained without indentation on the surface of the inclinometer pipe where the cable could stand. Then, as shown in Figure 17, a CNC machine was used to create small channels in the inclinometer pipes into which the fiber cables could be inserted.

Figure 17. The view of the small channels on the inclinometer pipe

5. A CASE STUDY IN YALOVA PROVINCE

5.1. Introduction

In this section, the geological formation of Yalova Province is reviewed. The seismic activity of the region and its vulnerability to earthquakes have been mentioned previously. The landslide vulnerability and climatic character of the province are discussed. All of the characteristics mentioned earlier are essential factors affecting landslide vulnerability, and their awareness reveals the vulnerability of Yalova Province in terms of landslides.

5.1. Geological Formation of Yalova Province

Yalova is located in the southeastern part of the Marmara Region in northwestern Türkiye. It borders the Marmara Sea to the north and west, Kocaeli to the east, Bursa (Orhangazi - Gemlik), and the Gemlik Gulf to the south. Yalova lies between 39°-40° North latitude and 29°-31° East longitude, with an altitude of 2 meters above sea level and its highest point reaching 926 meters. The province covers an area of 847 km^2, accounting for 0.11% of Türkiye’s total land area (Alparslan, 2011; Yalova Provincial Disaster Risk Mitigation Plan, 2022)

As a geomorphological structure, Yalova Province's coastline does not exhibit significant indentations or protrusions, and its coastal strip displays natural beach characteristics. Apart from the flat areas on its eastern coasts, Yalova has a mountainous terrain. The Samanlı Mountains cover the southern part of the region, also the prominent mountains of the province, and are located in the south of Yalova. The overall slope range of the province is between 0% and 80%. In areas where the alluvial unit is observed, the slope values are between 0-10%, while in other areas, they can increase up to 70-80% (Figures 18 and 19).

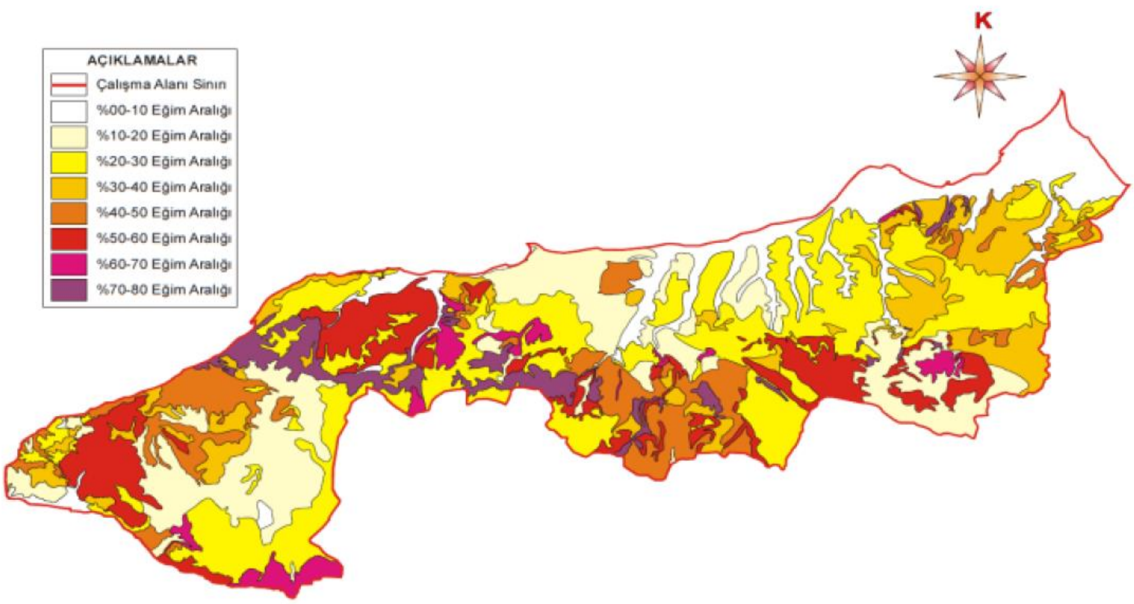

Figure 18. Slope Index Map of Yalova Province

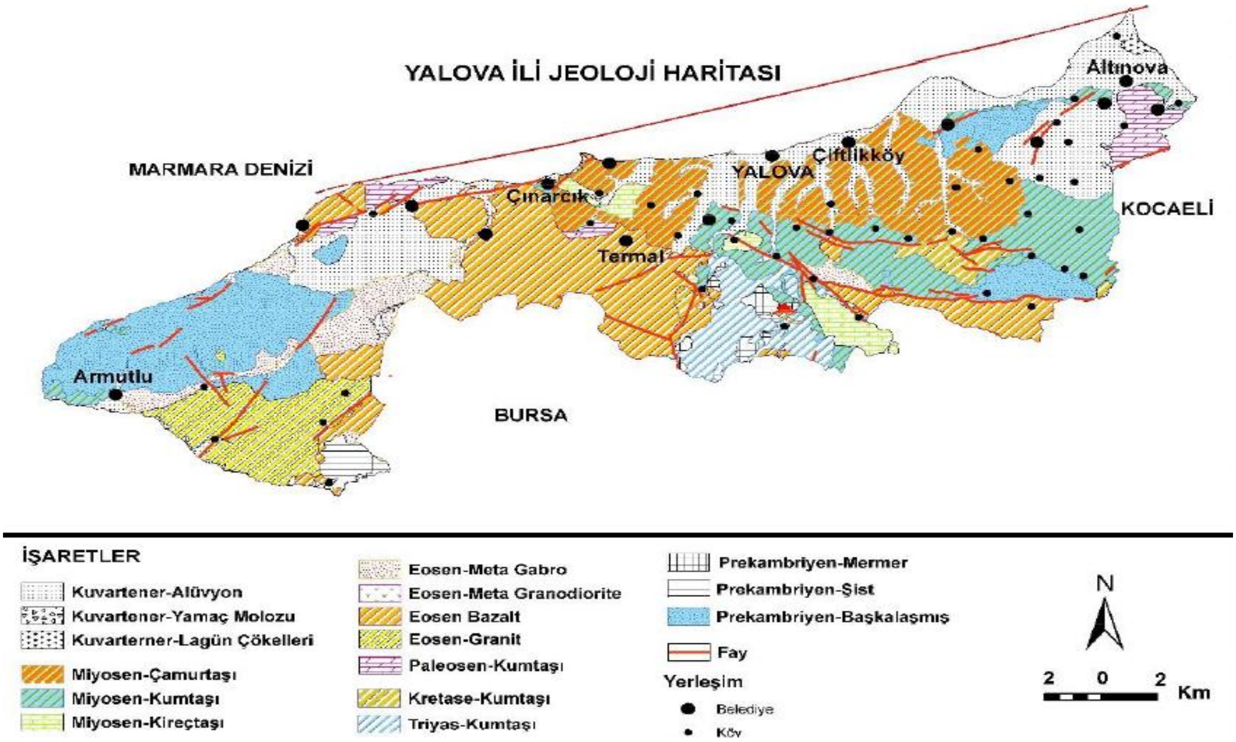

Figure 19. Geological Map of Yalova Province

One of the most critical parameters of landslide stability is geological structure. The geological structure of Yalova is diverse and represents various geological periods. Rock types from the Paleozoic era are exposed in the study area. Primarily, there are the Pamukova Metamorphites, believed to be of Pre-Cambrian-Lower Paleozoic age, and the İznik metamorphizes of Lower Triassic-Cretaceous age, which show less metamorphism. Above these, in sequence, are the Upper Cretaceous-aged Bakacak formation, the Upper Paleocene-Middle Eocene-aged İncebel formation, and the Eocene-aged Sarısu formation, which are sedimentary and volcano-sedimentary units. During the Eocene period, the Fıstıklı Granitoid was established in the region. Furthermore, the area also features the Miocene-aged Kılıç formation, Upper Miocene-Lower Pliocene-aged Yalakdere formation, Pleistocene-aged marine terraces, and current alluviums.

5.2. Seismicity

The Marmara region, encompassing Yalova, has a long history of seismic activity. This region has endured several intense earthquake activities, with moment magnitudes larger than 7. These tremors are primarily due to the tectonic movements along the North Anatolian Fault Zone (NAFZ). Over the centuries, the region has been shaken by significant earthquakes, the impacts of which have been measured by assessing the damage they caused, the length of the fault rupture, and the observed lateral shifts. One of the most recent seismic events was the earthquake on 17 August 1999, the Kocaeli Earthquake. The devastation from this earthquake was most pronounced along the fault's trajectory. In the aftermath of this event, there has been a renewed emphasis on urban planning in Yalova, focusing on future infrastructure development and urban renewal initiatives. The geological characteristics of the region, including soil type and its response to seismic activities, are crucial in determining the magnitude of earthquake damage, particularly with secondary effects such as landslides and liquefaction, as noted by Kendir (2010).

Additionally, studies have chronicled the seismic history of the Marmara region, highlighting the recurring nature of earthquakes over the past few centuries. This historical data underscores the region's vulnerability and the imperative for ongoing preparedness and mitigation efforts (Ambraseys & Finkel, 1991). Figure 20 indicates that the early earthquake-related studies took place in Yalova Province. The extensive damage in the August 17th earthquake in Yalova, a province with intense seismic activity, is shown in Table 6.

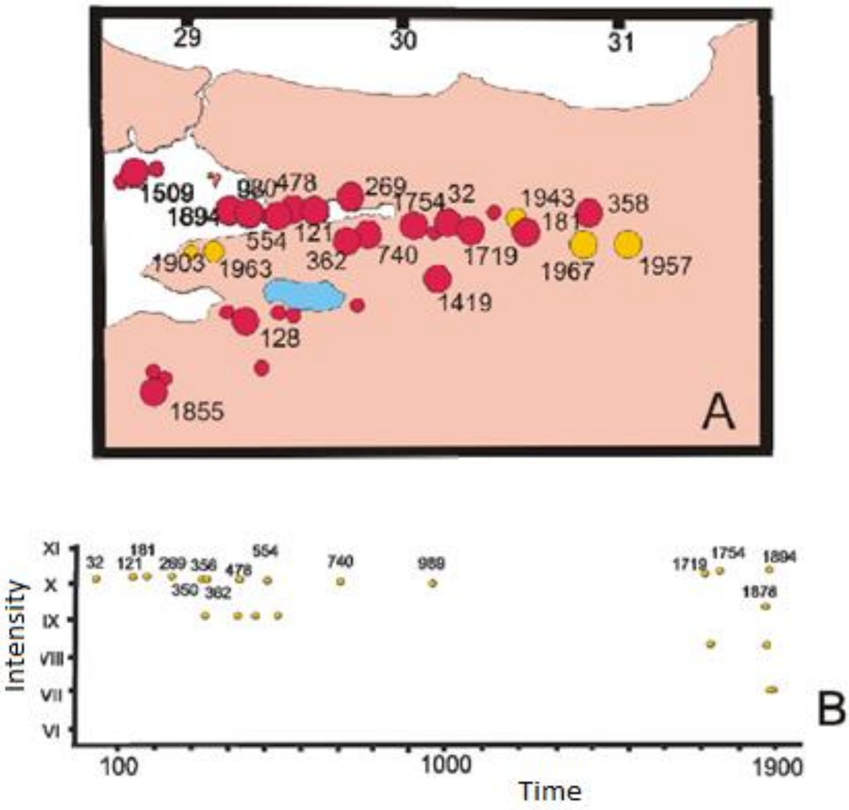

Figure 20. Historical earthquakes affecting the eastern Marmara region a) years of occurrence and epicenters, b) intensity (Ambraseys and Finkel, 1991)

Table 6. After the August 17 Earthquake, the number of people causalities and injuries in Yalova and its counties (Özmen, 2000)

Yalova Province	**Number of Causalities**	**Number of Injured**
Yalova-Center	1450	3395
Altınova	14	27
Armutlu	0	0
Çiftlikköy	672	2297
Çınarcık	365	314
Termal	3	0
TOTAL	**2504**	**6042**

5.3. Landslide Susceptibility in Yalova Province

Yalova Province, located in northwestern Türkiye, faces a heightened risk of landslides due to its geographical and geological attributes. It occupies a delicate position between the Sea of Marmara to the south and the active NAF to the north, rendering it susceptible to seismic activity, a key trigger for landslides. Moreover, Yalova's topography, characterized by steep slopes and hilly terrain, amplifies its vulnerability to mass movements. This susceptibility is increased by soft and easily erodible sedimentary rocks, like clay and siltstone, making the region prone to landslides during heavy rainfall or seismic events. Due to these factors, conducting comprehensive geological and geotechnical studies and implementing early warning systems in Yalova is imperative. Additionally, land-use planning must account for the region's unique geological and geographical conditions. These measures are essential to mitigate the risks associated with landslides.

Based on the presence or absence of landslide features, whether they are passive or active, the type of slope failure (shallow or deep-seated), the density of landslide distribution, the geological formation of the area, and the general slope angle, Lubkowski et al. (2002) created a landslide hazard map. In addition, as shown in Figure 21, Alparslan (2011) created a landslide susceptibility map with the methodology they developed by processing geology, hydrology, soil, and elevation data available from institutions in Türkiye. They categorized landslide risk into four according to landslide vulnerability index values:

- None (LSI <= 0.248)
- Low (0.248 < LSI <= 0.486)
- Moderate (0.486 < LSI <= 0.724)
- High (LSI > 0.724)

The Mineral Research and Exploration Organization (MTA) has also created a map showing the landslide susceptibility of entire Türkiye using high technology and GIS. Figure 22 presents the vulnerability map of Yalova province prepared by MTA.

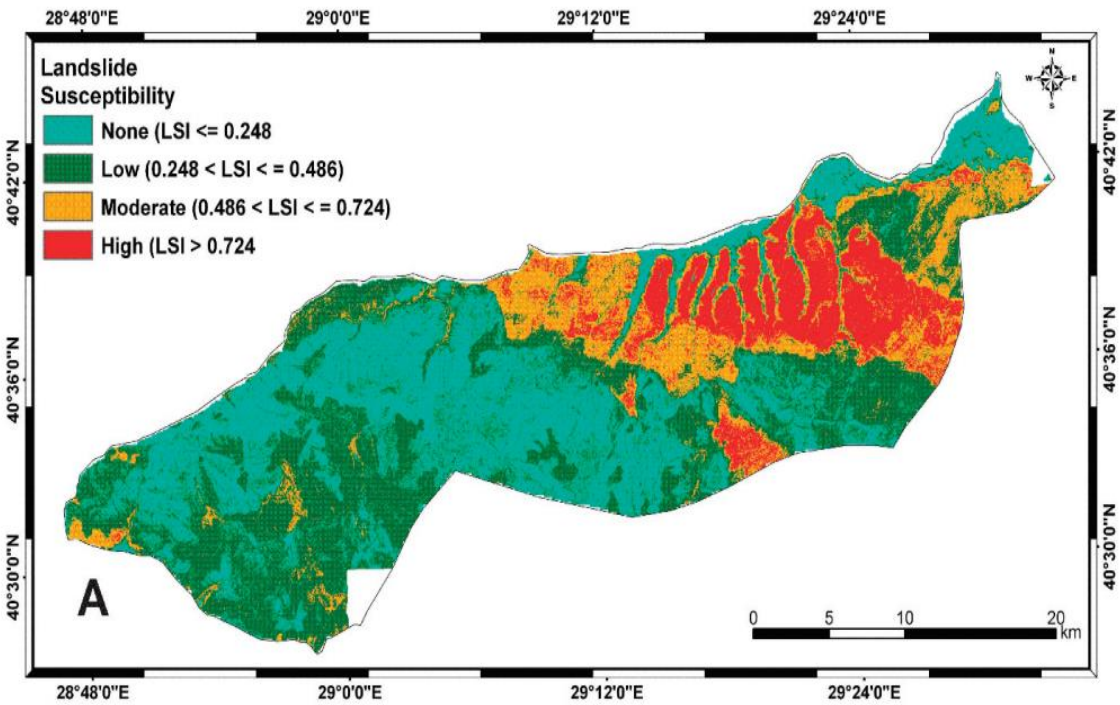

Figure 21. Landslide Susceptibility in Yalova Province (Alparslan, 2011)

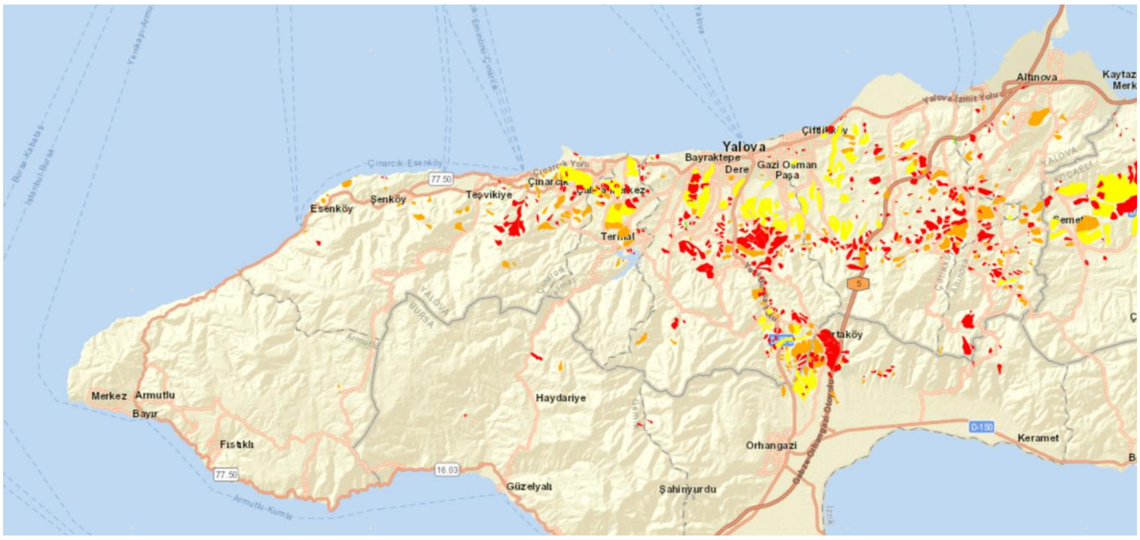

Figure 22. Landslide Map of Yalova Province: Red colors represent active landslides, yellow colors represent shallow landslides, and orange colors represent susceptible landslides. (Geosciences Map, General Directorate of Mineral Research and Exploration, MTA, 2021)

5.4. Climatic Characteristics of Yalova

Yalova is characterized by a Mediterranean climate, further influenced by continental and oceanic climatic features. The region's climate is classified within the Köppen classification system, which is one of the most widely used climate classification systems, as “Csa,” indicating a temperate climate with dry and hot summers (“Yalova – Wikipedia”; “Yalova, Türkiye – Climate - Weather Atlas”). The seasonal variations in Yalova exhibit warm, arid summers with clear skies, contrasting with the long, cold, and partially cloudy winters (“Yalova Climate, Weather By Month, Average Temperature - WeatherSpark"; “About Yalova - Urban Guide - YTSo.org.tr”).

The mean annual temperature in Yalova is recorded at 16.2ºC, with a slight deviation above this average, suggesting a trend towards warmer conditions (“Yalova, TR Climate Zone, Monthly Weather Averages and Historical Data - WeatherandClimate.com”). Precipitation is observed during the winter months, with October averaging 93.7 mm of rainfall, which contributes to the classification of Yalova's climate as having wet winters and comparatively dry summers as indicated in Table 7 (“Yalova Annual Weather Averages - WorldWeatherOnline.com”).

Table 7. Climate data for Yalova (1991–2020, extremes 1931–2020) (Source: Turkish State Meteorological Service)

Month	Record High (°C)	Average High (°C)	Daily Mean (°C)	Average Low (°C)	Record Low (°C)	Average Precipitation (mm)	Average Precipitation Days
January	25	10.3	6.8	3.7	-9.6	84.6	15.77
February	27.2	11.2	7.2	3.9	-11	68.7	13.47
March	32	13.5	9	5.2	-7.4	73.9	13.57
April	36.5	17.6	12.6	8.3	-1.6	51.3	11.1
May	37	22.5	17.4	12.8	1.2	39	8.47
June	42.1	27.1	21.9	16.9	7.1	47.4	6.83
July	39.2	29.8	24.3	19.1	10	22	4.1
August	40.2	30.1	24.5	19.6	10.3	34.5	3.87
September	37.5	26.2	20.8	16.1	6	52.9	8.1
October	36.6	21.1	16.5	12.7	1.3	93.7	12.03
November	29.7	16.3	12	8.4	-3.2	75.9	11.77
December	27.4	12	8.6	5.5	-9.2	105	15.4
Year	42.1	19.8	15.1	11	-11	748.9	124.5

5.5. Site Investigation of the Monitoring area

The study area that lies between Yalova Center and Çınarcık is shown by the red circle in Figure 23. This area is located on the northern side of Yalova. It is near the sea, which has significant implications for the local microclimate and the potential for land-water interactions. Given its closeness to the sea and apparent elevation changes, the area is at risk of landslides, primarily because water bodies or water flow contribute to soil saturation. Water availability, whether from precipitation or groundwater, acts as a triggering mechanism for landslides, particularly after heavy rainfall or if there are changes in land use that affect drainage or the water retention capacity of soil.

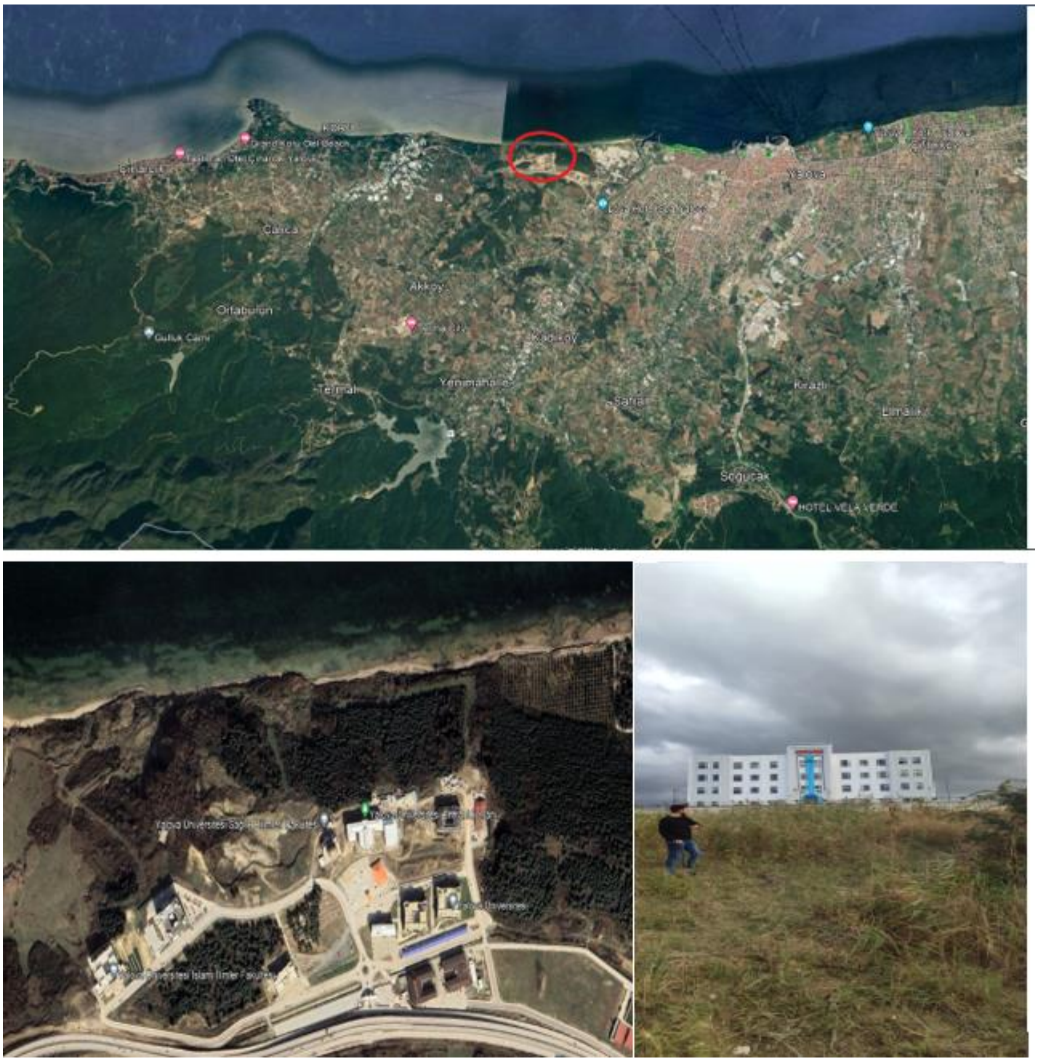

Figure 23. The study area (Google Inc., 2023)

For the reasons mentioned, the study area is highly susceptible to landslides. It is clearly seen in the GeoScience Map published by the General Directorate of Mineral Research and Exploration of Türkiye (MTA) in Figure **24**. The study was carried out in the orange zone, which was preferred because of terrain conditions, logistical situations, and available cable lengths.

Figure 24. Landslide Map of the study area: Red represents an active landslide, and orange represents the susceptible slope for a landslide. (Geosciences Map, General Directorate of Mineral Research and Exploration, MTA, 2021)

Figure 25 illustrates the proximity of the retaining wall and a building adjacent to the monitoring area, which contributes to the surcharge effect. It is readily discernible that this area exhibits susceptibility to landslides. This vulnerability is exemplified by the damage in front of the building, as illustrated in Figures 26 and 27.

Figure 25. The retaining wall and building adjacent to the monitoring area

Figure 26. The surface deformations and cracks near the building

Figure 27. The surface deformations and cracks near the building

5.5.1. Slope Stability Analysis of Study Area

An in-depth examination of the geotechnical borehole logs (Figure 28) reveals a stratification profile in which "Stiff Clay" constitutes the primary soil material up to a depth of seven meters. Below this superficial stratum, the material transitions to "Very Stiff Clay," are indicative of the compaction and consolidation characteristics typical of the subsoil environment. These findings are documented comprehensively in Appendix A, which includes detailed boring logs and SPT data.

Figure 28. Borings and their locations compiled from the study area

Before the field implementation, an investigation was conducted to determine the field configuration. The region with appropriate soil conditions was defined. It is critical to analyze this favorable area's landslide stability. As can be seen in Figures 29 and 30, a 3D image and then a Digital Elevation Model (DEM) were obtained with over 500 drone footage.

Figure 29. The sliding area highlighted in red represents where drone footage was taken from the site

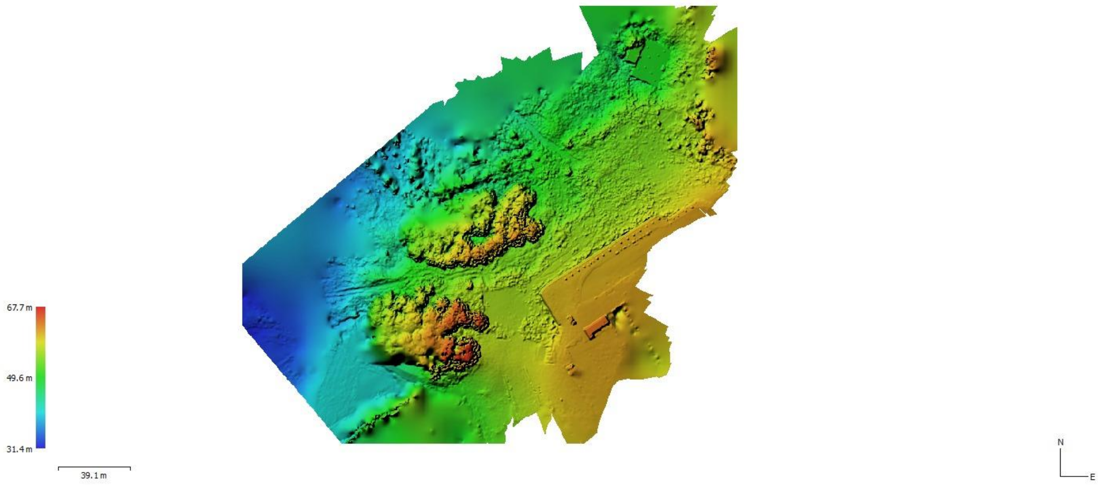

Figure 30. DEM of the sliding area in Figure 29, where drone footage was taken from the site

A profile of the study area was obtained from this DEM using the Profile Tool of the QGIS program. This profile was analyzed with the Geostudio 2012- Slope/W program using the Janbu Method, LEM, considering the properties of the soil materials given above (Figure 31). The Janbu method is widely utilized in LEM analysis in slope stability concepts. It is particularly effective in complex soil conditions and for various sliding surfaces. The method employs force equilibrium calculations for circular and particularly non-circular slip planes, as outlined in Table 3. Additionally, the Janbu Method's effectiveness in evaluating slopes with more moderate inclines was significant (Janbu, 1973). Due to these attributes, the LEM method was preferred for this research.

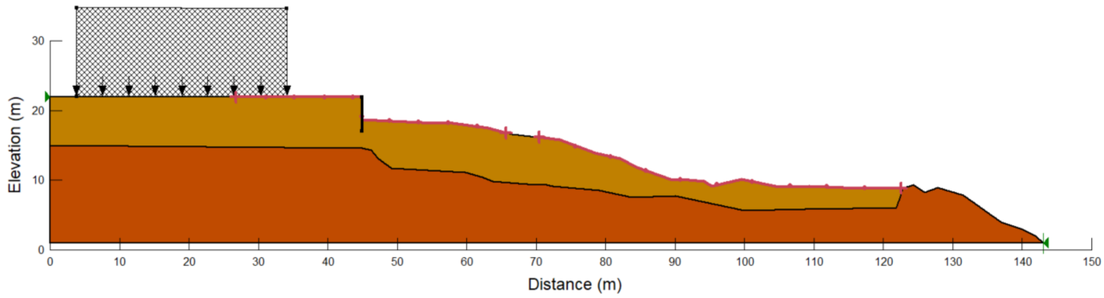

Figure 31. The geometry of the sliding surface from the study area

As a result of the detailed in-situ site investigation study and laboratory test results complied from previous studies, it was possible to recover geological formation information about the sliding mass spread over a local and wide area, as well as geotechnical shear strength parameters such as soil structure, natural unit volume weight (γ), cohesion (c) and internal friction angle (ϕ). The data of four different boreholes drilled to a depth of 15-20 meters instead of a single borehole to be drilled within the scope of the thesis around both landslide areas were examined. Accordingly, in the landslide area, soils related to the two-layered Yalakdere formation (Ty), consisting of a stiff clay layer (CH-CL) extending from the surface to depths of 6.5 to 10 meters and a layer of very stiff clay layer (CH) extending from depths of 6.5-10 meters to a depth of 20 meters under this layer, are encountered. According to the results obtained from the triaxial compressive strength tests (UU), the average cohesion and internal friction angle results from the upper layer of soil with stiff clay in the landslide area spreading over a large area are 74.35 kPa and 7.0°, respectively, and the average cohesion and internal friction angle values of the second layer soil with stiff clay are 83.40 kPa and 7.8°, respectively. In the local landslide area, the average cohesion (c) and internal friction angle values of the top layer soil with stiff clay are 76.61 kPa and 6.0°, respectively, and the average cohesion and internal friction angle values of the second layer soil with very stiff clay are 229.13 kPa and 9°, respectively. In addition, after the investigations, it was determined that the natural unit weights in the landslide area spread over a large area are 14.67 kN/m³ and 14.42 kN/m³ in the stiff clay and very stiff clay layers, respectively, and these values varied from 13.80 kN/m³ and 19.13 kN/m³ in the local landslide area, respectively. Figure 32 illustrates the Factor of Safety (FS) value and the critical slip surface location because of the analysis of the given material properties. As seen in Figure 32, the slope analyzed in a static condition with the building surcharge on it has a low FS value of 1.115.

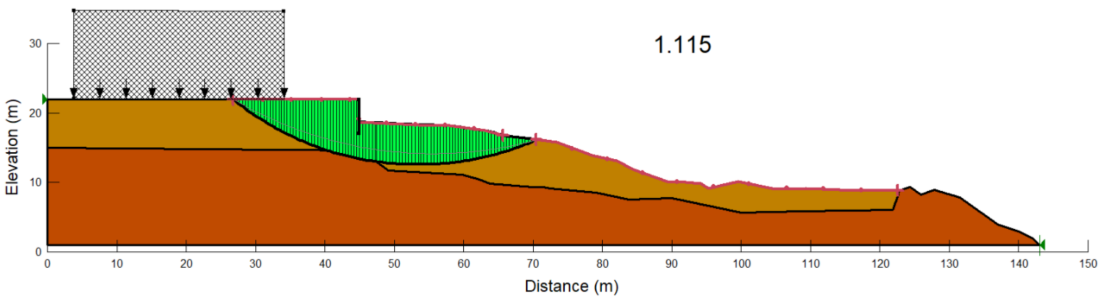

Figure 32. FS value for the critical failure surface (static conditions)

Given the seismic susceptibility of the region, it is clear that conducting static analysis only is insufficient. Dynamic analysis is also needed, which involves applying peak ground acceleration to the Slope/W program. The monitoring area's short-period design spectral acceleration (S_{DS}) data was obtained from the Earthquake Hazard/Risk Map of Türkiye, published by AFAD (Türkiye Earthquake Hazard Maps Interactive Web Application, 2018). This data was referenced following the DD-2 earthquake type and ZD soil type specific to the area. The acceleration value was determined in line with the Türkiye Building

Earthquake Code 2018 (Türkiye Building Earthquake Code- TBEC, 2018) Part 16.13.9 and 16.13.10.

$$a_h = 0.5\ (0.4\ S_{DS} S_T) \qquad ; \qquad a_v = \pm 0.5\ a_h \qquad (Eq. 12)$$

The S_{DS} data obtained from AFAD for the monitoring area is 1.46. Given that the slope's angle is approximately 16 degrees, the ST value is 1.2 (TBEC, 2018; Section 16.13.10). Based on these parameters, the horizontal acceleration coefficient (ah) is calculated to be 0.35, and the vertical acceleration coefficient (av) is ±0.18. Figure 33 illustrates that in the event of a potential DD2-type earthquake, the Factor of Safety (FS) of the monitoring area drops to 0.932 under combined dynamic and static loads, indicating slope failure. These analyses substantiate the decision regarding selecting the monitoring area location, which was made following thorough field investigations.

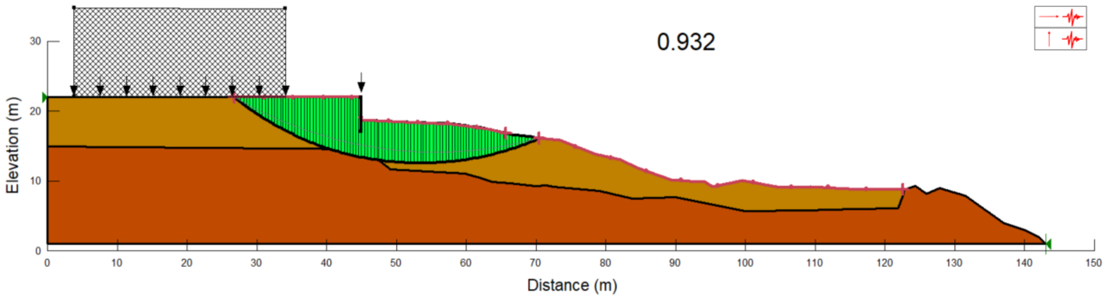

Figure 33. FS value for the critical failure surface under dynamic conditions

6. METHODOLOGY

6.1. Introduction

The subject of this thesis was carried out in an area susceptible to landslides in Yalova province after completion of the laboratory studies. A fiber optic system using a Brillouin Optical Time Domain Analyzer (BOTDA) device based on the Brillouin frequency shift was used for the data acquisition. In addition to BOTDA, an Optical Time Domain Reflectometer (OTDR), which works on the principle of energy loss, was used to check the condition of the fiber optic cable instantaneously, especially during cable deployment. Before the initiation of the continuous data acquisition process, several steps were followed in the field. These steps are digging, cable placement, and backfilling.

The laboratory studies used fiber cables with 1-, 2-, and 3-mm diameters. After the analysis, it was decided that the 3 mm cable was the most suitable among these three different cables for field conditions. In addition, a 4.5-mm cable was supplied and used in field studies since it is expected to be more resistant to adverse field conditions.

6.2. The Monitoring System

The BOTDA requires two laser beams pointing in a fiber cable structure in opposing directions. Light is launched in one direction and backscattered to the cable in the other. When the frequency difference between these two lasers coincides with a fiber's Brillouin frequency, a peak point appears on the measurement graph (Xiaofei et al., 2011).

As the strain and temperature change, the peak point forms at a different location than the previous. A shift in frequency of the peak point is detected due to this change. High-precision measurements over a lengthy fiber configuration may be obtained via the BOTDA system (Xiaofei et al., 2011; Yin et al., 2010).

The research used a Distributed Strain and Temperature Sensor (DSTS) device manufactured by OZ Optics, Ltd (Figure 34).

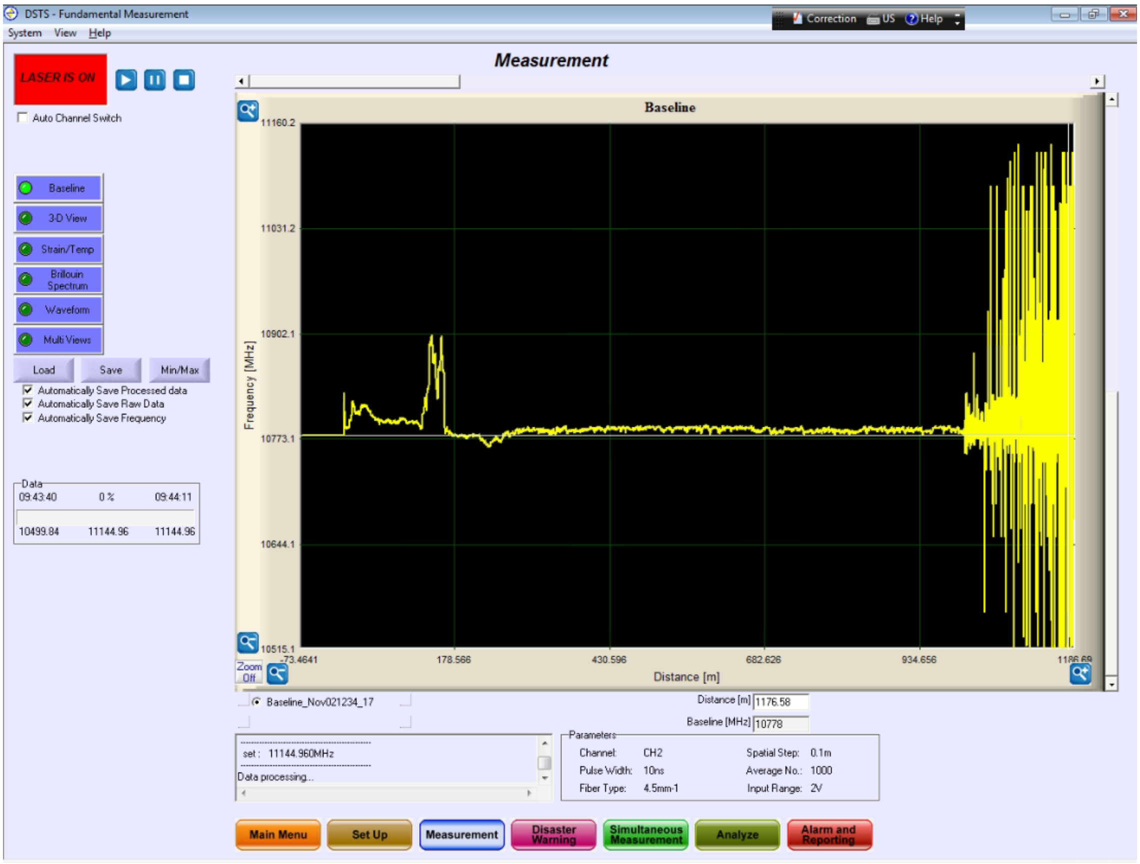

Figure 34. Fiber optic system interface showing baseline measurement of fiber optical cable

Important notes about the system:

- "Baseline" measures the first and raw frequency data from the fiber cable.
- Strain data is processed in "Absolute Strain" and "Relative Strain". Absolute strain gives data that shows only the current state of the cable without asking for Baseline data beforehand. Relative strain data is strain data comparable to baseline data. Within the scope of this study, studies will be carried out with Relative Strain. The cumulative analysis of these data will be discussed in the following chapters.

6.3. Field Installation of Fiber Optic System

The site must be prepared before any field study data acquisition and analysis. This optimization is essential for collected data to be accurate and reliable. Within the scope of this thesis, a 40 cm wide, 30-40 cm deep, and approximately 50 m boring channel was excavated in the crown of the landslide.

Afterwards, respectively:

- 50-80 cm boreholes were drilled in the appropriate sections with the help of a hand auger (Figure 35).

Figure 35. Boring applications with the hand auger method

- Small channels were opened in the inclinometer pipes due to the situation mentioned in Section 4.3, Preliminary Trials. The 1-meter-long inclinometer pipes shown in Figure 36, on which the fiber cables could be easily fixed, the small cable channel and cable wrapping part prepared using a CNC machine, were placed in the drilled holes with the fiber cable (Figure 37).

Figure 36. Fiber optic fixing inclinometer pipe

Figure 37. Appearance of an inclinometer pipe with two different fiber optic cables after placement in the monitoring site

- This process was repeated for the other fifteen drilling holes, and the fiber optic installation process in the study area was completed with a total of sixteen inclinometer pipes. Immediately after the installation, the channel was filled with fine sand to create a soft cushioning layer. This process minimized the contact of the fiber cables to be covered in the following steps with the sift soil ground and ensured that the cables were in contact with a soft material. For data acquisition, both the 3-mm fiber cable (yellow cable) and the 4.5-mm fiber cable (grey cable), considered more suitable for field conditions, were used (Figures 38, 39, and 40).

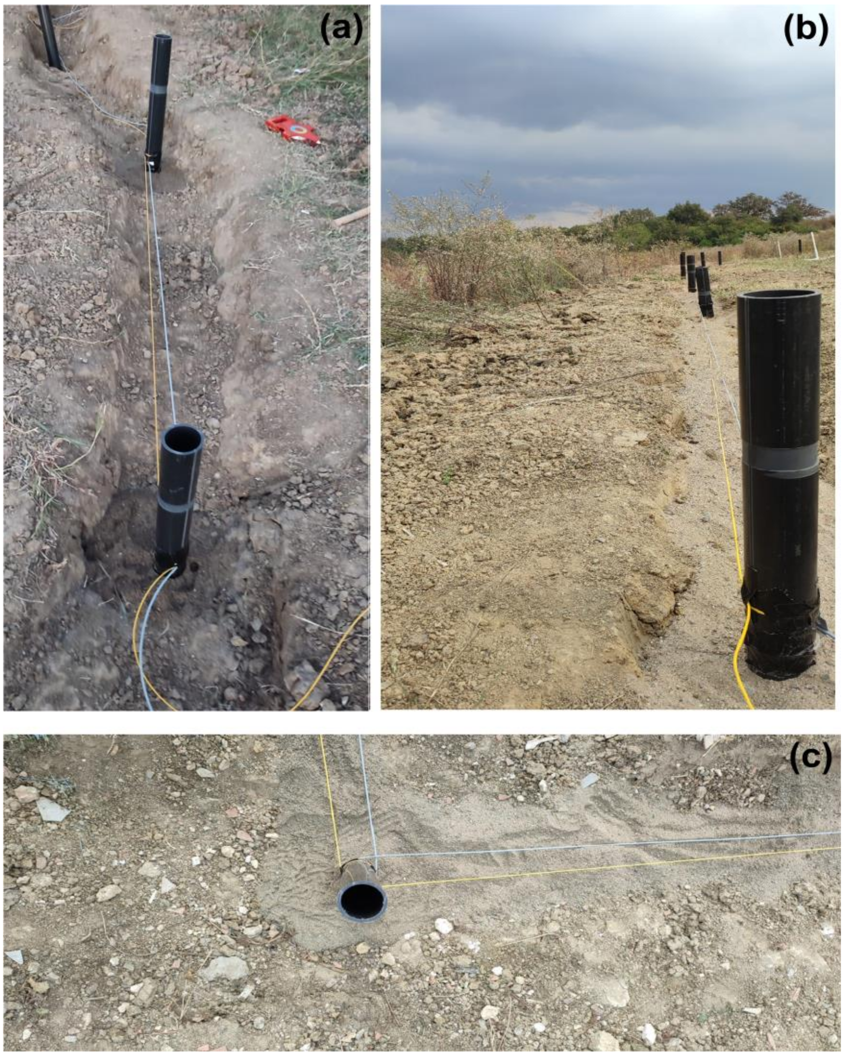

Figure 38. Installation Process a: before cushioning with sand; b) and c) after cushioning with sand

Figure 39. The entire configuration, after cushioning with sand

Figure 40. The entire configuration, after cushioning with a sand layer

- After cushioning, the channel in which the fiber cables had been installed was filled with a stiffer material at the top, available near the monitoring area. Figures 41 and 42 show the completed appearance of the filled channel.

Figure 41. The completion of the entire fiber cable channel area

Figure 42. The completion of the entire fiber cable channel area before monitoring

Since the monitoring area was approximately 150 m from the BOTDA device where the data would be received and processed, the fiber cable sections outside the channel were exposed to external factors. For the fiber cable protection, the portions of the cables outside the channel were placed in 14- and 18-mm plastic inclinometer pipes, as shown in Figure 43. OTDR was used to monitor the condition of the cable instantaneously during fiber cable installation operations (Figure 44).

Figure 43. Fiber protection inclinometer pipes

Figure 44. The energy loss check of fiber optic cable by OTDR

Additionally, in the event of significant data loss resulting from the splitting or buckling the fiber optic cable during installation or monitoring, implementing a fusion process becomes essential for cable maintenance. To facilitate this, a

Fujikura FSM 60S fusion splicer (Figure 45 was utilized for splicing the cables, and a Fujikura CT-30 high-precision cleaver (Figure 46) was employed to execute perpendicular cuts on the cables). These tools were kept ready to ensure prompt and efficient maintenance and repair of the cable system when needed during the monitoring period.

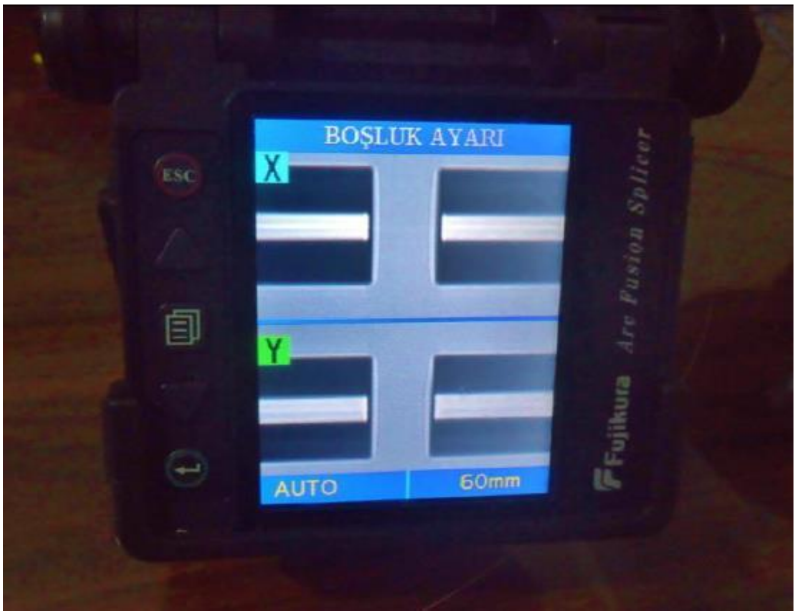

Figure 45. The utilized fusion splicer (Fujikura FSM 60S) to fuse two cables without signal loss

Figure 46. A view of the cleaver used to cut the fiber cables properly

Figures 47 and 48 show the distance values of two different fiber cables (3 mm and 4.5 mm) at the end of the installation completion, and Figure 49 shows the fiber cable distances in the channel and configuration in the monitoring area in detail. Table 8 shows the distance information of 3-mm and 4.5-mm fiber cables on the boreholes separately.

Figure 47. Site installation configuration of 3-mm fiber optical cable (yellow cable)

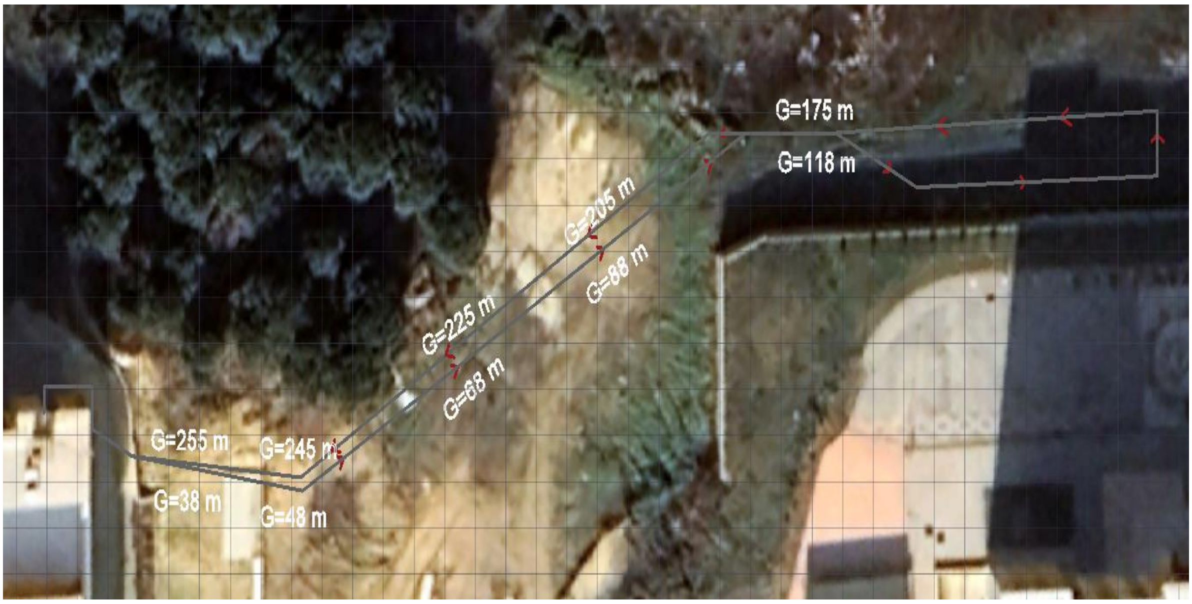

Figure 48. Site installation configuration of 4.5-mm fiber optical cable (gray cable)

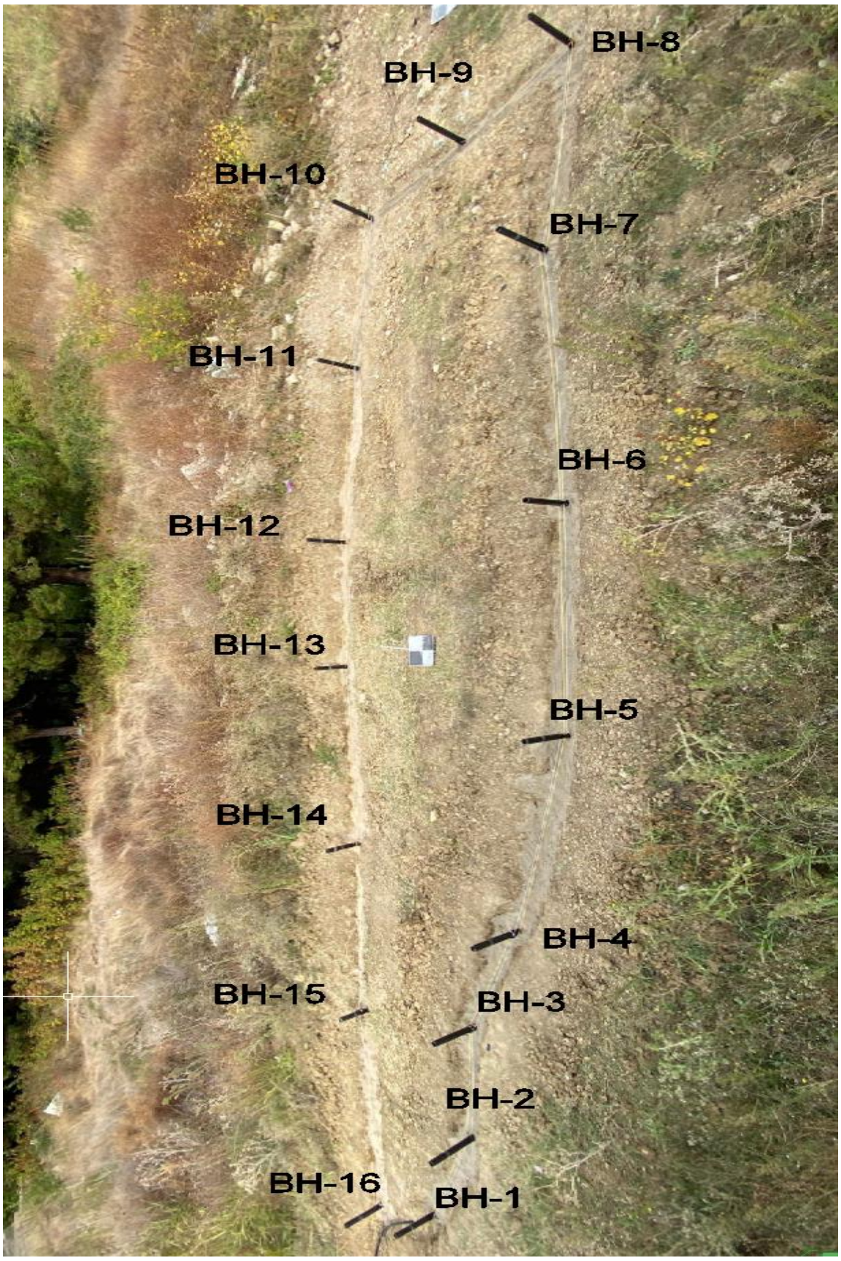

Figure 49. The view of the boreholes after completion in the monitoring area

Table 8. Monitoring configuration points of fiber optical cables based on the BH locations

	BH-1		BH-2		BH-3 (T)		BH-4	
Cable	Entry (m)	Exit (m)	Entry (m)	Exit (m)	Entry (m)	Exit (m)	Entry (m)	Exit (m)
3 mm (Y)	282.00	281.17	278.80	278.56	277.00	277.24	274.85	273.98
4.5 mm(G)	123.00	123.24	125.00	125.77	127.55	127.79	130.00	130.24

	BH-5		BH-6 (T)		BH-7		BH-8 (T)	
Cable	Entry (m)	Exit (m)	Entry (m)	Exit (m)	Entry (m)	Exit (m)	Entry (m)	Exit (m)
3 mm (Y)	271.00	270.76	268.00	267.76	267.00	266.20	261.85	261.61
4.5 mm(G)	133.00	133.78	137.00	137.26	140.55	140.79	144.00	144.24

	BH-9 (T)		BH-10 (T)		BH-11		BH-12	
Cable	Entry (m)	Exit (m)	Entry (m)	Exit (m)	Entry (m)	Exit (m)	Entry (m)	Exit (m)
3 mm (Y)	259.00	258.76	257.95	257.71	253.00	252.76	249.00	248.19
4.5 mm(G)	145.50	145.74	148.00	148.24	150.87	161.65	155.00	155.24

	BH-13 (T)		BH-14		BH-15		BH-16 (T)	
Cable	Entry (m)	Exit (m)	Entry (m)	Exit (m)	Entry (m)	Exit (m)	Entry (m)	Exit (m)
3 mm (Y)	245.80	245.56	242.10	239.86	239.00	238.07	234.00	234.24
4.5 mm(G)	158.00	158.24	161.60	162.47	165.80	166.04	169.90	170.14

(T) refers only to the boreholes used to ensure the tension of the cables. In other words, boreholes were not installed to install the cables deeper but to provide tension and allow them to run over the channel's bottom layer at this study stage.

6.4. Data Acquisition Process

After all these processes and controls, both ends of the fiber optic cables were installed in different channels (3-mm cable in channel 1, 4.5-mm cable in channel 2) of the DSTS device, which is the primary data receiver of the system (Figure 50).

Figure 50. DSTS with two different fiber optical cables entrance and exit jacks

To obtain and process the strain data, it is first necessary to take the baselines for the two cables separately. Figures 51 and 52 show the first baseline of the 3-mm and the 4.5-mm cable, respectively. In Figure 51, it is clear that the 3-mm cable has a high noise level, which is not detectable with OTDR. One of the significant advantages of BOTDA is that it is more sensitive than energy loss based on devices, i.e., OTDR. Various adjustments were made on-site and along the cable to optimize the noise level, and the noise level was reduced to reasonable levels, making it suitable for measurement (Figure 53). Although this noise level affects the measurement accuracy of the 3-mm fiber optic cable, the fiber cable installation is similar to the one used in the laboratory, making it possible to compare. After all these arrangements, strain data acquisition started on both cables at 10-minute intervals for each cable.

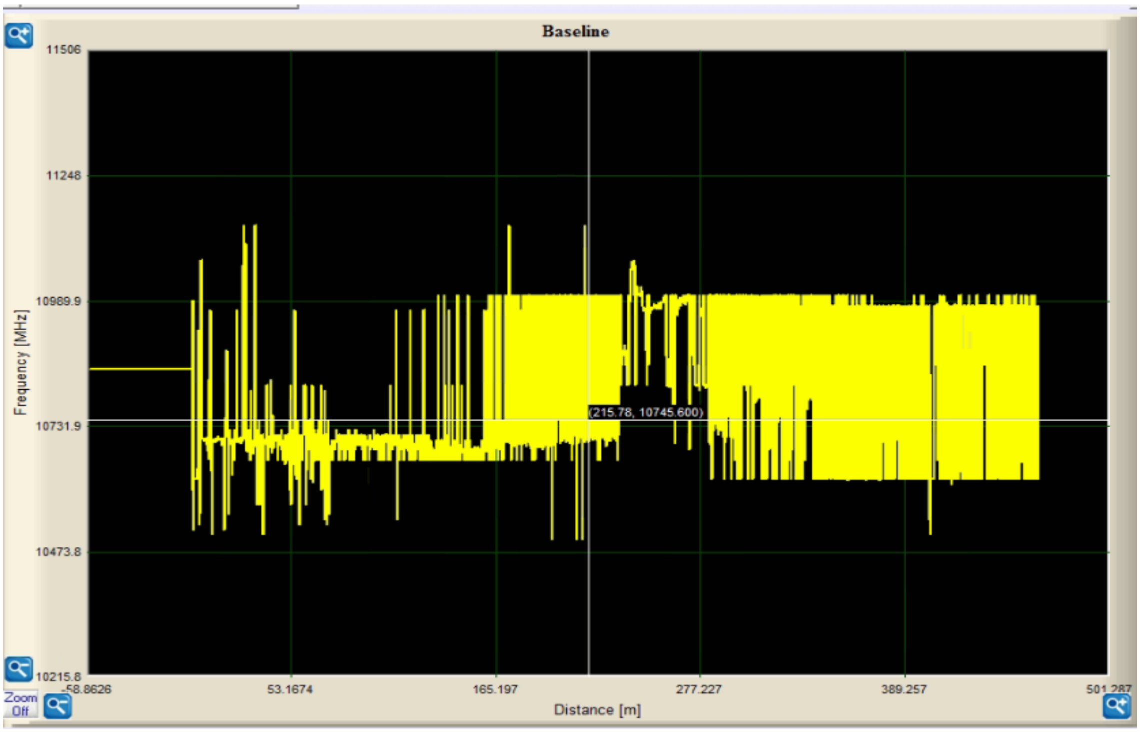

Figure 51. First baseline of 3-mm fiber cable

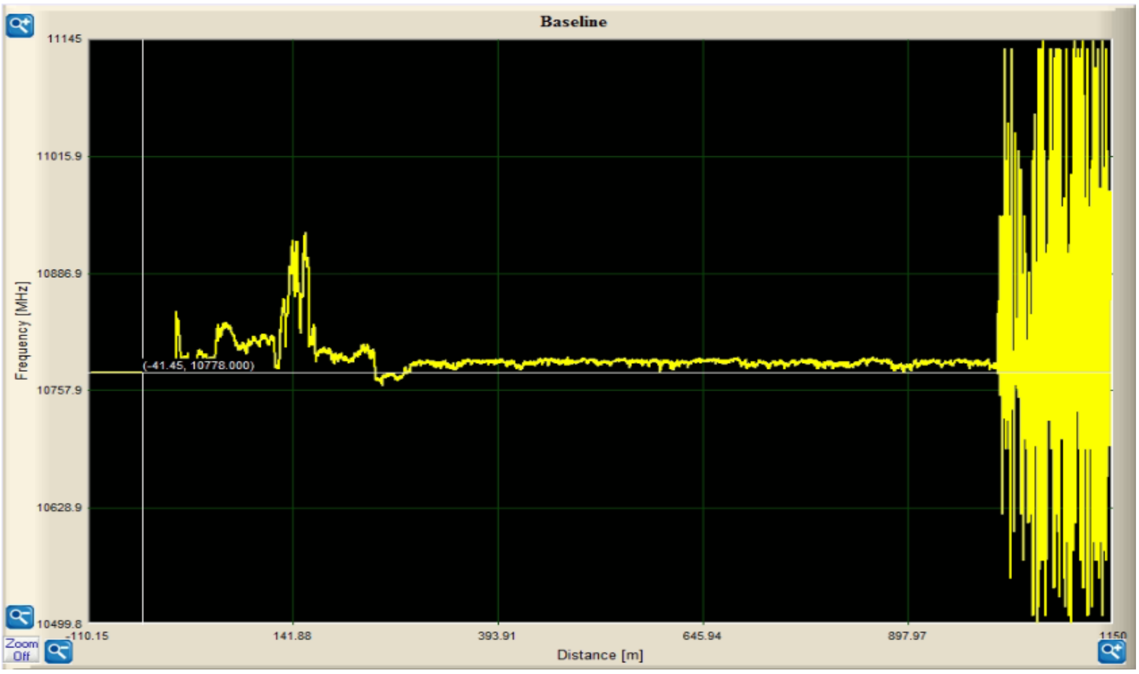

Figure 52. Baseline of 4.5-mm fiber cable

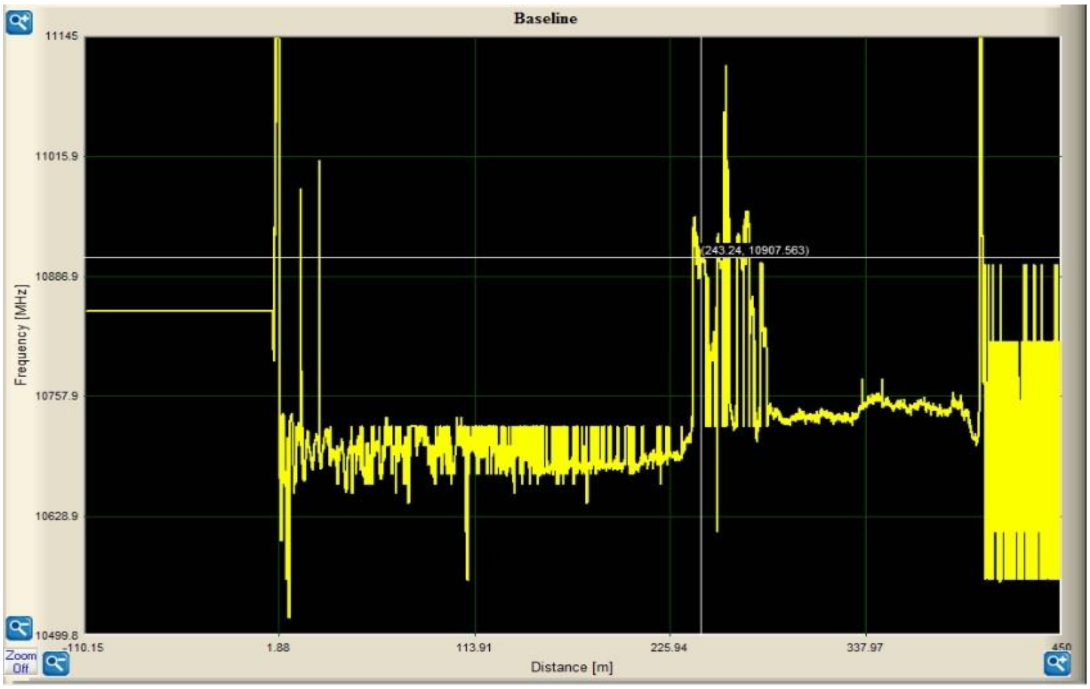

Figure 53. Baseline in 3-mm fiber optic cable after modifications along the entire cable

The relatively high-frequency values between 120-170 meters of 4.5 mm cable and 230-280 meters of 3 mm cable are because these parts of the fiber cables are within the monitoring area. Inside the monitoring area, the fiber cables are stretched to measure the slightest difference in strain. In addition to the DSTS used to measure the strain data, a strong ground motion accelerometer was also installed in the data control room to record the seismic activity in the region, as shown in Figures 54 and 55.

Figure 54. A strong ground motion accelerometer was installed in the study area.

Figure 55. The strong ground motion station antenna is installed outside the data control room.

7. RESULTS AND DISCUSSION

7.1. Introduction

The main objective of this thesis is to perform long-term and continuous landslide monitoring with light-based fiber-optic methods. Fiber optic systems have been preferred over other methods because of their advantages: compact size, extensive bandwidth, immunity to electromagnetic interference, resilience in various environmental conditions, fast data transfer, affordability, and the ability to perform real-time monitoring.

After the baseline processes, the operation of the system was tested with various manipulations (such as moving the inclinometer pipes manually) from October 18 to November 1 (Pre-Monitoring Testing Phase). After the test phase, the system was monitored for 50 days without any external intervention between November 2, 2023, and December 21, 2023, which is the scope of this thesis.

A total of twelve files were recorded on the system, with six separate files coming from each fiber optical cable (3 mm and 4.5 mm) per hour. Each file contains strain data measured on every 0.1 m along the cable. In this case, 15000 strain data from two different fiber cables at a time and 300000 separate strain data per hour were recorded on the system. Such a large amount of data brought two problems up. One was the storage, and the other was the analysis of this data. The storage problem was easily solved by uploading data from the field computer to cloud systems weekly. Several different Python codes were used to extract the desired data from the files and export them to Excel format to facilitate the analysis of this data. Then, the appropriate strain graphs were plotted by using Python and Excel.

A comparison was conducted throughout the system monitoring process between the strain and precipitation data acquired from the General Directorate of Meteorology (MGM). In addition to precipitation (rainfall), earthquakes are a primary landslide-triggering mechanism. During the monitoring period, four earthquakes with a magnitude larger than Mw 3.5 occurred in the Marmara Region, two of which were close to the monitoring area, having magnitudes Mw 5.1 and 4.1:

- 26/10/2023 17:18:24, Marmara Sea - [depth: 13.22 km] Tekirdağ MW 3.6
- 07-11-2023 23:05:48, Marmara Sea - [depth: 03.10 km] Balıkesir MW 4.1
- 04/12/2023 10:42:20, Marmara Sea - [depth: 04.73 km] Bursa MW 5.1
- 17/12/2023 23:53:52, Marmara Sea - [depth: 08.52 km] Yalova MW 4.1

7.2. Pre-Monitoring Testing Phase

Conducting a system pre-monitoring phase is essential to ensure the system operates smoothly before a long-term monitoring effort. That is because any problem in the system can lead to incorrect data measurement and inaccurate results. Since this thesis aims to develop landslide monitoring using a fiber optic system in the field, false data could lead to significant problems, such as loss of property and life. For these reasons, the monitoring area was visited on various days between October 18 and November 2 to determine the status of the data received from the fiber cables.

In this process:

- The implementation area was visited at 4-day intervals. It was examined whether there was any adverse situation in the fiber cables and application channel.
- By pushing and pulling two different boreholes, it was determined whether there was a reaction in the strain data.
- Strain data were monitored instantaneously from OTDR and DSTS by remote connection.

Figures 56 and 57 display the measurements performed on the fiber cables after the tensile operation applied to BH 6 (137-137.26 m for 4.5 mm cable; 267.76-268 m for 3 mm cable) in the monitoring area during the pre-monitoring phase. As seen from these figures, the system works sensitively against any movement. The deformation of the BH 6 in this cable can be clearly observed in the DSTS device. The 3 mm cable has significant strain changes in a noisy data set.

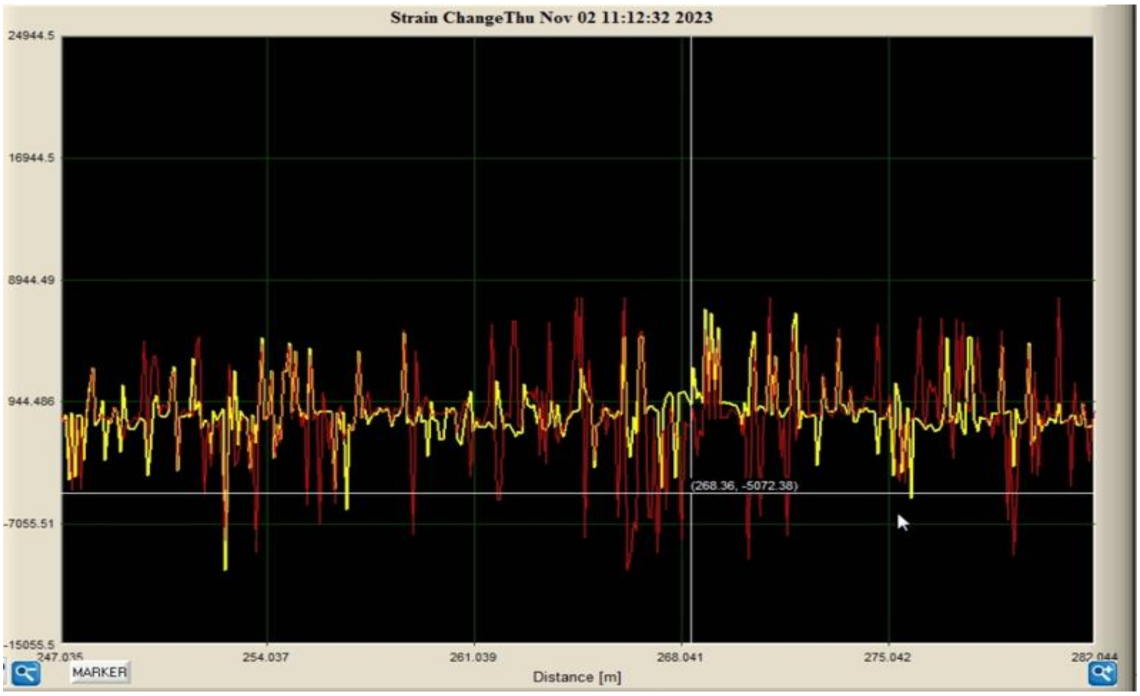

Figure 56. Strain variation with 3-mm fiber cable during the tensile operation to BH 6

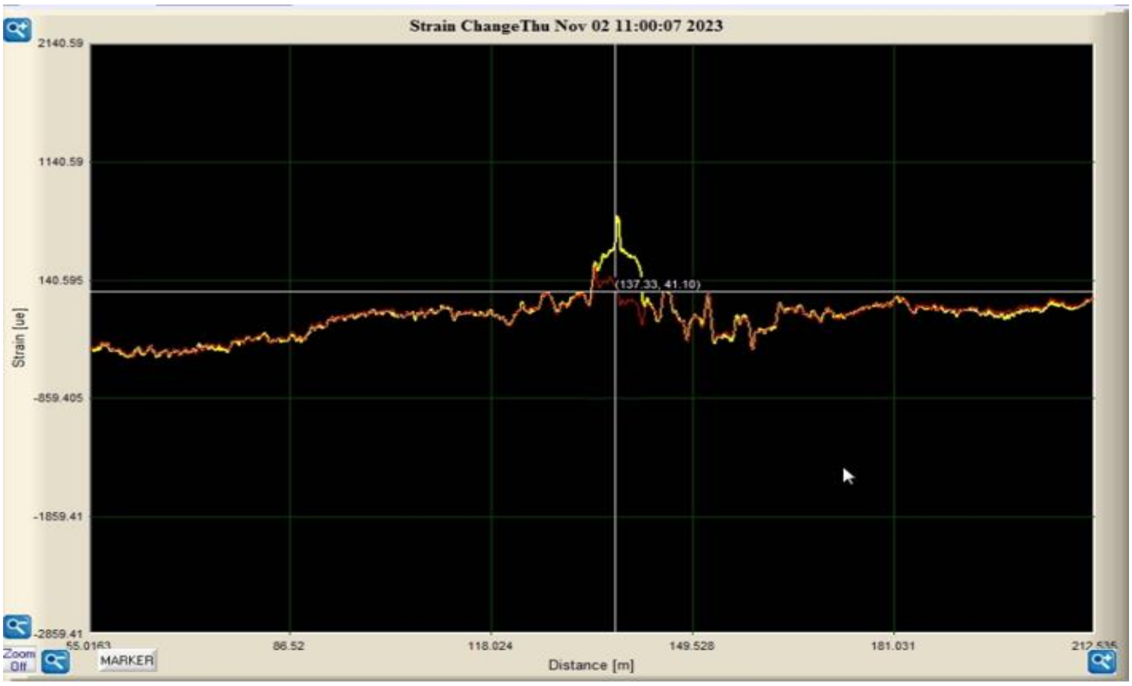

Figure 57. Strain variation with 4.5-mm fiber cable during the tensile operation to BH 6

7.3. Identifying Significant Sensitive Stress Points in the Monitoring Area

To analyze the data reliably, it is necessary to identify the places where the results of the strain data in the monitoring system are the highest. The reasons for this are the following:

- In particular, a noisy graph was obtained from the 3-mm fiber optic cable for various reasons (such as production problems and disruptions during the laying process), making comparing precipitation difficult. It was appropriate to identify sensitive points (SP) and determine the existence of a relationship with precipitation data.
- The data were obtained along the cable. In other words, με-Distance data were received. When comparing hourly precipitation data with strain data on the cable, it was necessary to use data from a certain point at different hours. Analyzing SPs offers a streamlined and easily manageable approach to hourly data processing.

Strain data in November were analyzed to identify the most active sections. Figures 58 and 59 show the με-distance data for 3-mm and 4.5-mm cables during November. According to the data obtained from the fiber cables, a representation of the sensitive parts in the field is also given in Figure 60. SPs of the application site are tabulated Table 9.

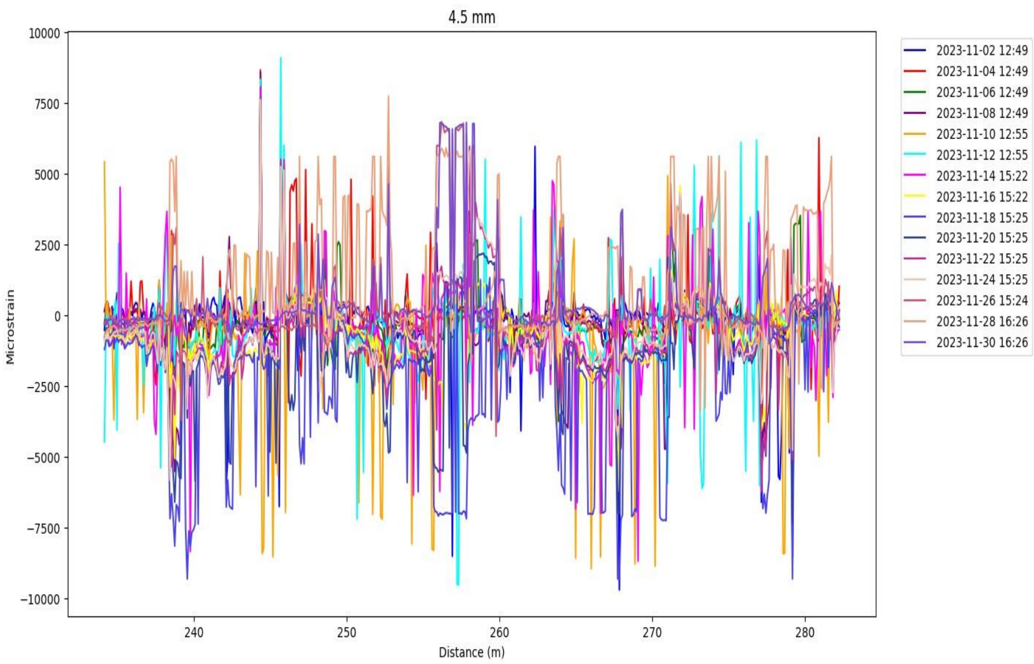

Figure 58. με vs. distance variations on the 3-mm fiber optic cable

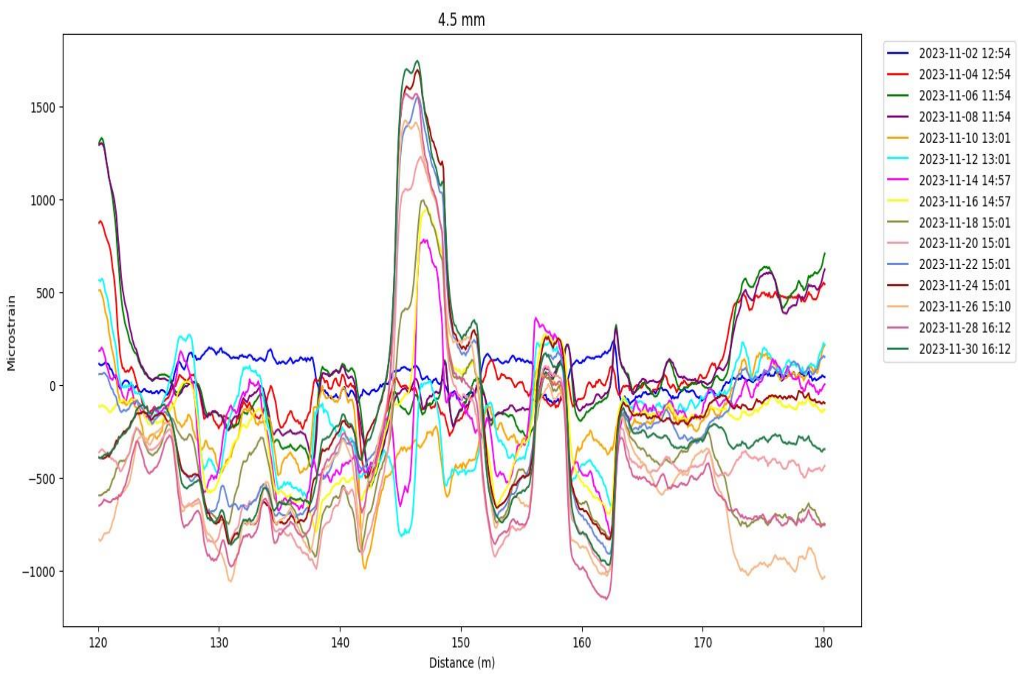

Figure 59. με vs. distance variation on the 4.5-mm fiber optic cable

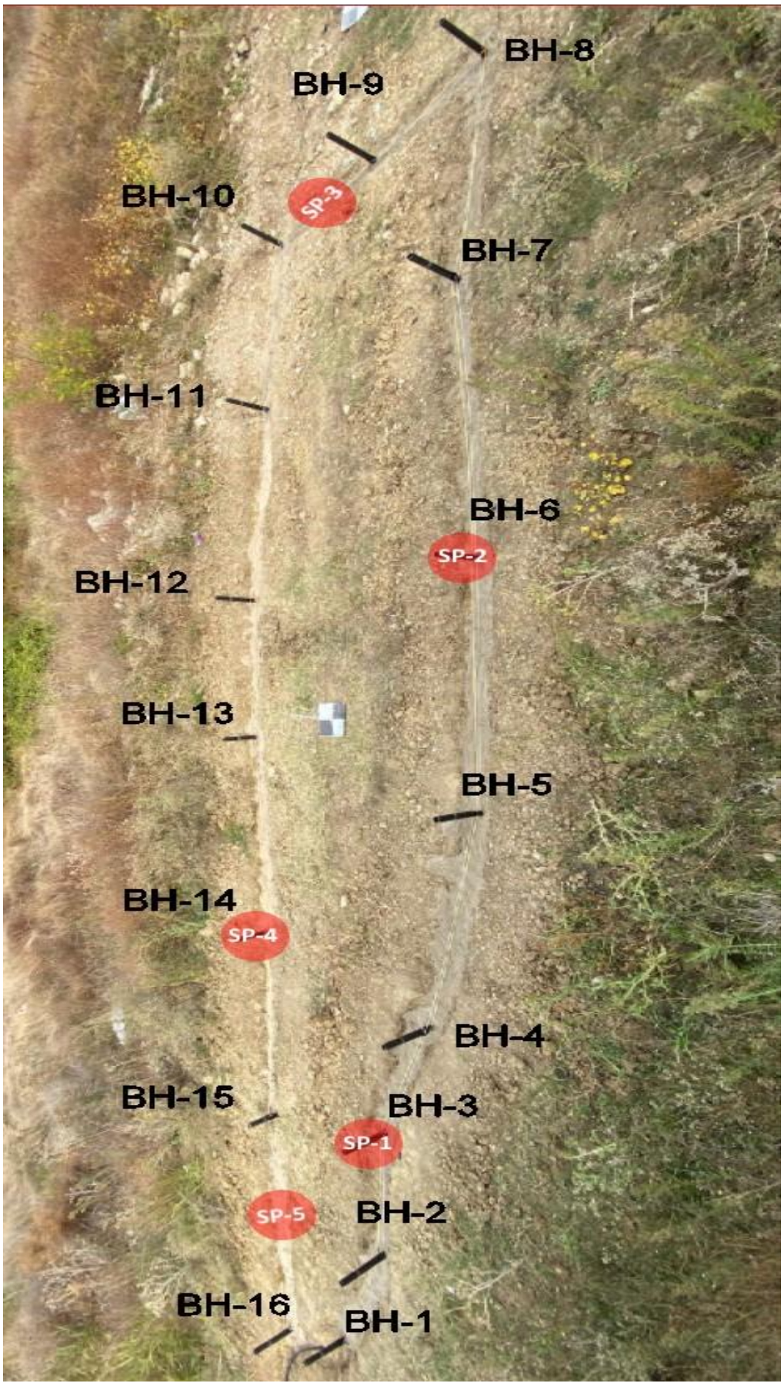

Figure 60. Schematic representation of sensitive points in the field

Table 9. Sensitive Points

Fiber Cable	# of Sensitive Point (SP)				
	1 (m)	2 (m)	3 (m)	4 (m)	5 (m)
3-mm	276.93	268.05	256.00	239.97	235.42
4.5-mm	127.53	136.92	146.11	162.03	166.52
BH #	BH 3	BH 6	BH 9-10	BH 14	BH 15-16

7.4. Investigation of Precipitation-Induced Stress Changes

Landslides are often triggered by rainfall due to the interaction of water with the soil and geological features. When heavy or prolonged rainfall occurs, the soil absorbs the water, gradually increasing its weight. This increased weight can push the soil or rock material beyond its capacity for slope stability. For these reasons, to better understand the effects of precipitation and to examine how it causes changes in με values, hourly precipitation data were obtained from MGM between November 2 and December 21. To determine the με-precipitation relationship, analyzing the hourly data of the identified SPs is critical. Figures 61 and 62 show that Yalova province received rainfall for 29 days in November and December, and heavy rain occurred on November 18 and 29. On November 18 and 29, 3-mm and 4.5-mm fiber optic cable data, especially hourly variation, were analyzed in this section to represent an example. Afterward, all data for November and December were analyzed together. In addition, while performing hourly analysis, it was deemed appropriate to make a cumulative evaluation in addition to relative data since the effect of precipitation continues throughout the day. These results enabled a comparison in line with the results obtained in the laboratory studies. See APPENDIX B for the precipitation table in November and December obtained from MGM.

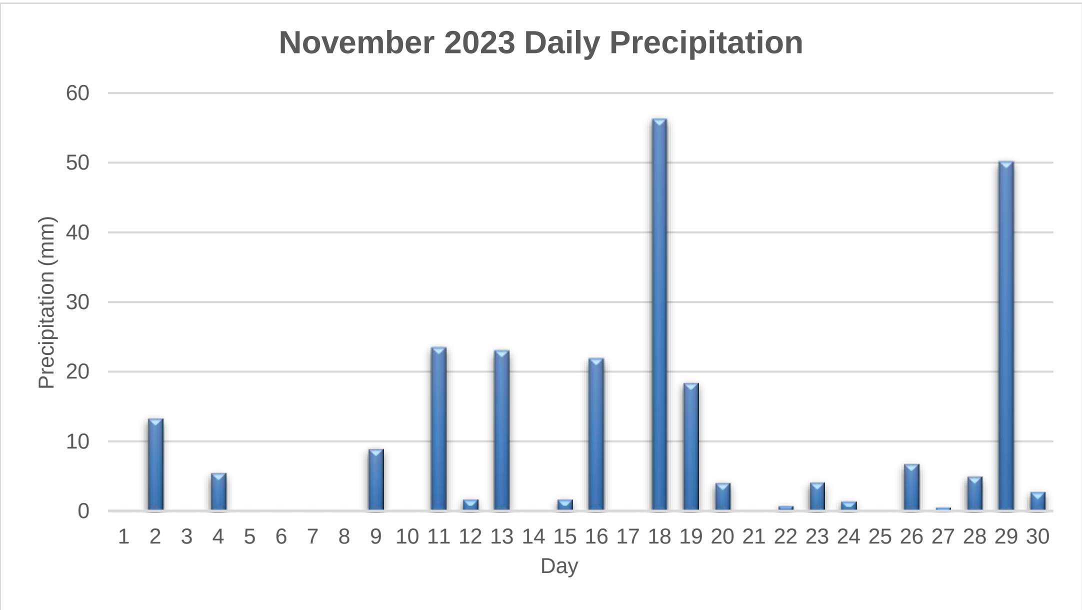

Figure 61. Daily precipitation data in Yalova Province during November 2023

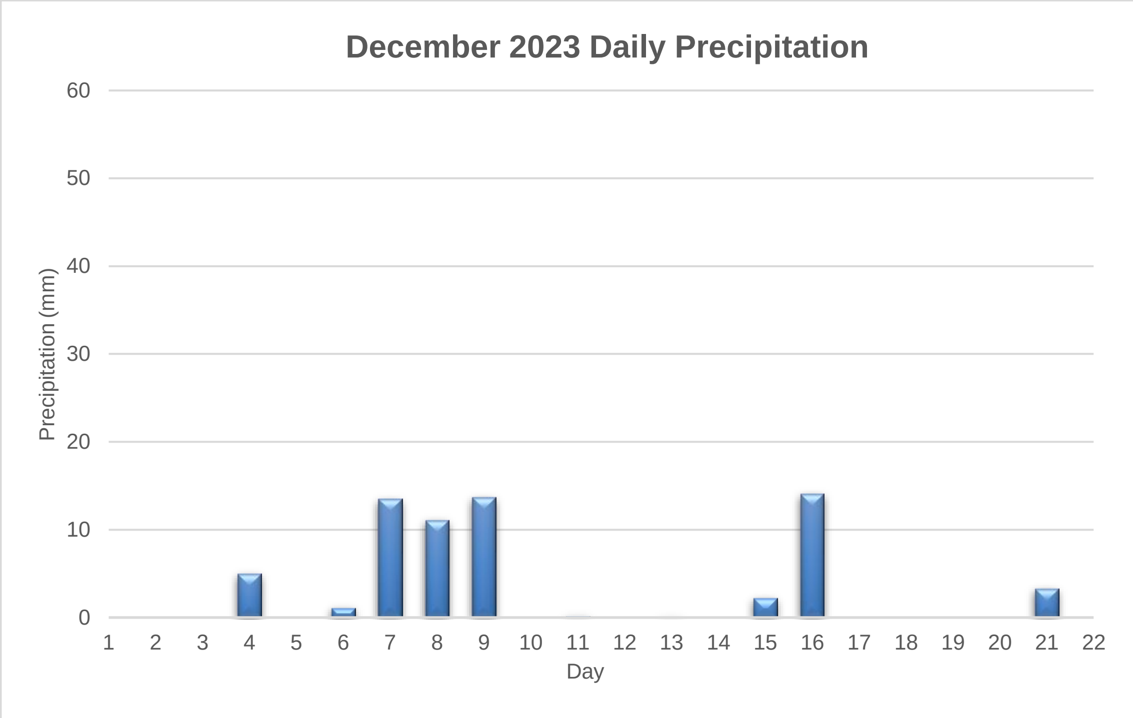

Figure 62. Daily precipitation data in Yalova Province during December 2023

7.4.1. Outcomes from the 3-mm Fiber Optic Cable Analysis

Figures 61 and 62 display that Yalova province received rainfall for 19 days in November, and heavy rain occurred on November 18 and 29. The relationship between fiber cables and precipitation was analyzed in this section for November 18 and 29.

7.4.1.1. Assessment of SP 1 in the 3-mm Diameter Fiber Optic Cable

Figures 63 and 64 show the hourly 3-mm fiber cable με vs. precipitation relationship for SP 1 (BH 3) on November 18 and 29. According to these data, it was observed that there were variations in the strain values of 3-mm fiber cable with the onset of precipitation on November 18. The strain values, which reached -5000 με levels, fluctuated during the day for several reasons, such as temperature and sunshine duration. On November 29, the rainfall caused multiple variations in the fiber cable data as on other days after the rainfall. The strain data, which peaked at 7000 με, shows daily variations.

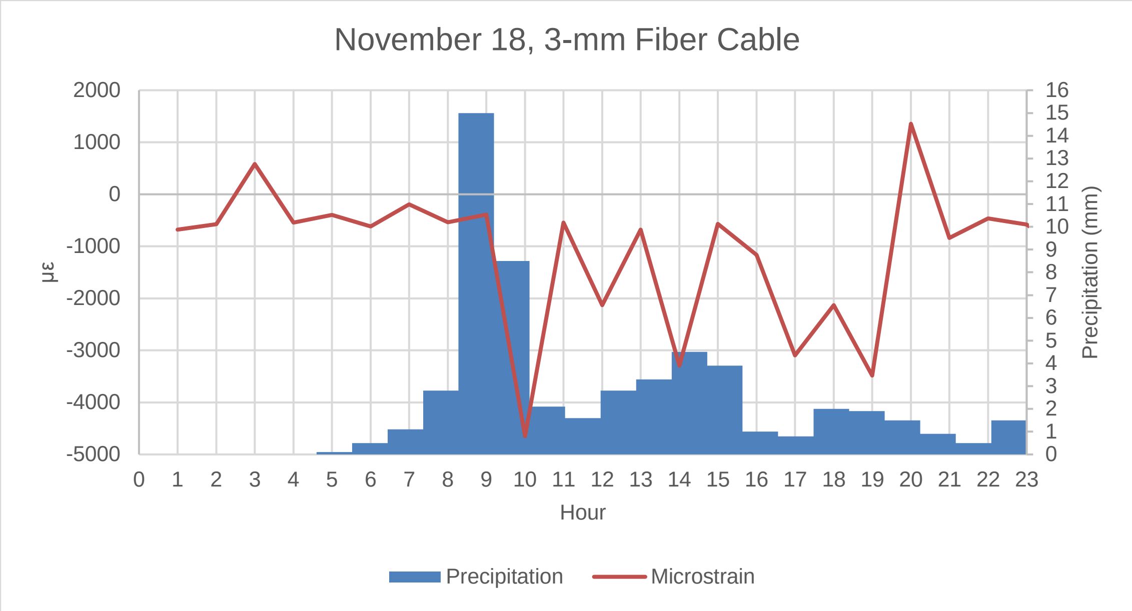

Figure 63. Hourly relation of με vs. precipitation results with 3-mm cable for SP 1 on November 18 (BH 3)

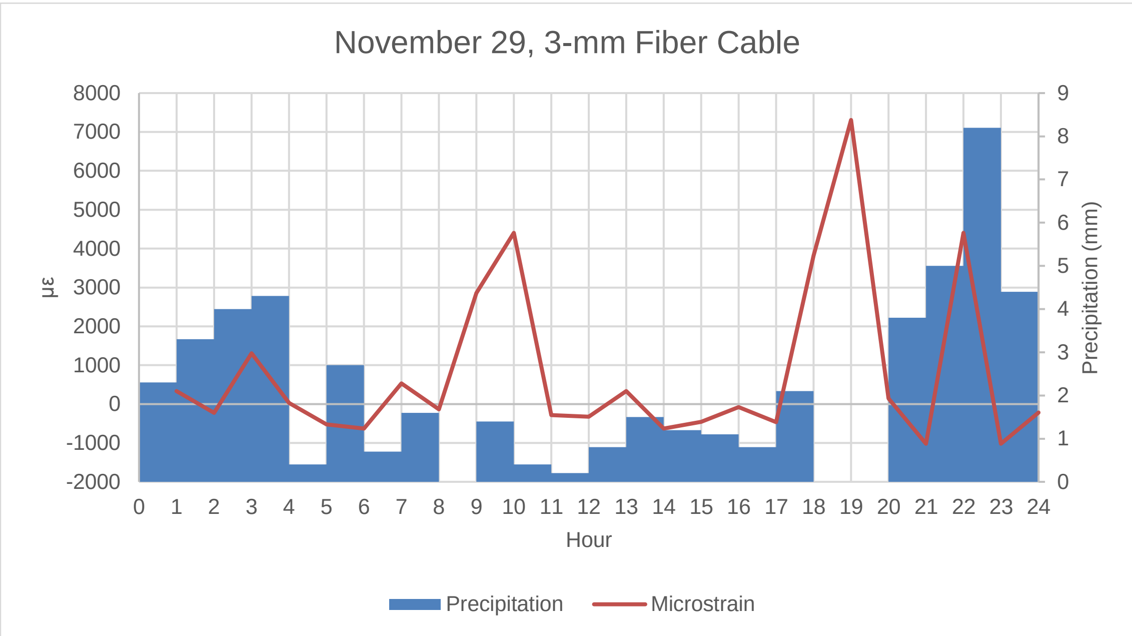

Figure 64. Hourly relation of με vs. precipitation results with 3-mm cable for SP 1 on November 29 (BH 3)

Interpreting daily data through the utilization of cumulative information stands as a justifiable approach, given the inherent nature of precipitation data as a short-term process in which hourly observations progressively contribute to the daily cumulative total. The cumulative method, which will simplify the analysis in short-term monitoring as in laboratory studies, is suitable for hourly data analysis.

For SP 1, Figures 65 and 66 for the 3-mm cable represent the cumulative με vs. precipitation relationship. As indicated in Figure 25, SP 1 is positioned close to the retaining wall, which may be the beginning of the monitoring area. In line with the results obtained, cumulative fiber optic measurements reached a με value of 39714.63 with 56.3 mm rainfall on November 18. After 50.2 mm of rainfall on November 29, fiber optic measurement results reached up to 31481.38 με.

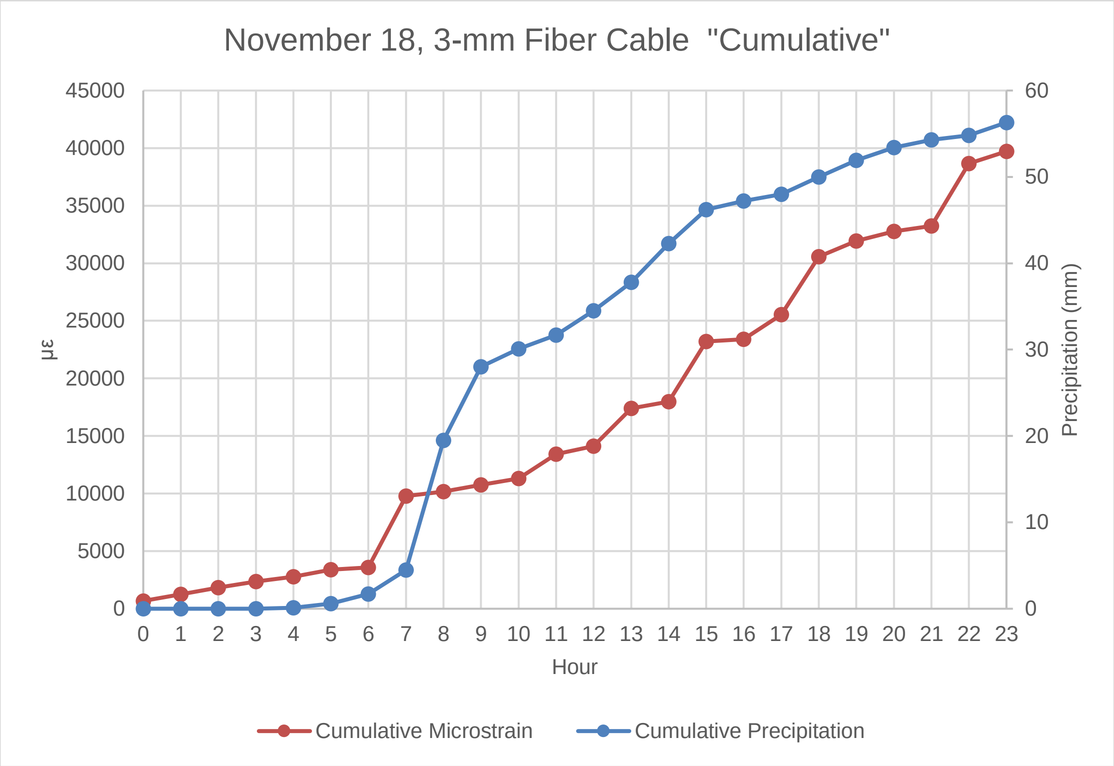

Figure 65. Hourly relation of cumulative με vs. precipitation results with 3-mm cable for SP 1 on November 18 (BH 3)

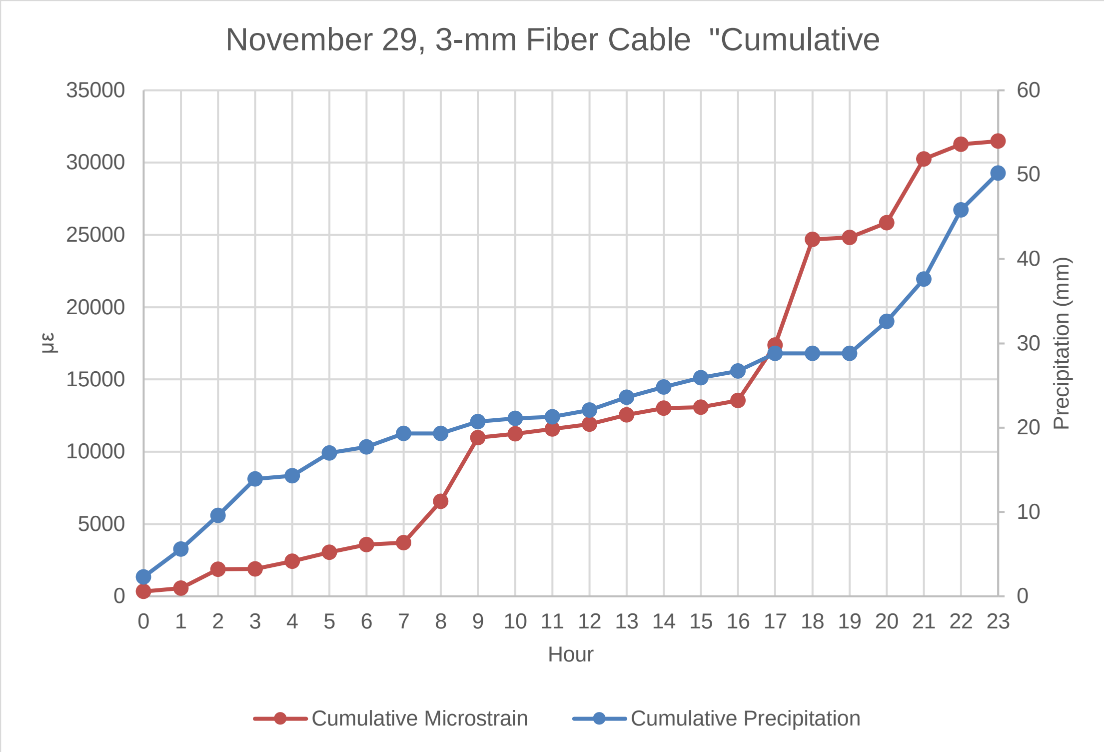

Figure 66. Hourly relation cumulative με vs. precipitation results with of 3-mm cable for SP 1 on November 29 (BH 3)

When the fiber optic and precipitation data for SP1 on both November 18 and 29 are analyzed, it becomes evident that strain variations in the fiber optic cable are induced by precipitation, and this will also be the case for other SPs.

While examining the hourly data that offers insights into the behavior of the site throughout the day, it is crucial to view landslide monitoring comprehensively. It is equally critical to consider daily variations alongside the hourly data. Figure 67 illustrates the correlation between weekly precipitation and με data between November 2- December 21. This figure clearly demonstrates the effect of precipitation on the με data collected from the fiber cables. This data shows that SP 1, which was 2500 με at the beginning of the month, decreases with increasing precipitation and drops to around -1000 με.

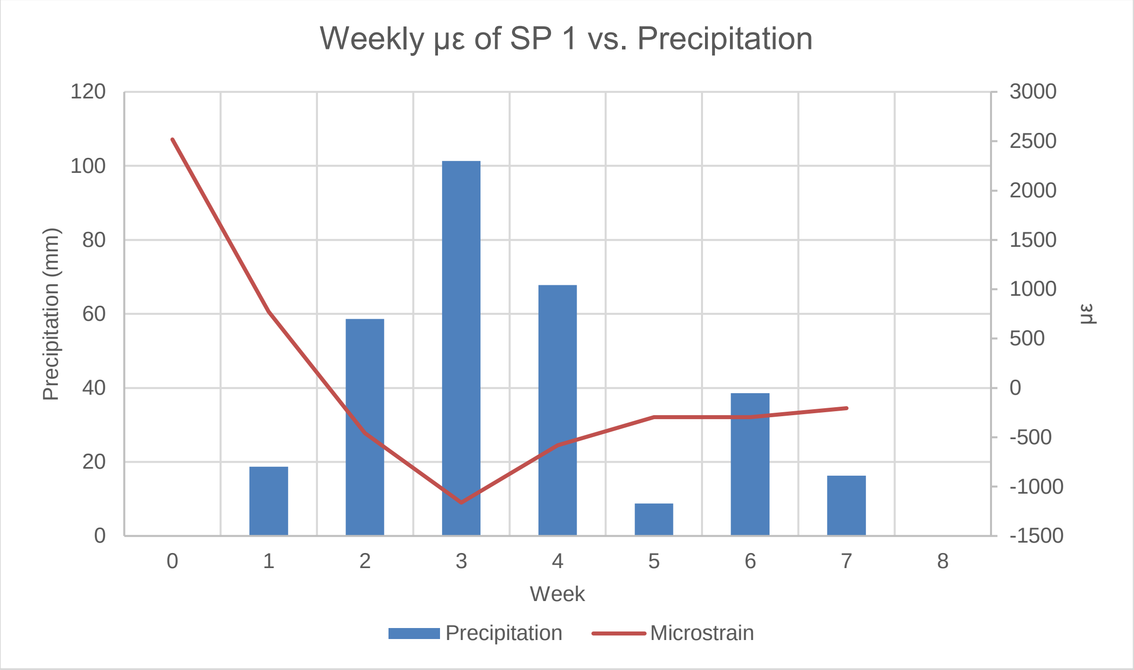

Figure 67. Weekly relation of με vs. precipitation results with 3-mm cable for SP 1 during the monitoring (BH 3)

7.4.1.2. Assessment of SP 2 in the 3-mm Diameter Fiber Optic Cable

Figures 68 and 69 display the hourly 3-mm fiber cable με vs. precipitation relationship for SP 2 (BH 6) on November 18 and 29. According to these data, it was observed that there were variations in the strain values of 3-mm fiber cable with the onset of precipitation on November 18. Strain values, which reached up to -8000 με levels, fluctuated during the day. On November 29, the rainfall caused variations in the fiber cable data as on other days after the rainfall. The strain data fluctuated between -3000 and 4500 με with a maximum value of approximately 4500 με.

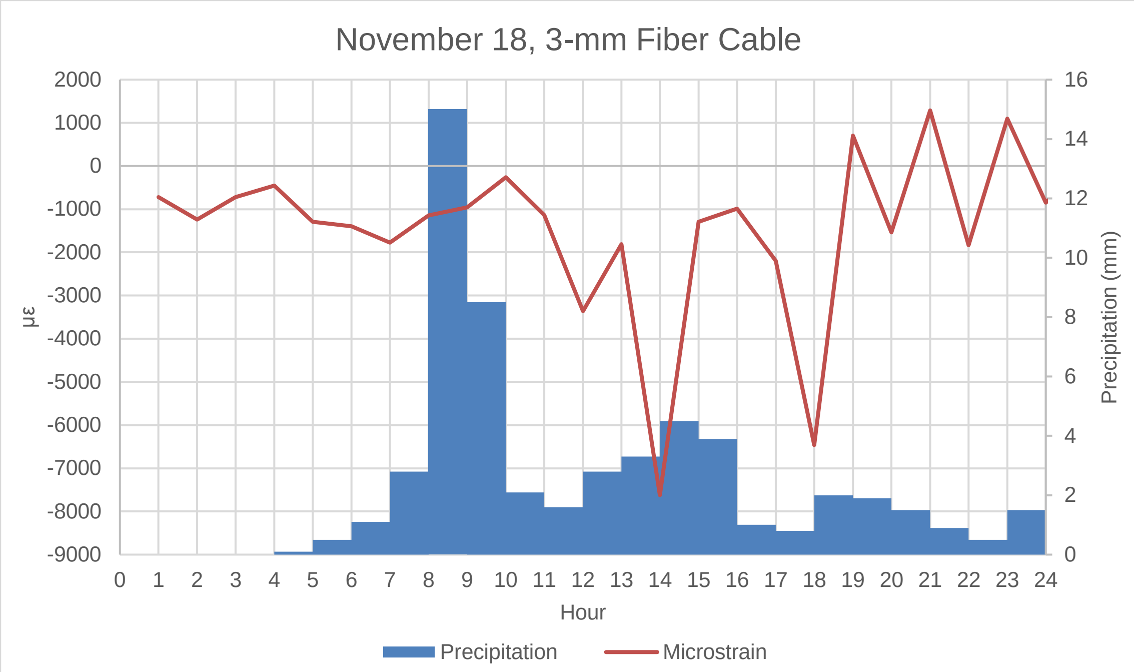

Figure 68. Hourly relation of με vs. precipitation results with 3-mm cable for SP 2 on November 18 (BH 6)

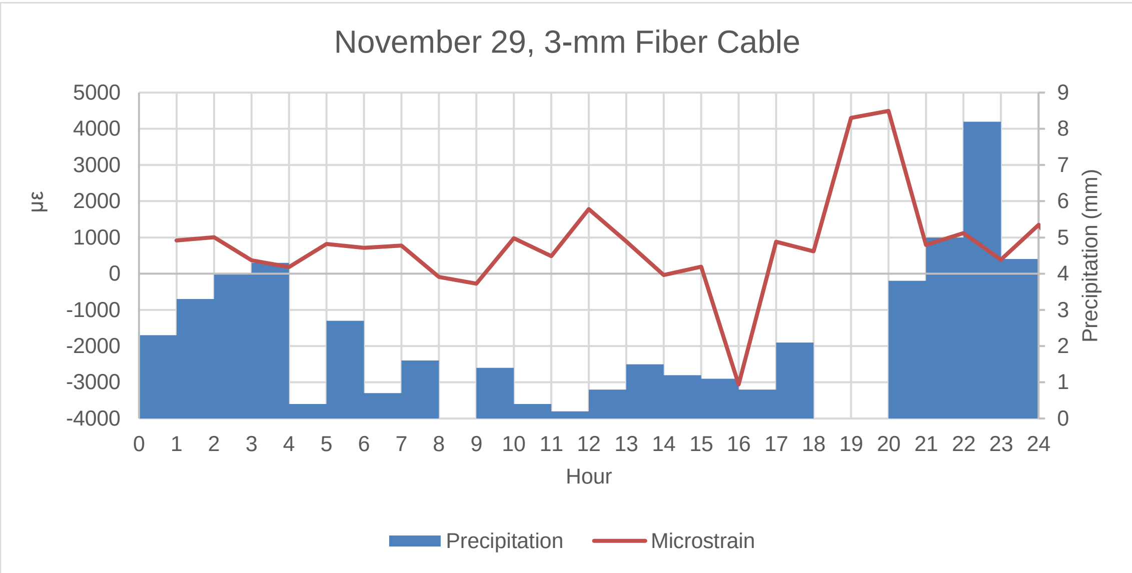

Figure 69. Hourly relation of με vs. precipitation results with 3-mm cable for SP 2 on November 29 (BH 6)

Figures 70 and 71 represent the cumulative με vs. precipitation relationship for SP 2 of the 3-mm cable. SP 2 is positioned close to the retaining wall, which may be in the middle of the upper side of the monitoring area. In line with the results obtained, cumulative fiber optic measurements reached a με value of

42134.03 with 56.3 mm rainfall on November 18. After 50.2 mm of rainfall on November 29, fiber optic measurements reached up to 26508.97 με value.

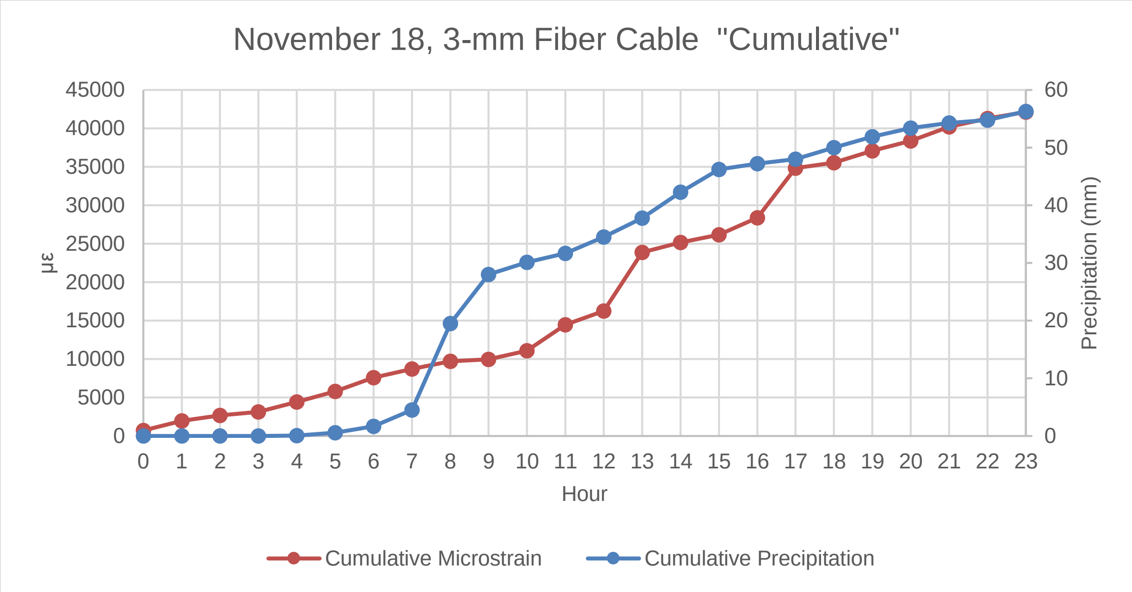

Figure 70. Hourly relation of cumulative με vs. precipitation results with 3-mm cable for SP 2 on November 18 (BH 6)

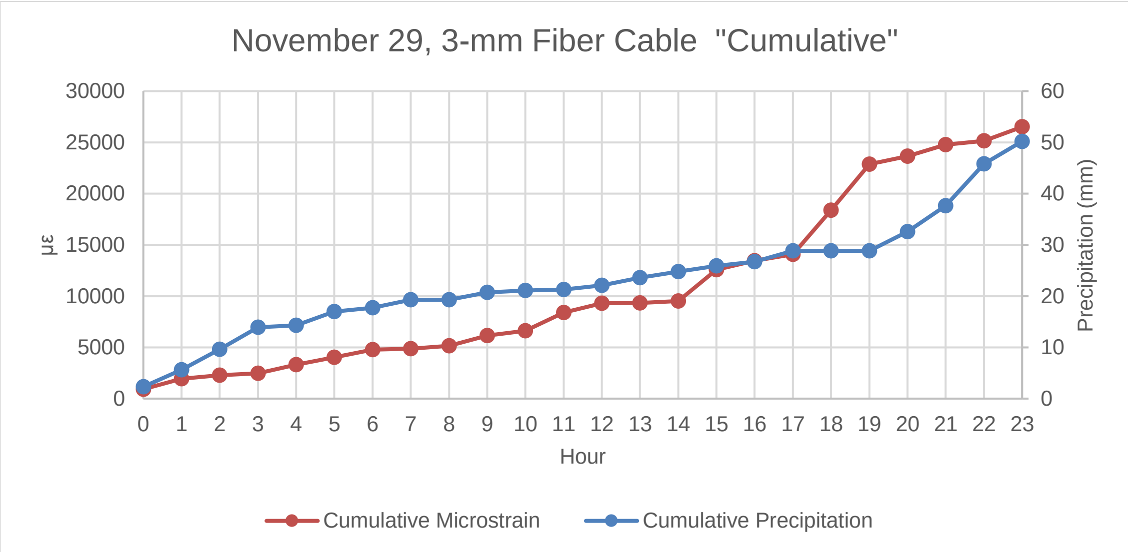

Figure 71. Hourly relation of cumulative με vs. precipitation results with 3-mm cable for SP 2 on November 18 (BH 6)

Figure 72 illustrates the correlation between weekly precipitation and με of SP 2 data between November 2- December 21. This figure demonstrates the effect of precipitation on the με data collected from the fiber cables. This data shows that SP 2, which was -1000 με at the beginning of the month, increased with precipitation and reached around 4500 με.

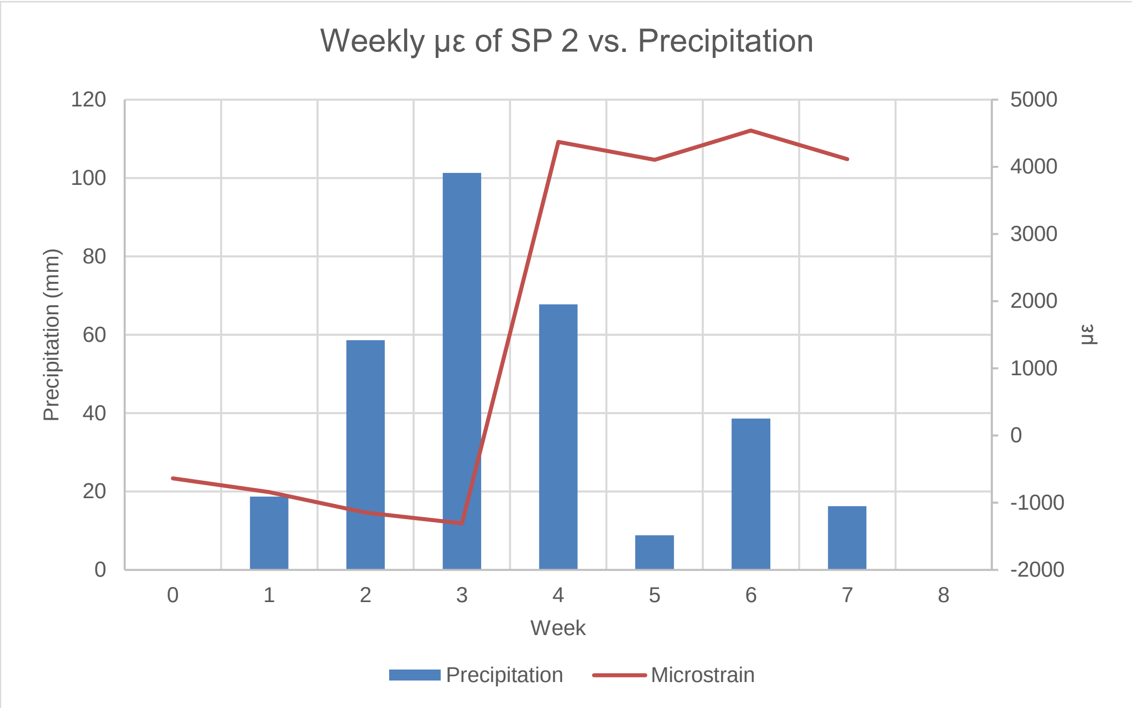

Figure 72. Weekly relation of με vs. precipitation results with 3-mm cable for SP 2 during the monitoring (BH 6)

7.4.1.3. Assessment of SP 3 in the 3-mm Diameter Fiber Optic Cable

Figures 73 and 74 display 3-mm fiber cable με vs. precipitation relationship hourly for SP 3 (BH 9-10) on November 18 and 29. According to these data, it was noticed that there were variations in the strain values of the 3 mm fiber cable due to precipitation on November 18. The strain values were at low με levels in the first hours of the day and reached up to -9000 με. On November 29, the values that were around -4000 με in the first hours of the day reached up to -8000 με after the rainfall.

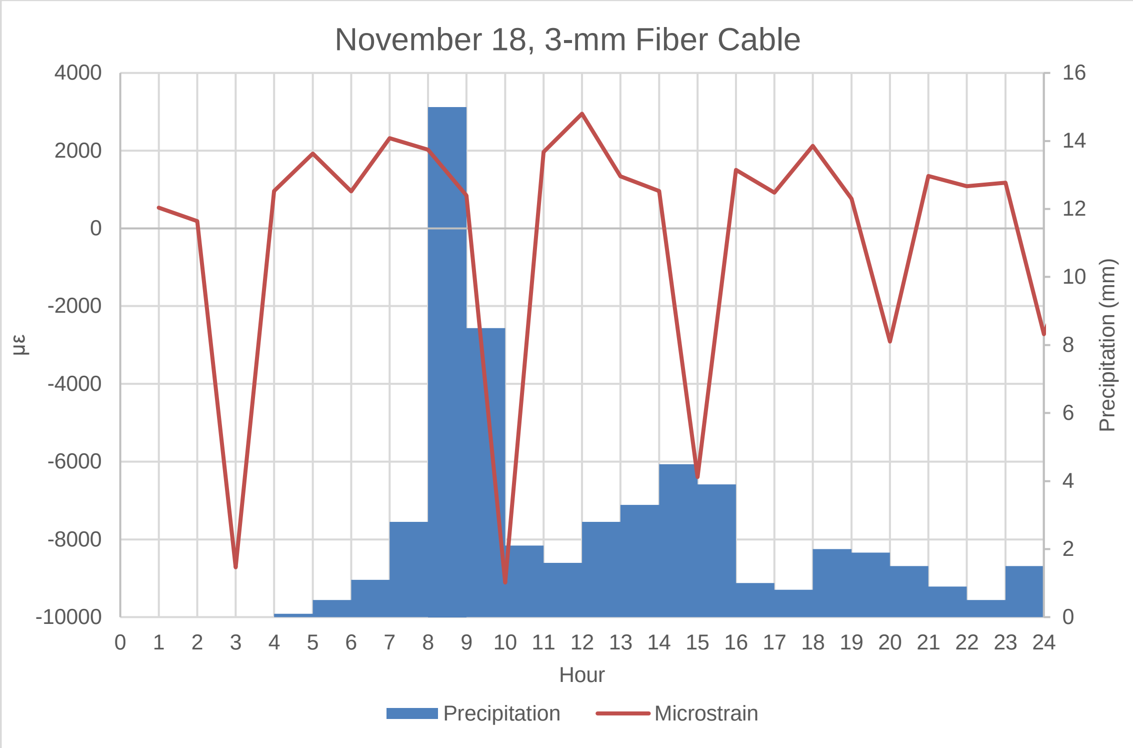

Figure 73. Hourly relation of με vs. precipitation results with 3-mm cable for SP 3 on November 18 (BH 9-10)

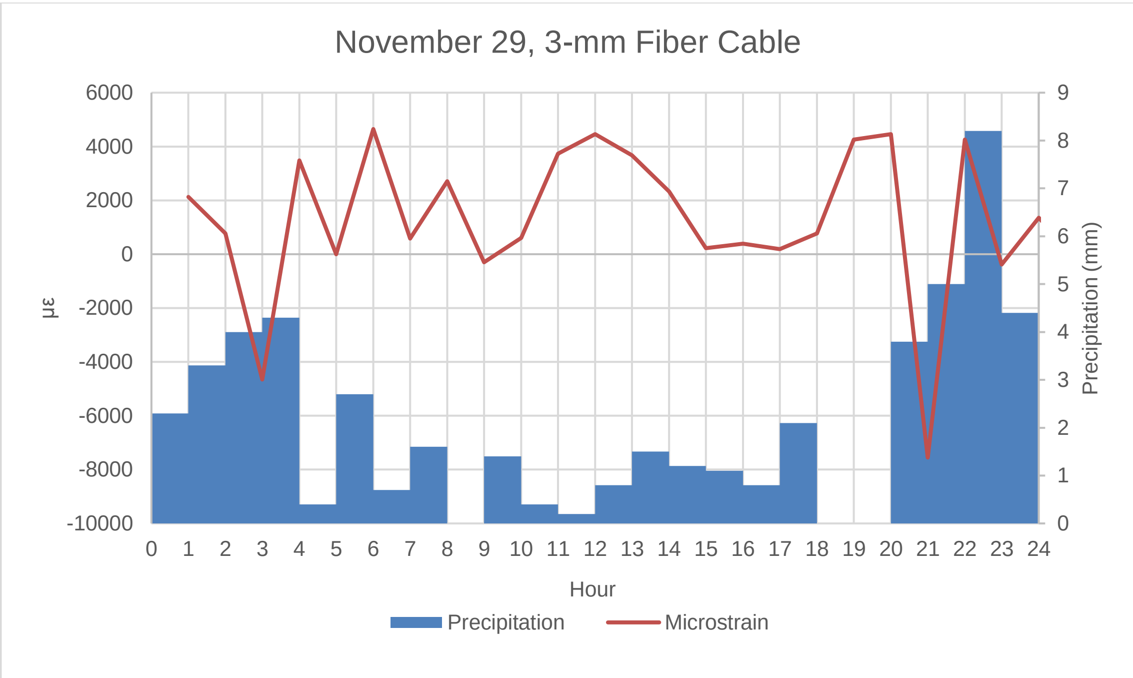

Figure 74. Hourly relation of με vs. precipitation results with 3-mm cable for SP 3 on November 29 (BH 9-10)

Figures 75 and 76 represent the cumulative με vs. precipitation relationship for SP 3 of the 3-mm cable. SP 3 is positioned in the corner of the monitoring area, which is the point in the monitoring area with the most strain difference in November. In line with the results obtained, cumulative fiber optic measurements reached a με value of 55570.28 with 56.3 mm rainfall on November 18. After 50.2 mm of rainfall on November 29, fiber optic measurements came to a 57919.36 με value.

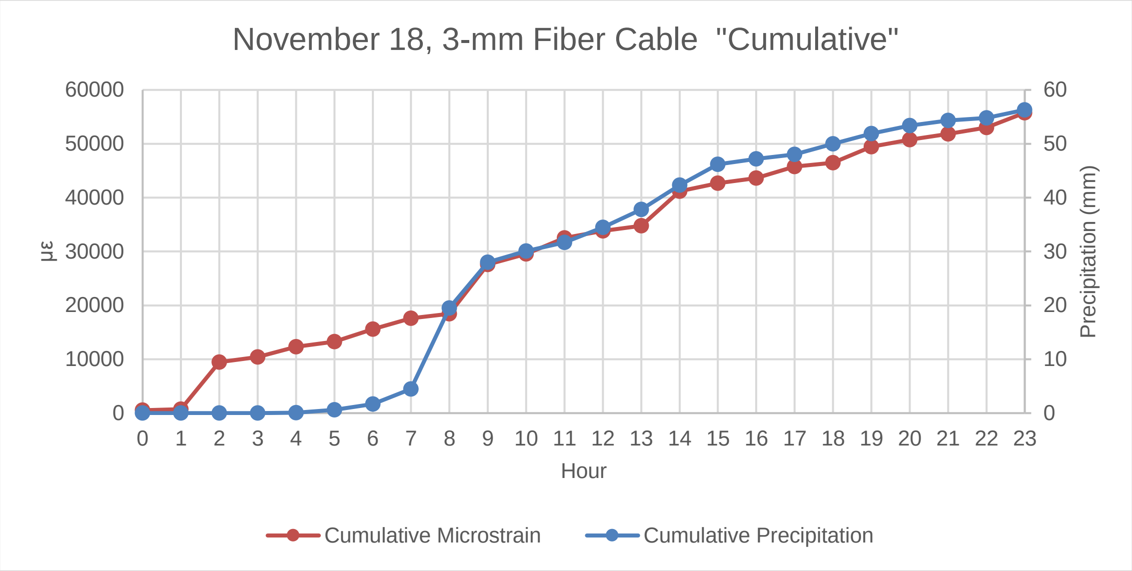

Figure 75. Hourly relation of cumulative με vs. precipitation results with 3-mm cable for SP 3 on November 18 (BH 9-10)

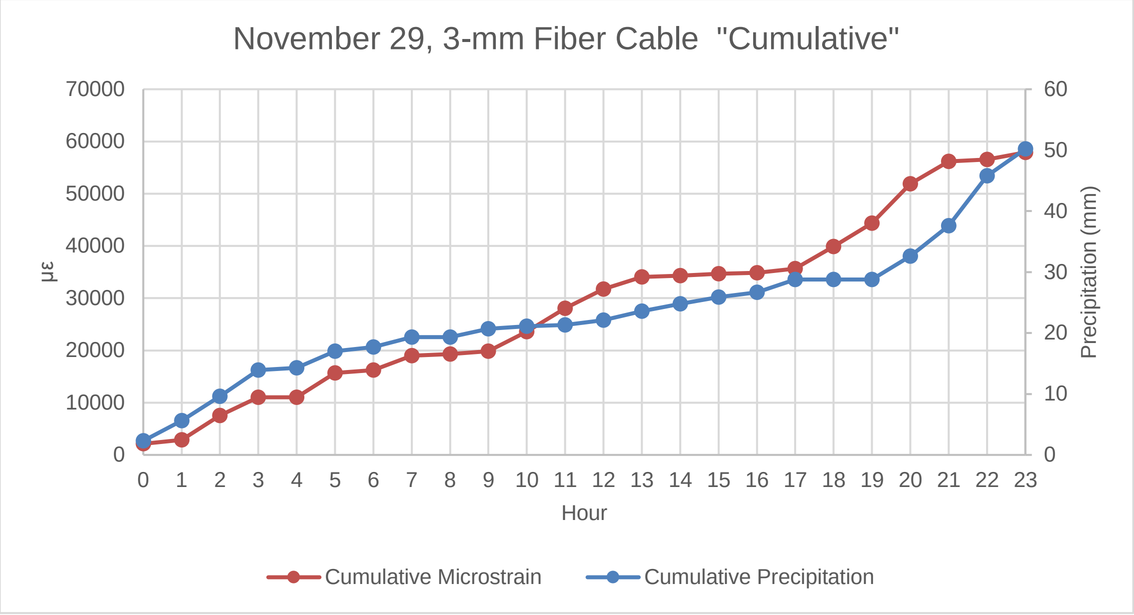

Figure 76. Hourly relation of cumulative με vs. precipitation results with 3-mm cable for SP 3 on November 29 (BH 9-10)

Figure 77 shows the correlation between weekly precipitation and με of SP 3 data between November 2- December 21. This figure demonstrates the effect of precipitation on the με data collected from the fiber cables. These data show that SP 3, which was -2000 με at the beginning of the month, increased with precipitation and reached around 7000 με.

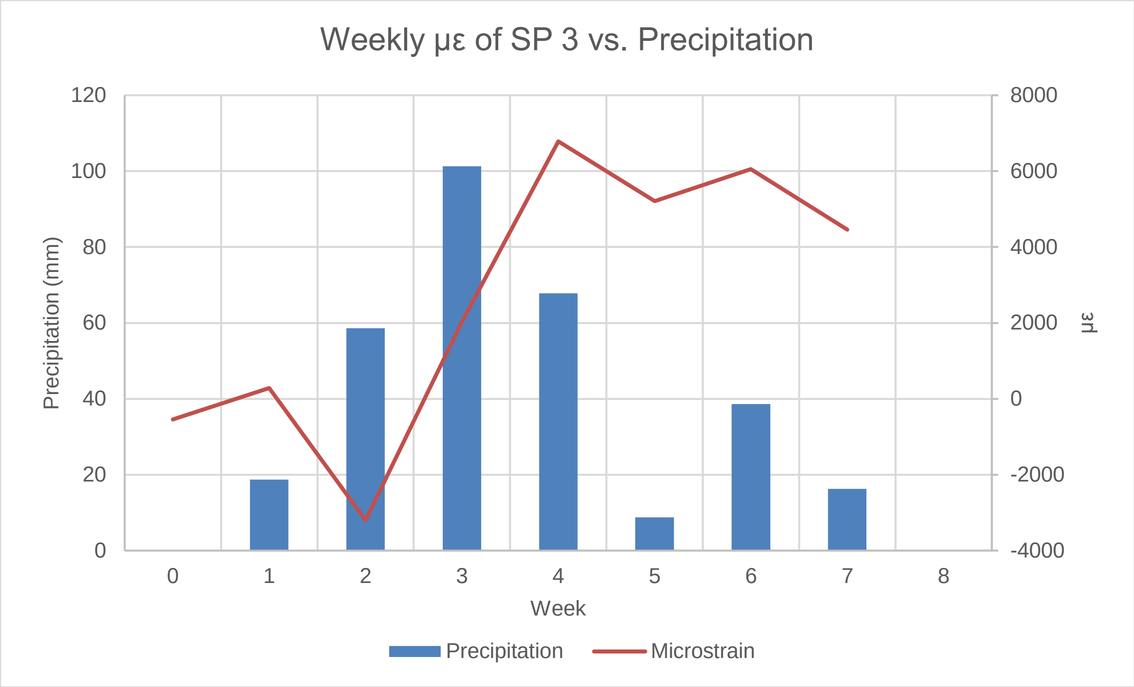

Figure 77. Weekly relation of με vs. precipitation results with 3-mm cable for SP 3 during the monitoring (BH 9-10)

7.4.1.4. Assessment of SP 4 in the 3-mm Diameter Fiber Optic Cable

Figures 78 and 79 show the hourly 3-mm fiber cable με vs. precipitation relationship for SP 4 (BH 14) on November 18 and 29. According to these data, it was stated that there were variations in the strain values of 3-mm fiber cable with the onset of precipitation on November 18. Strain values reached up to -3500 με levels. On November 29, the rainfall caused multiple variations in the fiber cable data as on other days after the intense precipitation. The strain data, which peaked at 4500 με, shows daily variations.

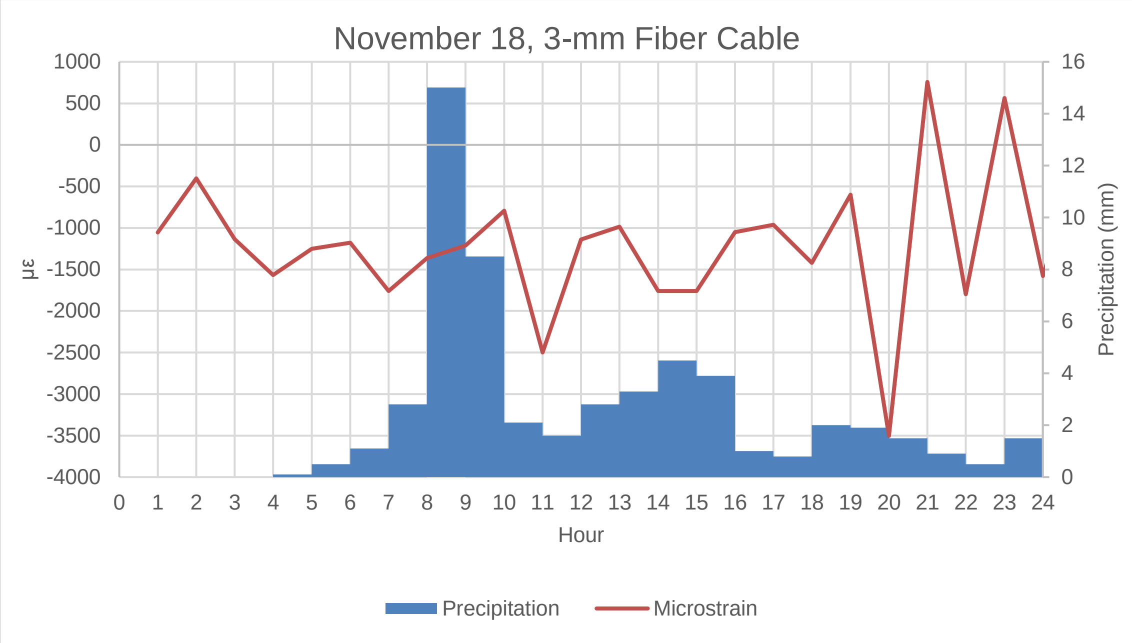

Figure 78. Hourly relation of με vs. precipitation results with 3-mm cable for SP 4 on November 18 (BH 14)

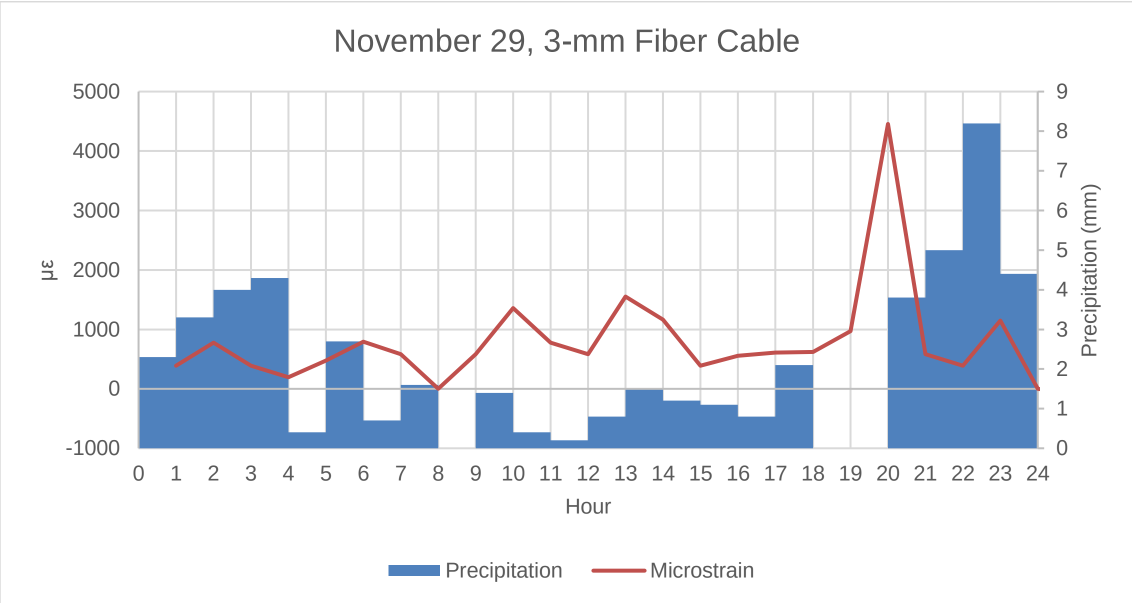

Figure 79. Hourly relation of με vs. precipitation results with 3-mm cable for SP 4 on November 29 (BH 14)

Figures 80 and 81 represent the cumulative με vs. precipitation relationship for SP 3 of the 3-mm cable. SP 4 is positioned in the middle site of the bottom side of the monitoring area. In line with the results obtained, cumulative fiber optic measurements reached a με value of 32089.85 with 56.3 mm rainfall on

November 18. After 50.2 mm of rainfall on November 29, fiber optic measurements reached a 19308.28 με value.

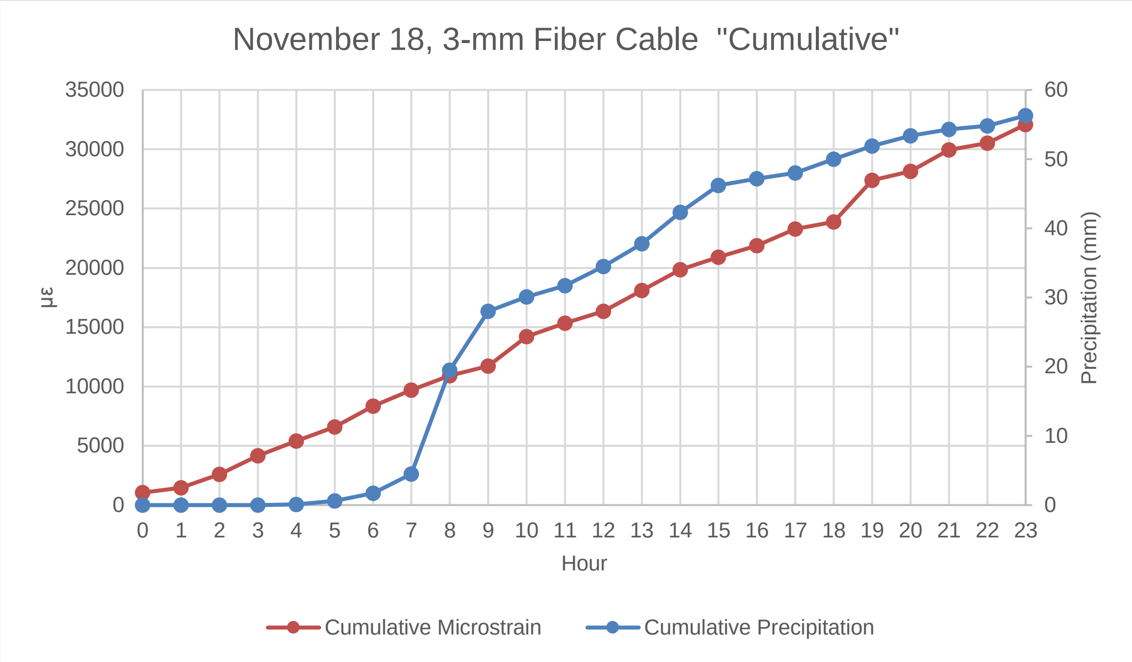

Figure 80. Hourly relation of cumulative με vs. precipitation results with 3-mm cable for SP 4 on November 18 (BH 14)

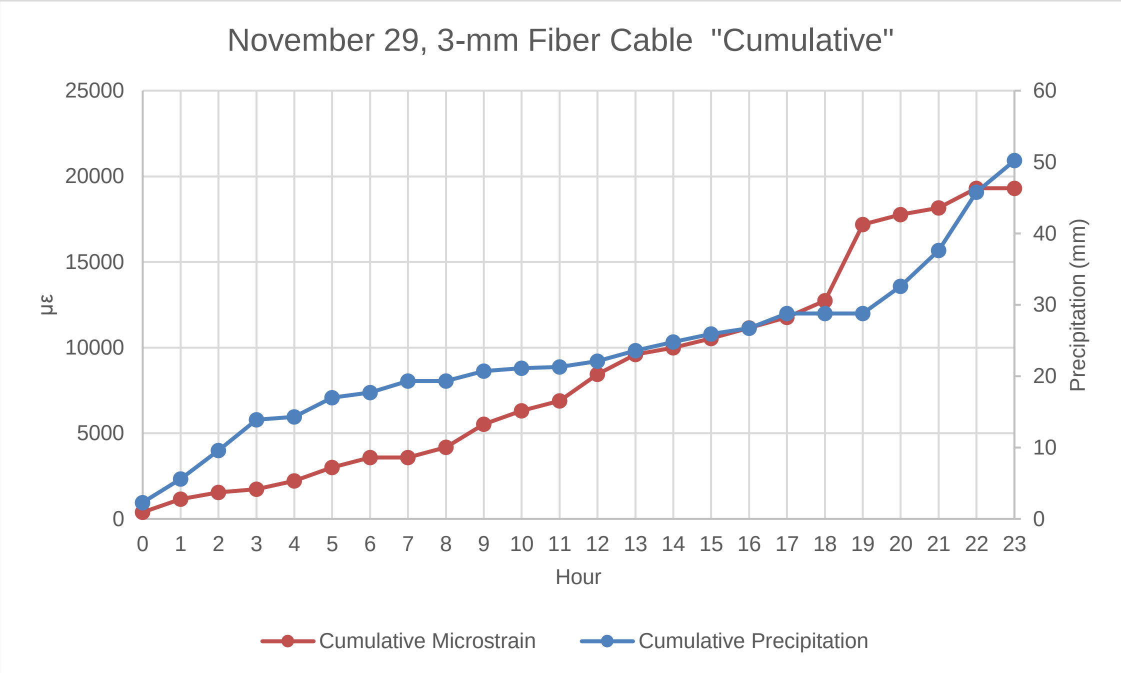

Figure 81. Hourly relation of cumulative με vs. precipitation results with 3-mm cable for SP 4 on November 29 (BH 14)

Figure 82 depicts the relationship between weekly precipitation levels and the με (με) values at SP 4, spanning the period from November 2 to December 21. The graph reveals that SP 2 initially registered a με of -1500 με at the month's onset. With progressive rainfall, there is a notable increase in strain, culminating in a value of approximately 500 με.

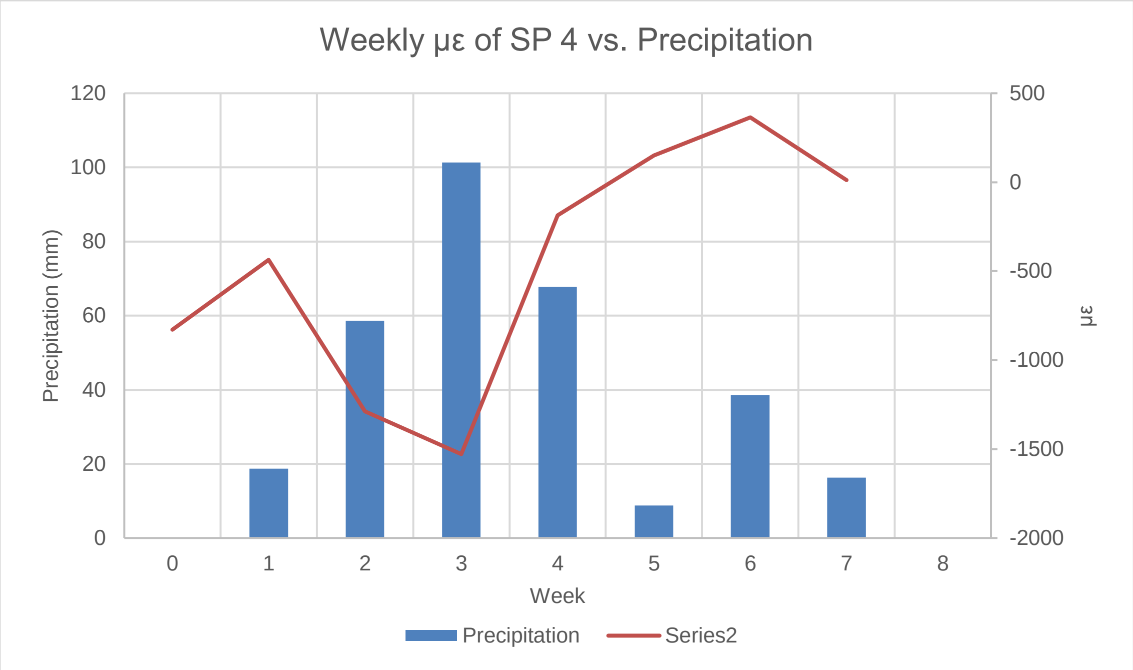

Figure 82. Weekly relation of με vs. precipitation results with 3-mm cable for SP 3 during the monitoring (BH 14)

7.4.1.5. Assessment of SP 5 in the 3-mm Diameter Fiber Optic Cable

Figures 83 and 84 present the hourly 3-mm fiber cable με vs. precipitation relationship for SP 5 (BH 15-16) on November 18 and 29. According to these data, με values, which were more stable in the first hours of the day on November 18, fluctuated between -4000 με and 6000 με after the rainfall event. On November 29, strain values were slightly between -700 με and 100 με after precipitation.

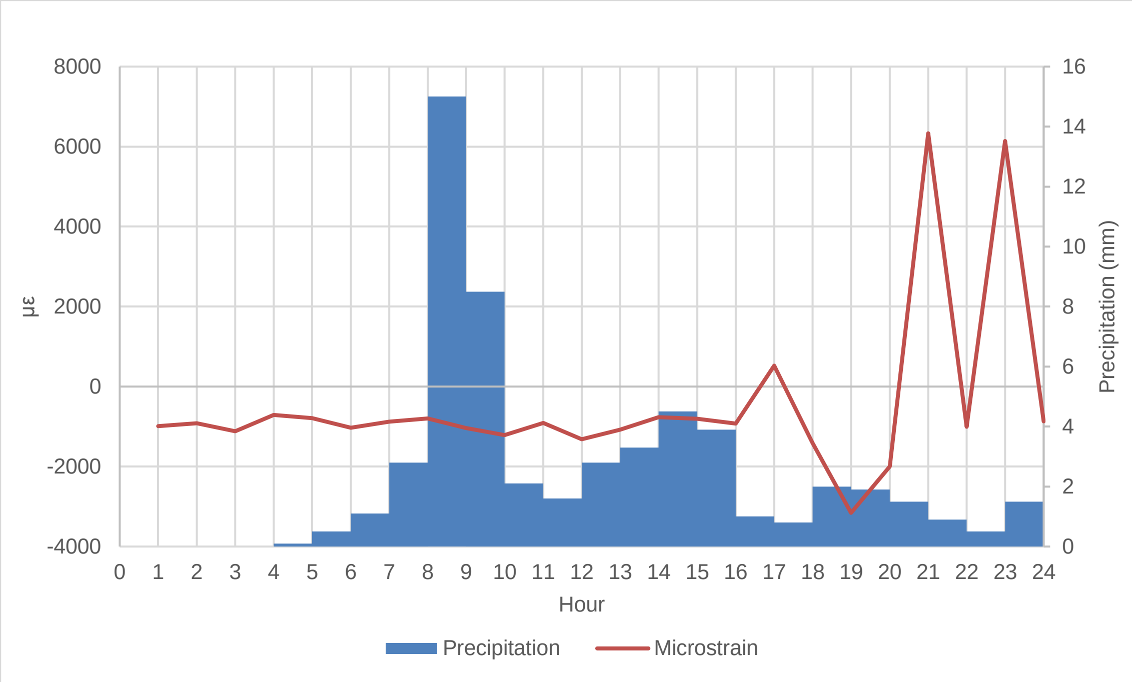

Figure 83. Hourly relation of με vs. precipitation results with 3-mm cable for SP 5 on November 18 (BH 15-16)

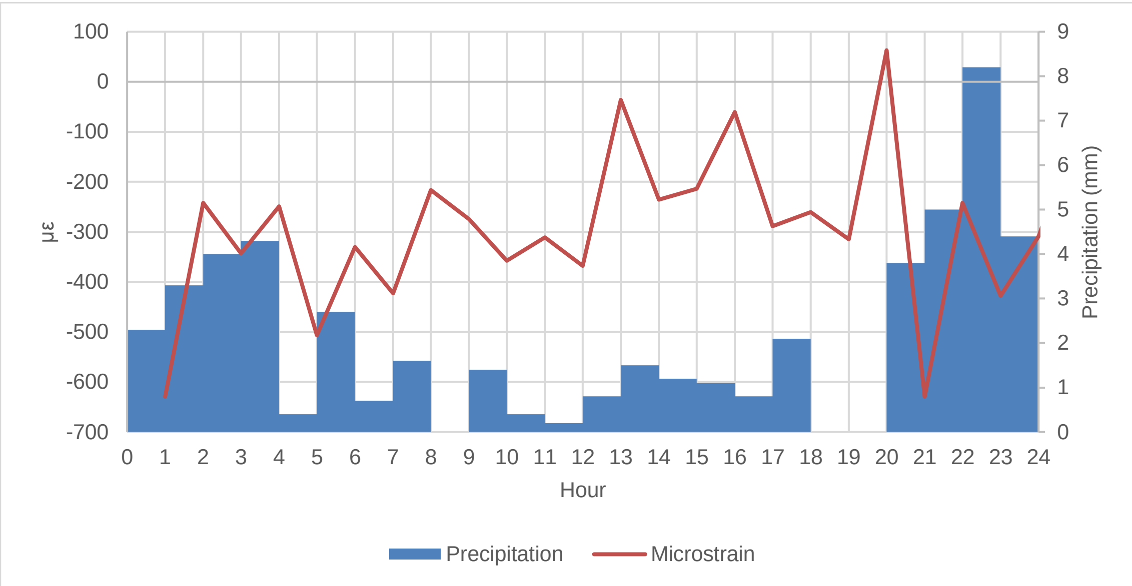

Figure 84. Hourly relation of με vs. precipitation results with 3-mm cable for SP 5 on November 29 (BH 15-16)

Figures 85 and 86 represent the cumulative με vs. precipitation relationship for SP 5 of the 3-mm cable. SP 5 is positioned at the end of the bottom side of the monitoring area. In line with the results obtained, cumulative fiber optic measurements reached a με value of 36772.97 with 56.3 mm rainfall on

November 18. After 50.2 mm of rainfall on November 29, fiber optic measurements reached up to 7331.97 με value.

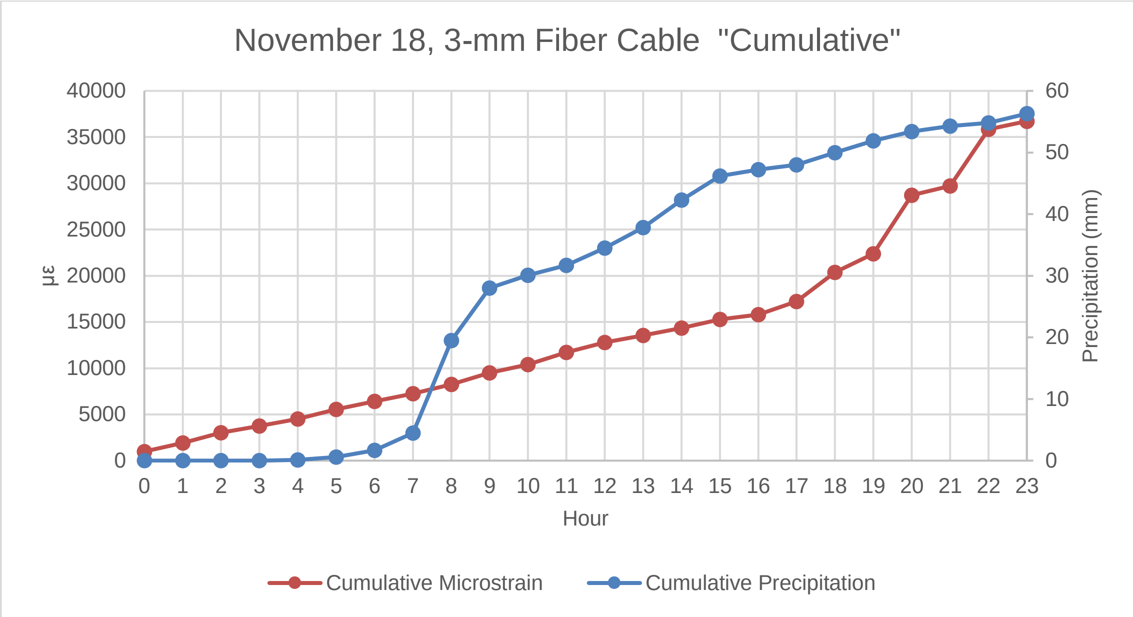

Figure 85. Hourly relation of cumulative με vs. precipitation results with 3-mm cable for SP 5 on November 18 (BH 15-16)

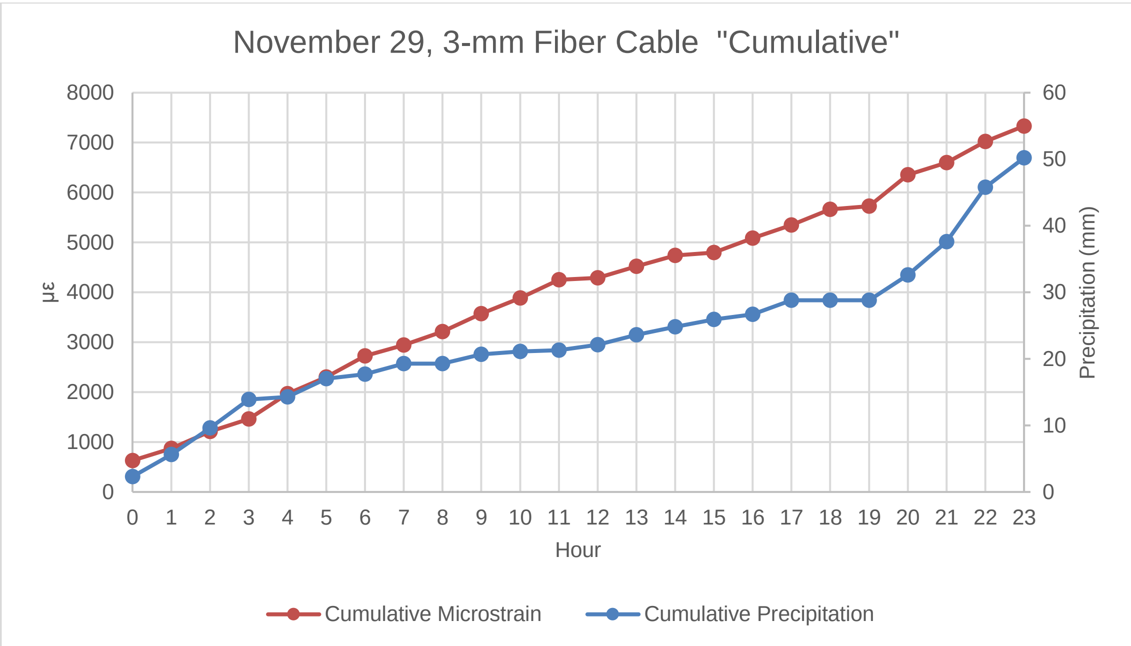

Figure 86. Hourly relation of cumulative με vs. precipitation results with 3-mm cable for SP 5 on November 18 (BH 15-16)

Figure 87 indicates the relationship between weekly precipitation levels and micro-strain (με) values at SP 5, covering the period from November 2 to December 21. The graph reveals that SP 2 recorded a micro-strain of -1200 με at the beginning of the month. A significant increase in strain with subsequent rainfall resulted in a value of around 100 με.

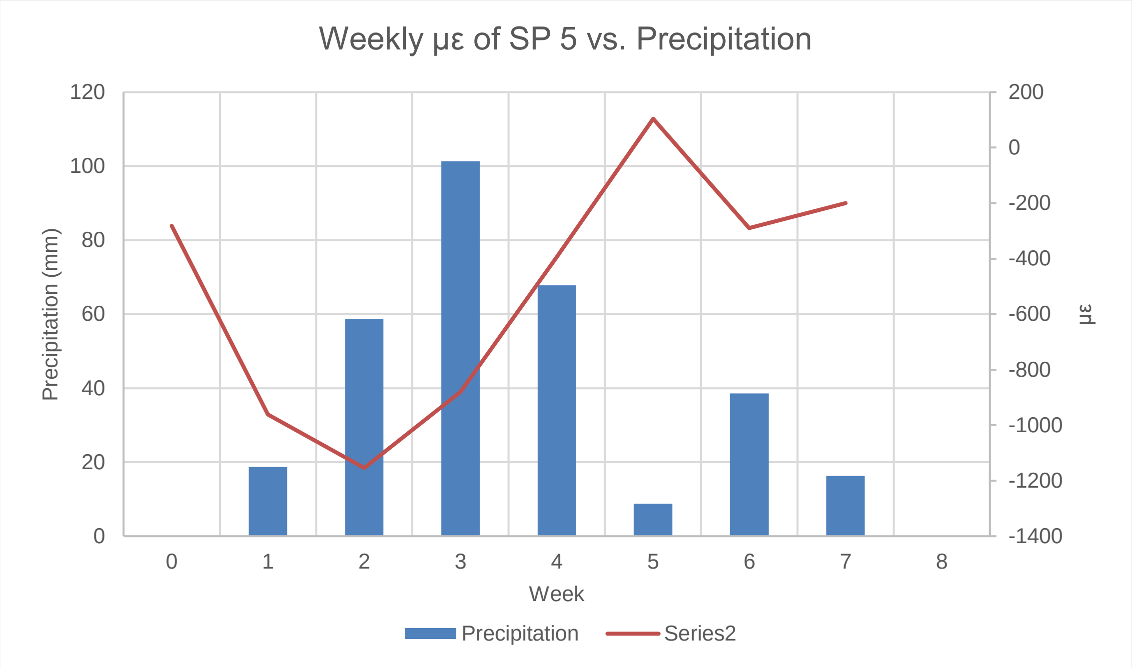

Figure 87. Weekly relation of με vs. precipitation results with 3-mm cable for SP 5 during the monitoring (BH 15-16)

7.4.2. Outcomes from the 4.5-mm Fiber Optic Cable Analysis

As mentioned, strain changes will be considered separately for precipitation and seismic activity. After analyzing the data of November 18 and 29 for the 4.5-mm fiber cable, which is more suitable for monitoring the effect of rainfall more clearly due to its noiselessness, the changes along the cable during the whole study period will be given.

7.4.2.1. Assessment of SP 1 in the 4.5-mm Diameter Fiber Optic Cable

Figures 88 and 89 display the hourly 4.5-mm fiber cable με vs. precipitation relationship for SP 1 (BH 3) on November 18 and 29. With the increase in precipitation on November 18, the change of approximately 400 με in the 4.5-mm fiber cable is clearly seen in the graph.

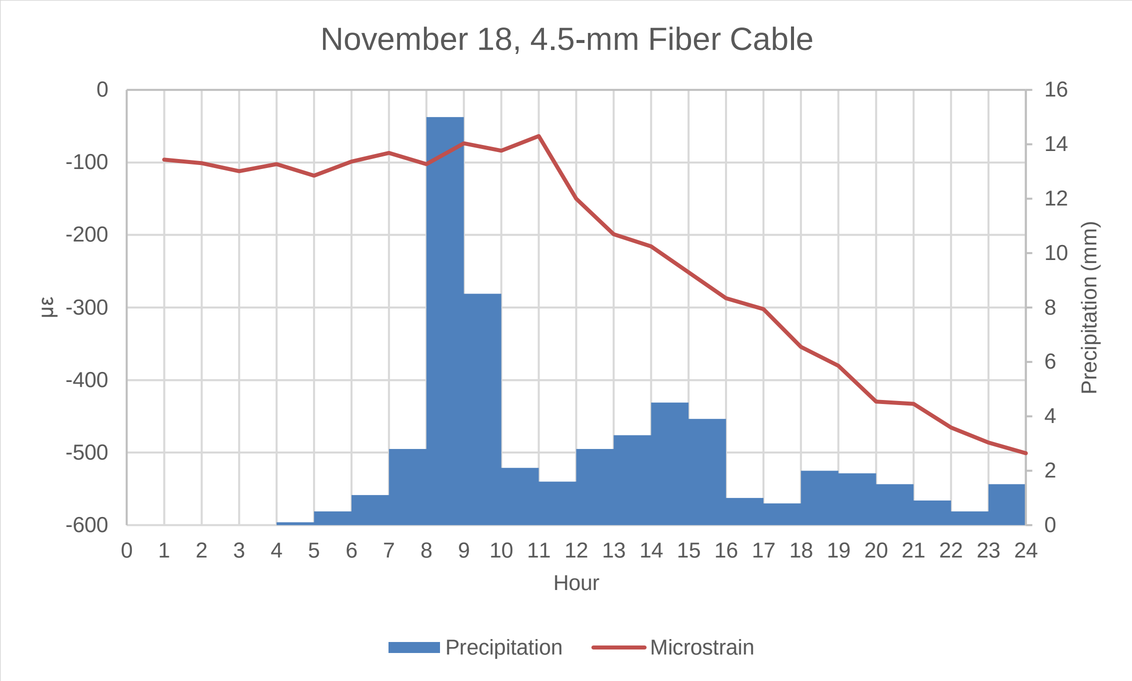

Figure 88. Hourly relation of με vs. precipitation results with 4.5-mm cable for SP 1 on November 18 (BH 3)

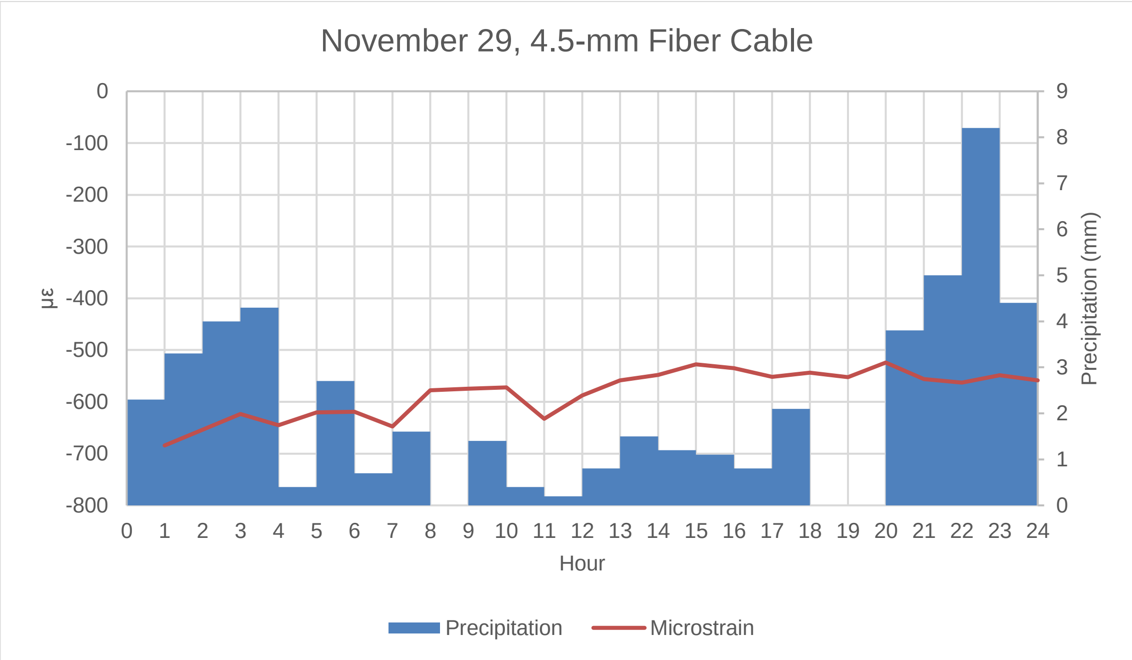

Figure 89. Hourly relation of με vs. precipitation results with 4.5-mm cable for SP 1 on November 29 (BH 3)

Figures 90 and 91 represent the cumulative με vs. precipitation relationship for SP 1 of the 4.5-mm cable. In line with the results obtained, cumulative fiber optic measurements reached a με value of 4992.82 with 56.3 mm rainfall on November 18. After 50.2 mm of rainfall on November 29, fiber optic measurements reached up to 14006.20 με value.

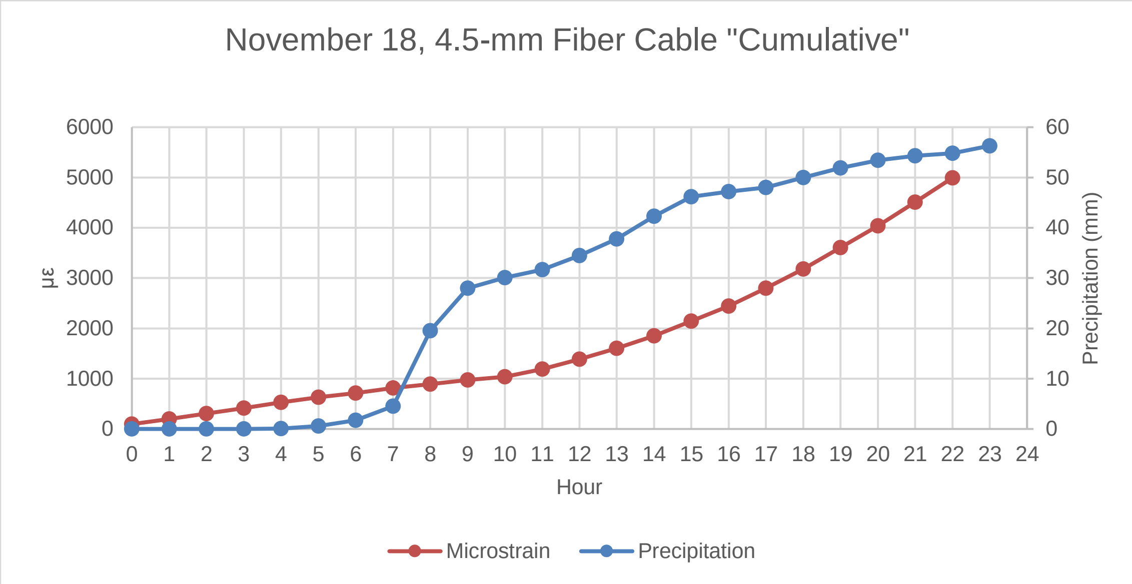

Figure 90. Hourly relation of cumulative με vs. precipitation results with 4.5-mm cable for SP 1 on November 18 (BH 3)

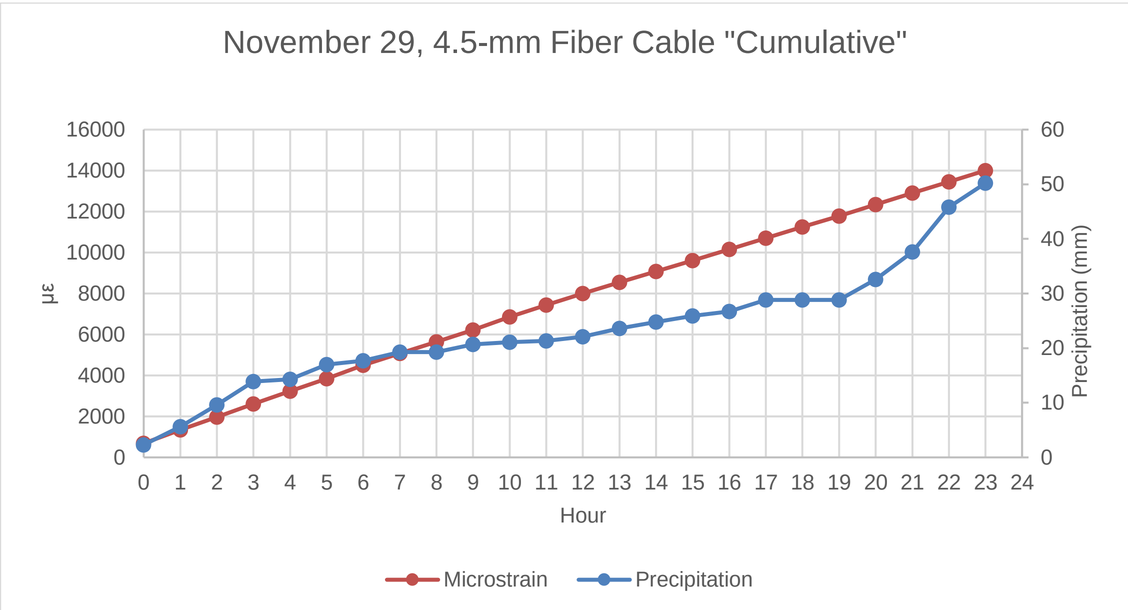

Figure 91. Hourly relation of cumulative με vs. precipitation results with 4.5-mm cable for SP 1 on November 29 (BH 3)

Figure 92 shows the relationship between weekly precipitation levels and micro-strain (με) values at SP 1, covering the period from November 2 to December 21. The graph reveals that SP 1 recorded a micro-strain of 120 με at the beginning of the month. A significant increase in strain with subsequent rainfall resulted in a value of around -600 με.

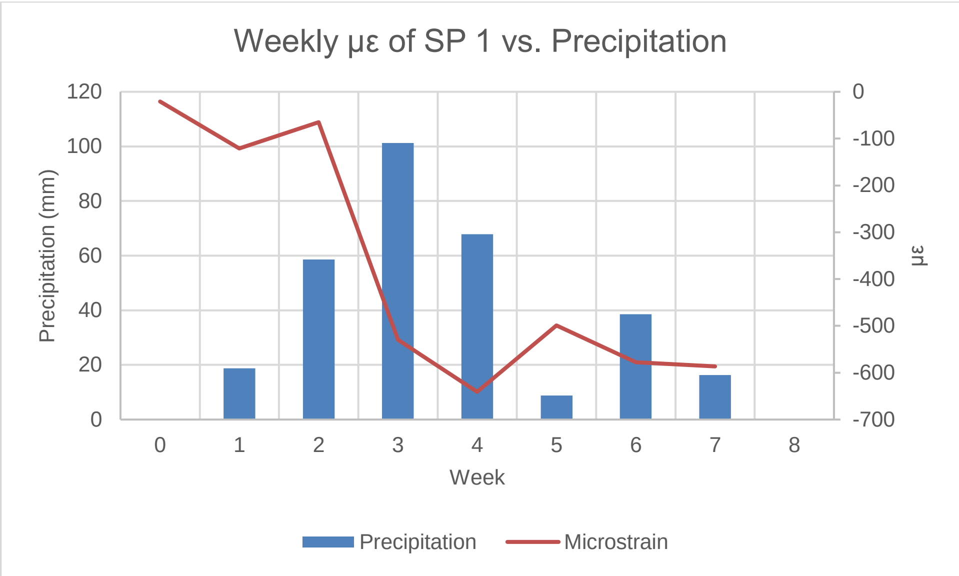

Figure 92. Weekly relation of με vs. precipitation results with 4.5-mm cable for SP 1 during the monitoring (BH 3)

7.4.2.2. Assessment of SP 2 in the 4.5-mm Diameter Fiber Optic Cable

Figures 93 and 94 show the hourly 4.5-mm fiber cable με-precipitation relationship for SP 2 (BH 6) on November 18 and 29.

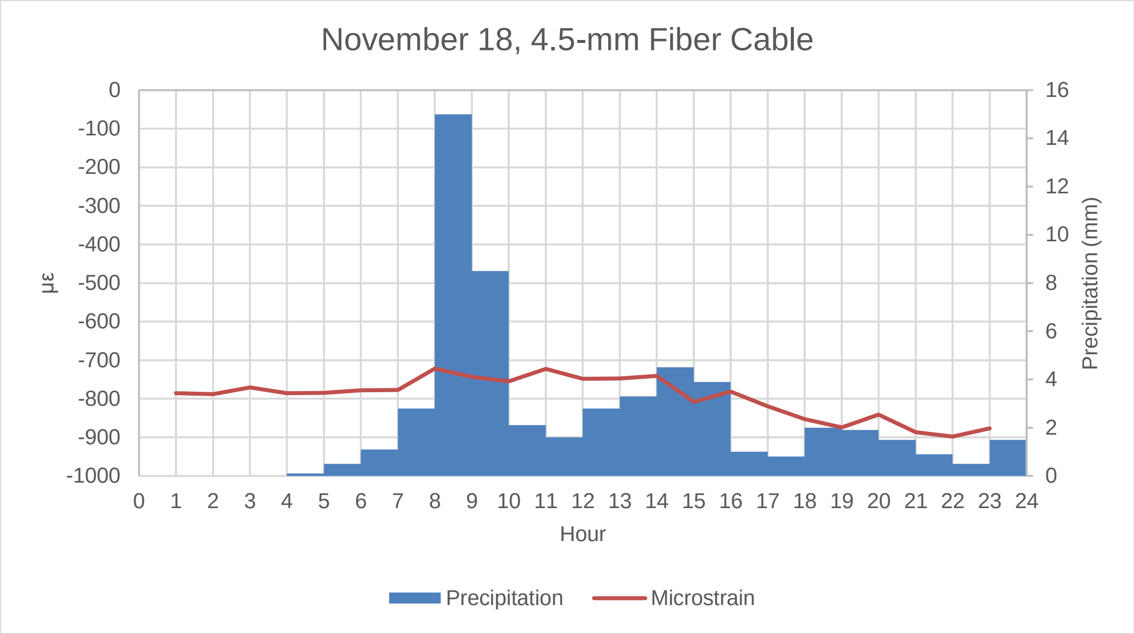

Figure 93. Hourly relation of με vs. precipitation results with 4.5-mm cable for SP 2 on November 18 (BH 6)

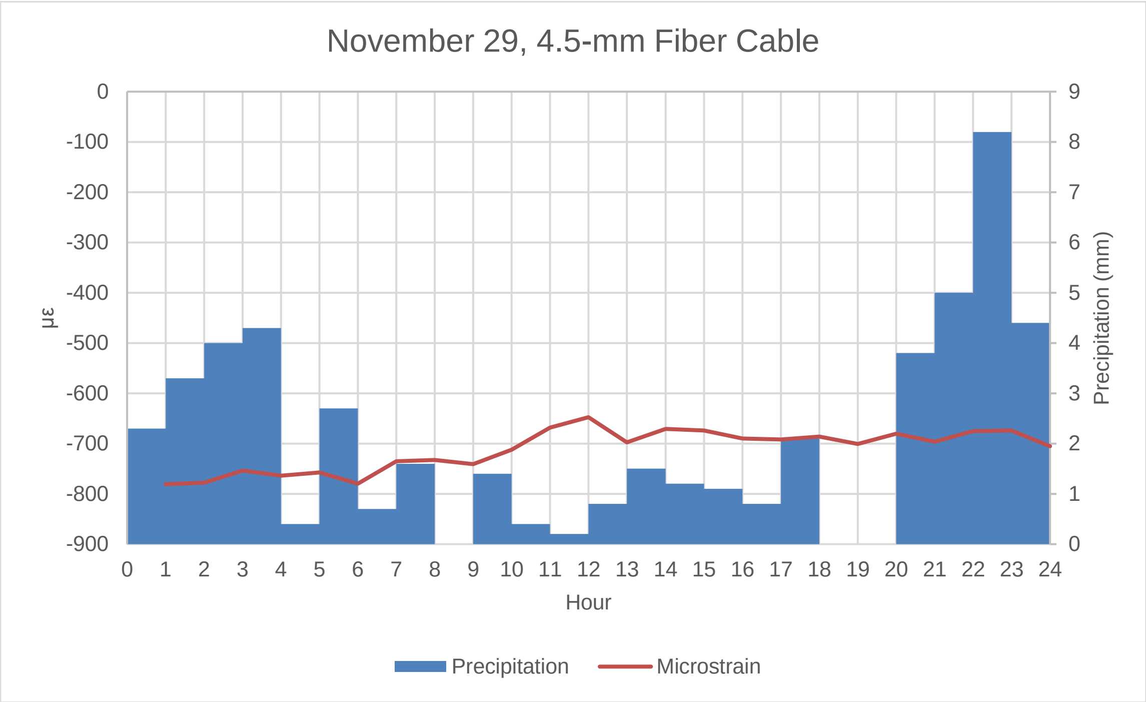

Figure 94. Hourly relation of με vs. precipitation results with 4.5-mm cable for SP 2 on November 29 (BH 6)

Figures 95 and 96 represent the cumulative με vs. precipitation relationship for SP 2 of the 4.5-mm cable. In line with the results obtained, cumulative fiber optic measurements reached a με value of 18286.55 with 56.3 mm rainfall on November 18. After 50.2 mm of rainfall on November 29, fiber optic measurements reached up to 17092.60 με value.

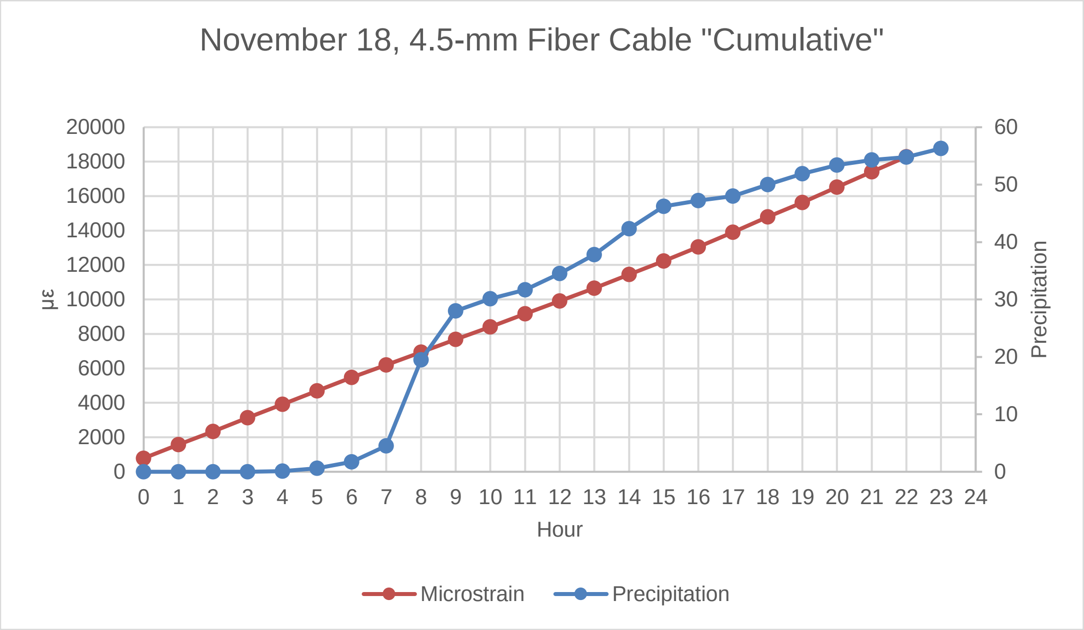

Figure 95. Hourly relation of cumulative με vs. precipitation results with 4.5-mm cable for SP 2 on November 29 (BH 6)

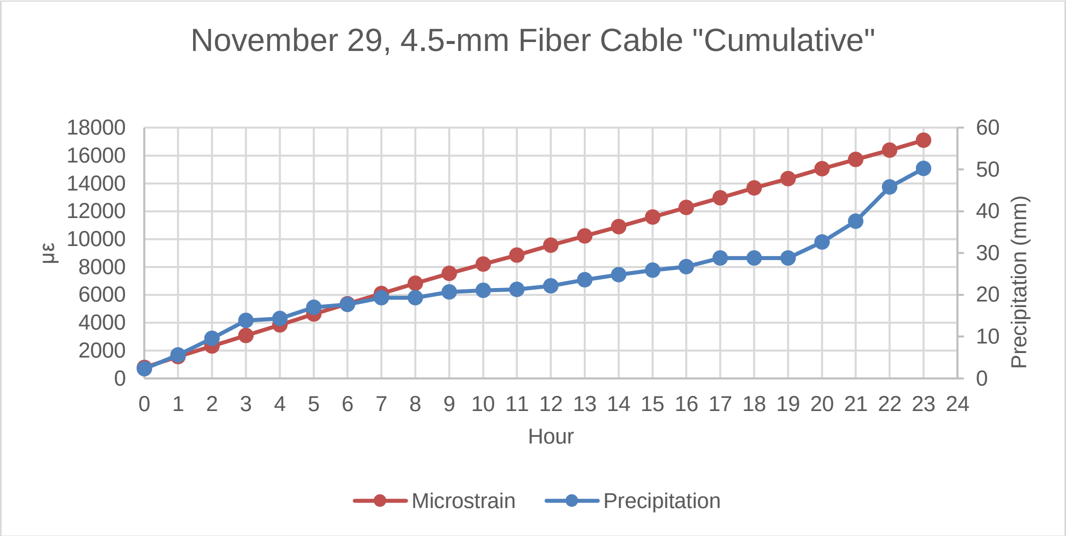

Figure 96. Hourly relation of cumulative με vs. precipitation results with 4.5-mm cable for SP 2 on November 29 (BH 6)

Figure 97 shows the relationship between weekly precipitation levels and micro-strain (με) values at SP 2, covering the period from November 2 to December 21. The graph reveals that SP 2 recorded a micro-strain of -100 με at the beginning of the month. A significant increase in strain with subsequent rainfall resulted in a value of around -900 με. With the decrease in precipitation, an increase in straits was observed again.

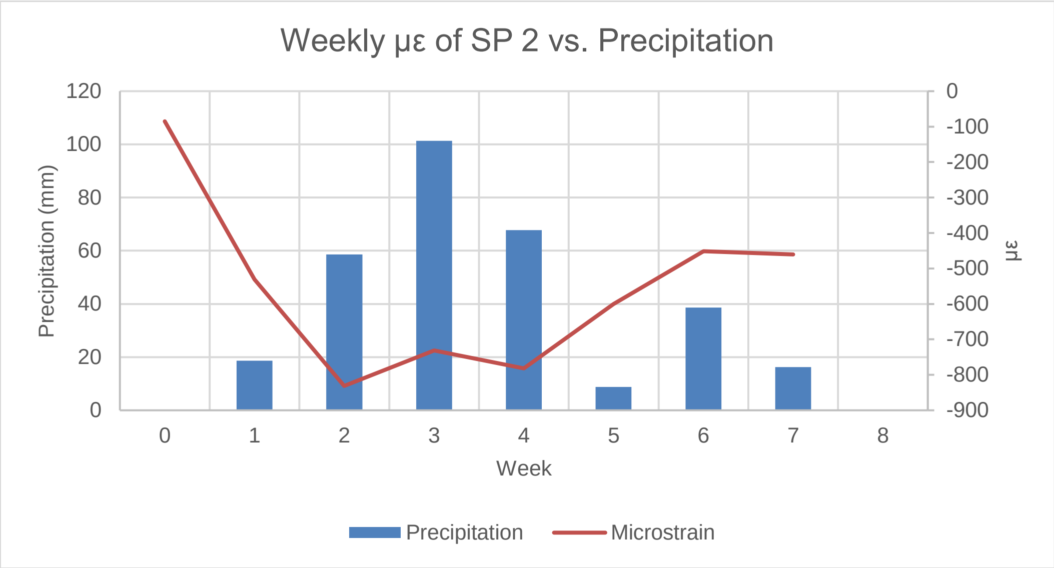

Figure 97. Weekly relation of με vs. precipitation results with 4.5-mm cable for SP 2 during the monitoring (BH 6)

7.4.2.3. Assessment of SP 3 in the 4.5-mm Diameter Fiber Optic Cable

Figures 98 and 99 show the hourly 4.5-mm fiber cable με vs. precipitation relationship for SP 3 (BH 9-10) on November 18 and 29. With the increase in precipitation on November 18, the change of approximately 250 με in the 4.5-mm fiber cable is displayed in the graph. Precipitation on November 29 caused 100 με changes in SP 3.

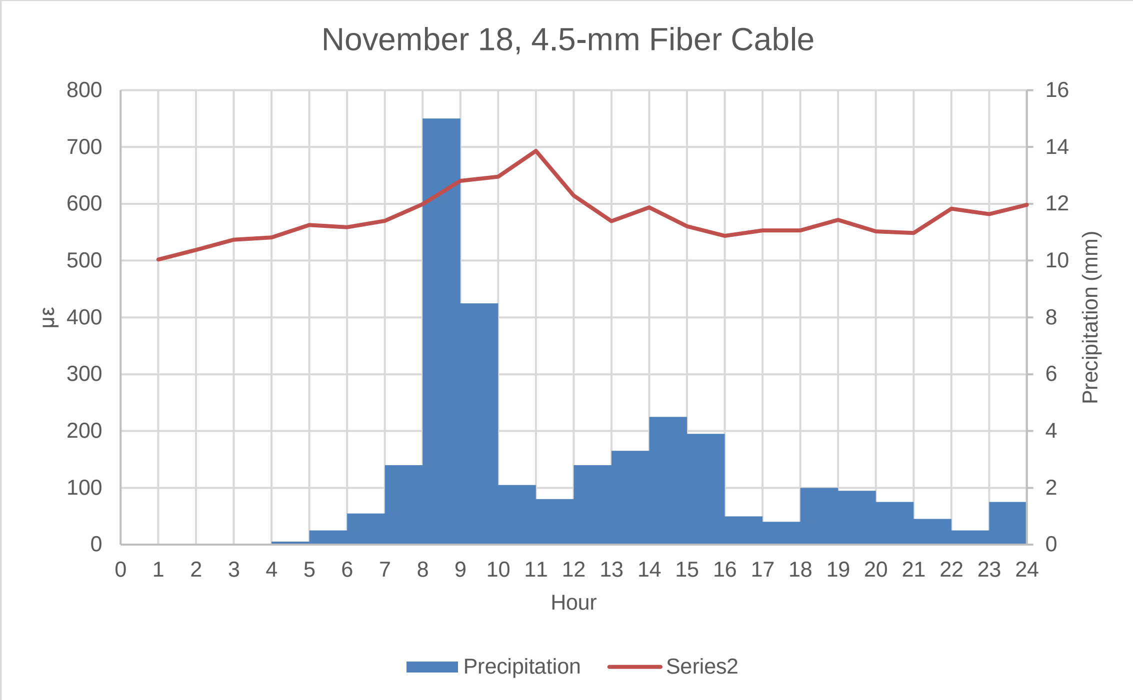

Figure 98. Hourly relation of με vs. precipitation results with 4.5-mm cable for SP 3 on November 18 (BH 9-10)

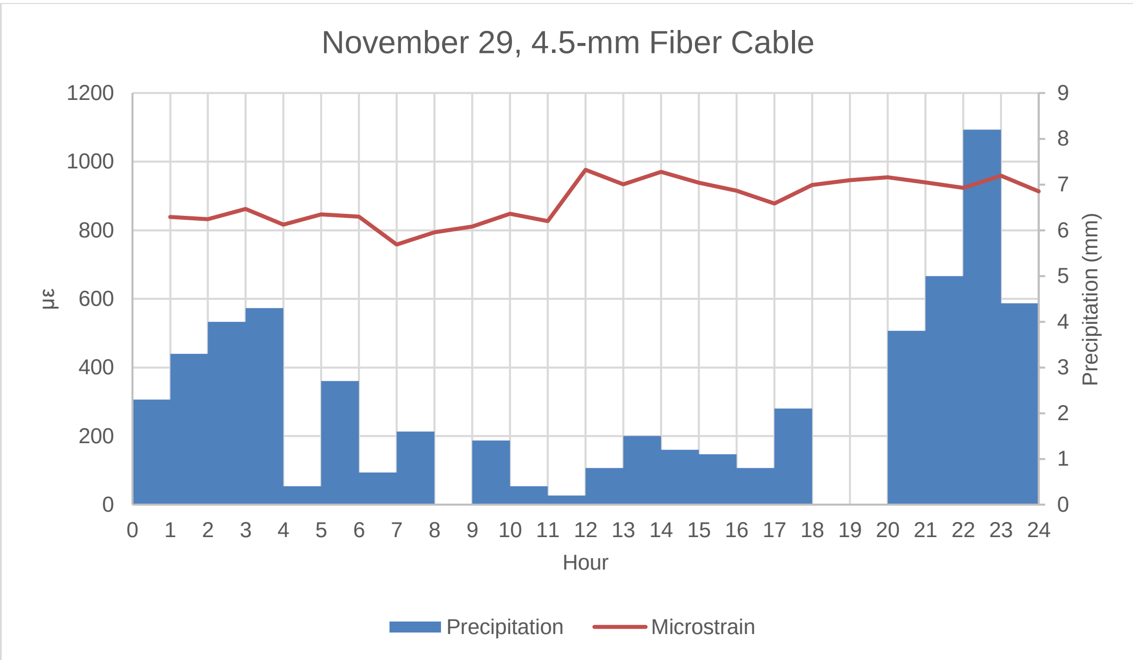

Figure 99. Hourly relation of με vs. precipitation results with 4.5-mm cable for SP 3 on November 29 (BH 9-10)

Figures 100 and 101 represent the cumulative με vs. precipitation relationship for SP 3 of the 3-mm cable. In line with the results obtained, cumulative fiber

optic measurements reached a με value of 13299.87 with 56.3 mm rainfall on November 18. After 50.2 mm of rainfall on November 29, fiber optic measurements reached up to 21253.48 με value.

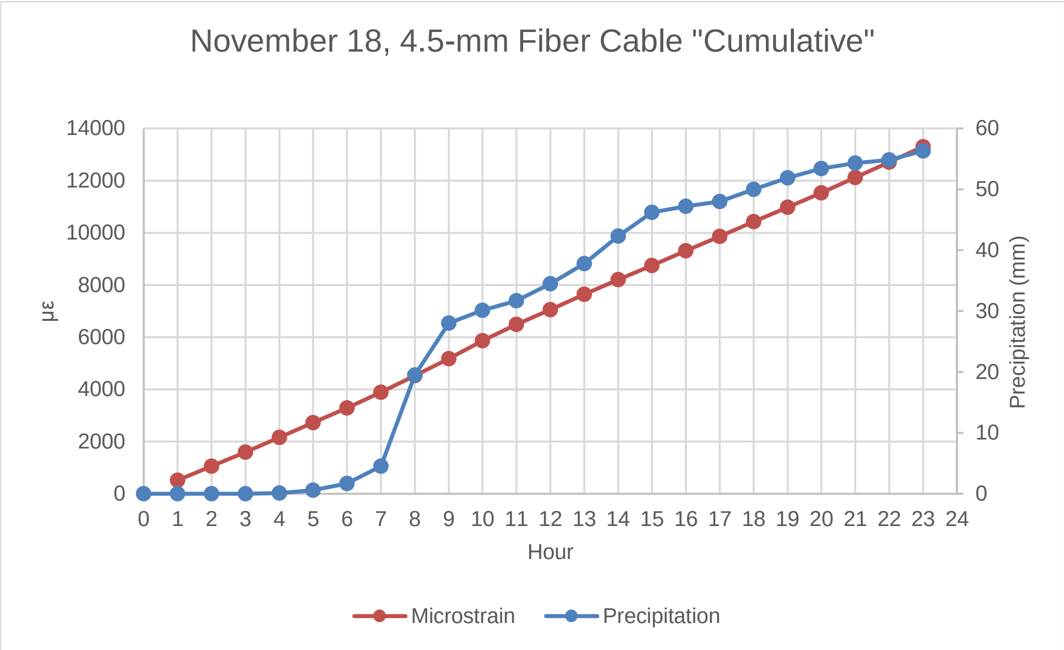

Figure 100. Hourly relation of cumulative με vs. precipitation results with 4.5-mm cable for SP 3 on November 18 (BH 9-10)

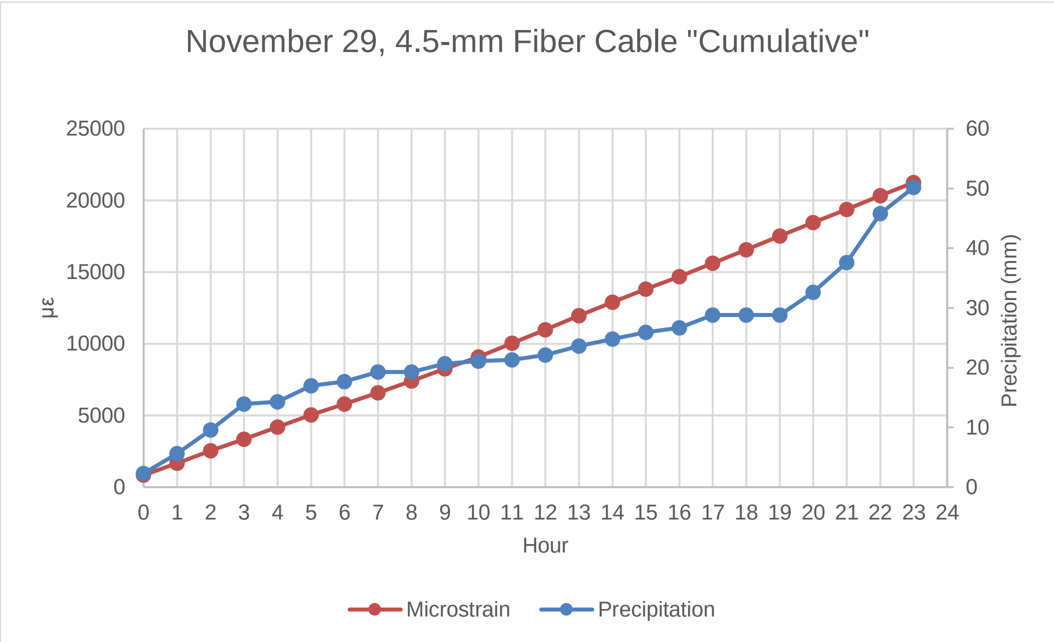

Figure 101. Hourly relation of cumulative με vs. precipitation results with 4.5-mm cable for SP 3 on November 29 (BH 9-10)

Figure 102 indicates the relationship between weekly precipitation levels and micro-strain (με) values at SP 3, which was the most active point, covering the period from November 2 to December 21. The graph reveals that SP 1 recorded a micro-strain of -500 με at the beginning of the month. A significant increase in strain with subsequent rainfall resulted in a value of around 2000 με.

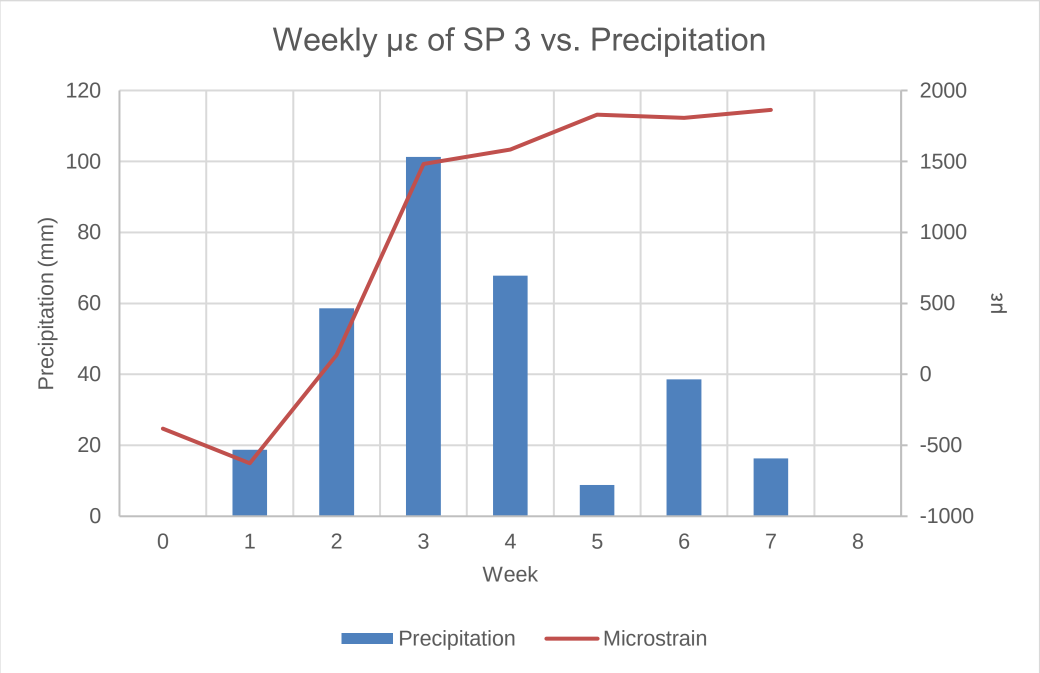

Figure 102. Weekly relation of με vs. precipitation results with 4.5-mm cable for SP 3 during the monitoring (BH 9-10)

7.4.2.4. Assessment of SP 4 in the 4.5-mm Diameter Fiber Optic Cable

Figures 103 and 104 show the hourly 4.5-mm fiber cable με vs. precipitation relationship for SP 4 (BH 14) on November 18 and 29. With the increase in precipitation on November 18, the change of approximately 200 με in the 4.5-mm fiber cable is displayed in the graph. Precipitation on November 29 caused 100 με changes in SP 4.

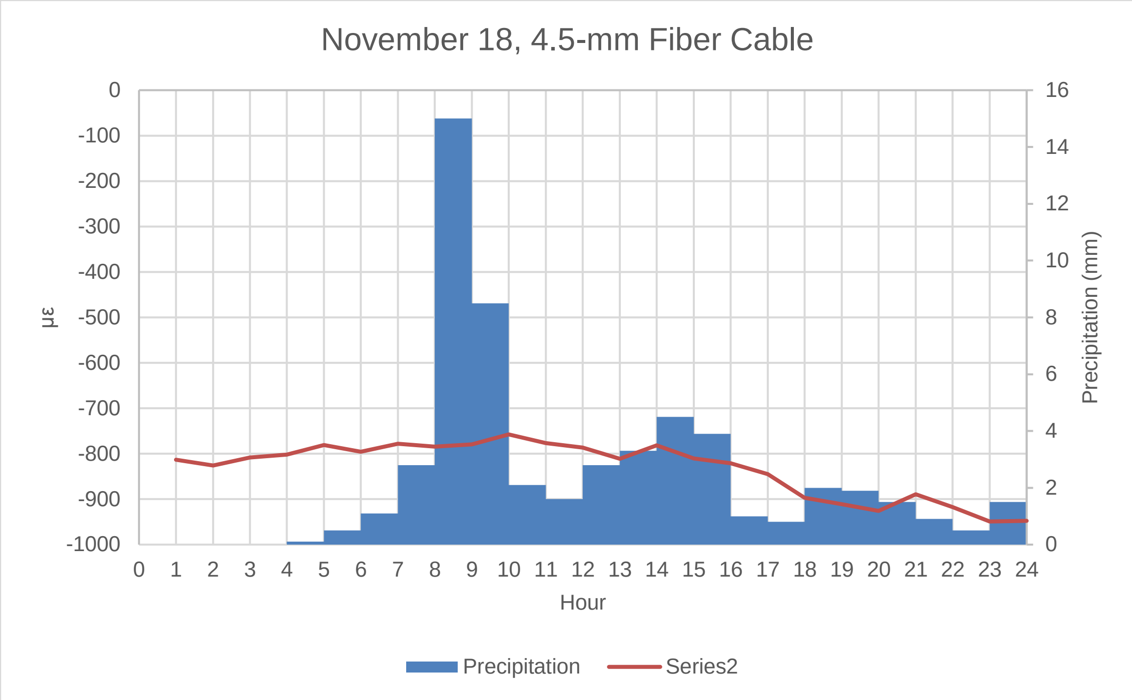

Figure 103. Hourly relation of με vs. precipitation results with 4.5-mm cable for SP 4 on November 18 (BH 14)

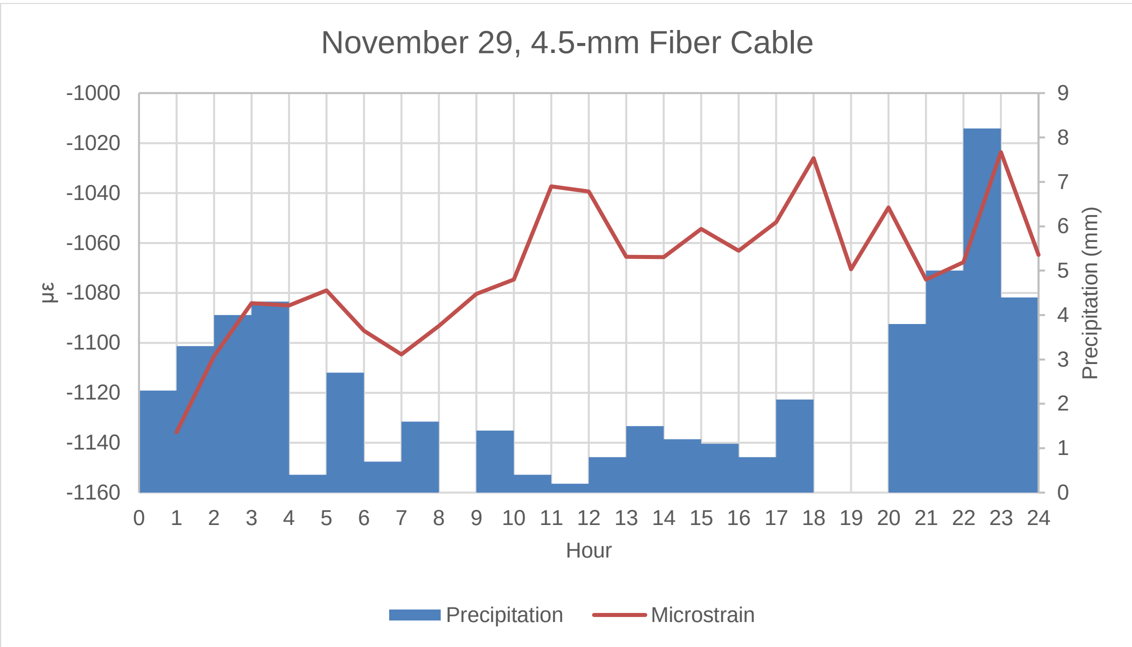

Figure 104. Hourly relation of με vs. precipitation results with 4.5-mm cable for SP 4 on November 29 (BH 14)

Figures 105 and 106 represent the cumulative με vs. precipitation relationship for SP 4 of the 4.5-mm cable. In line with the results obtained, cumulative fiber

optic measurements reached a με value of 19045.97 with 56.3 mm rainfall on November 18. After 50.2 mm of rainfall on November 29, fiber optic measurements reached up to 25688.36 με value.

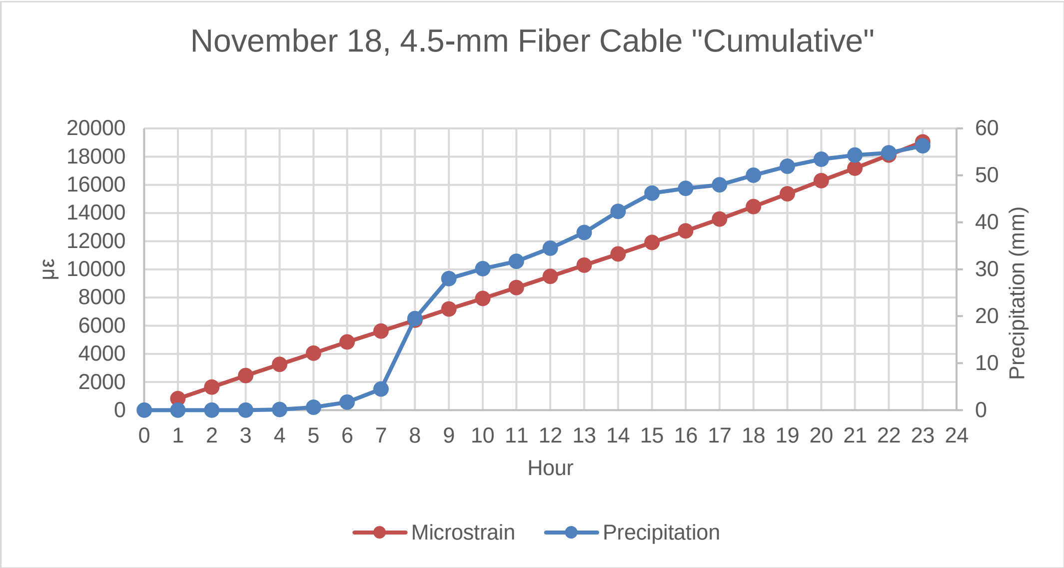

Figure 105. Hourly relation of cumulative με vs. precipitation results with 4.5-mm cable for SP 4 on November 18 (BH 14)

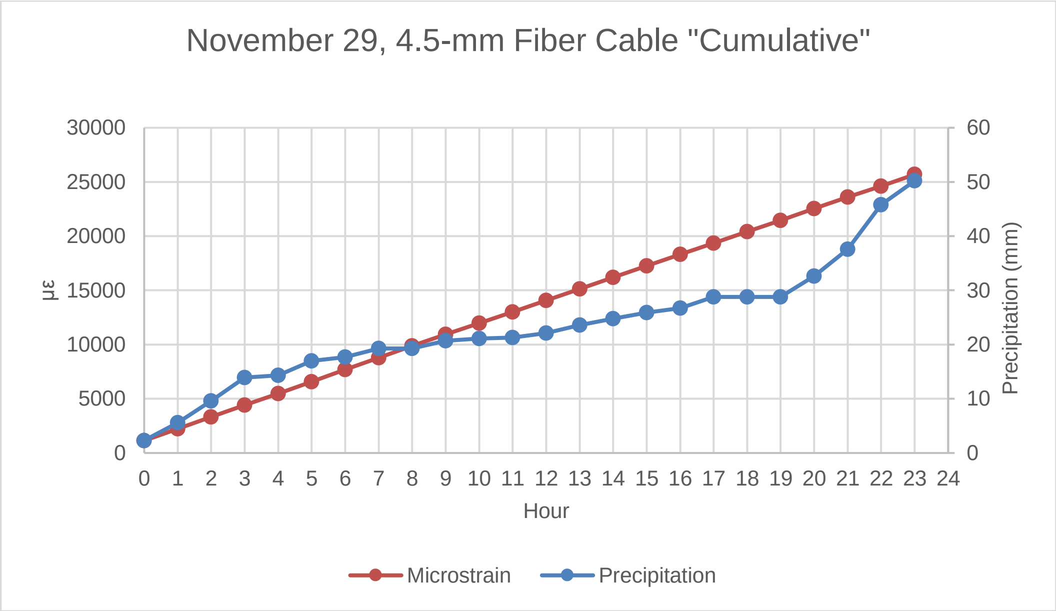

Figure 106. Hourly relation of cumulative με vs. precipitation results with 4.5-mm cable for SP 4 on November 29 (BH 14)

Figure 107 indicates the relationship between weekly precipitation levels and micro-strain (με) values at SP 4, which was the most active point, covering the period from November 2 to December 21. The graph reveals that SP 4 recorded a micro-strain of -100 με at the beginning of the month. There was a significant increase in strain with subsequent rainfall, resulting in a value of around -1200 με.

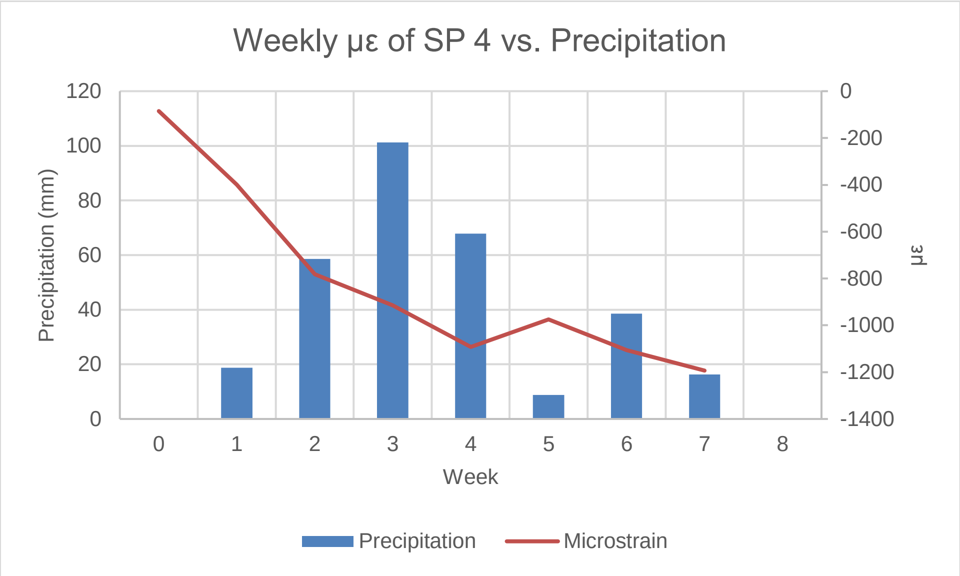

Figure 107. Weekly relation of με vs. precipitation results with 4.5-mm cable for SP 4 during the monitoring (BH 14)

7.4.2.5. Assessment of SP 5 in the 4.5-mm Diameter Fiber Optic Cable

Figures 108 and 109 show the hourly 4.5-mm fiber cable με-precipitation relationship for SP 5 (BH 15-16) on November 18 and 29. With the increase in precipitation on November 18, the change of approximately 300 με in the 4.5-mm fiber cable is tabulated in the graph. Precipitation on November 29 caused 150 με changes in SP 5.

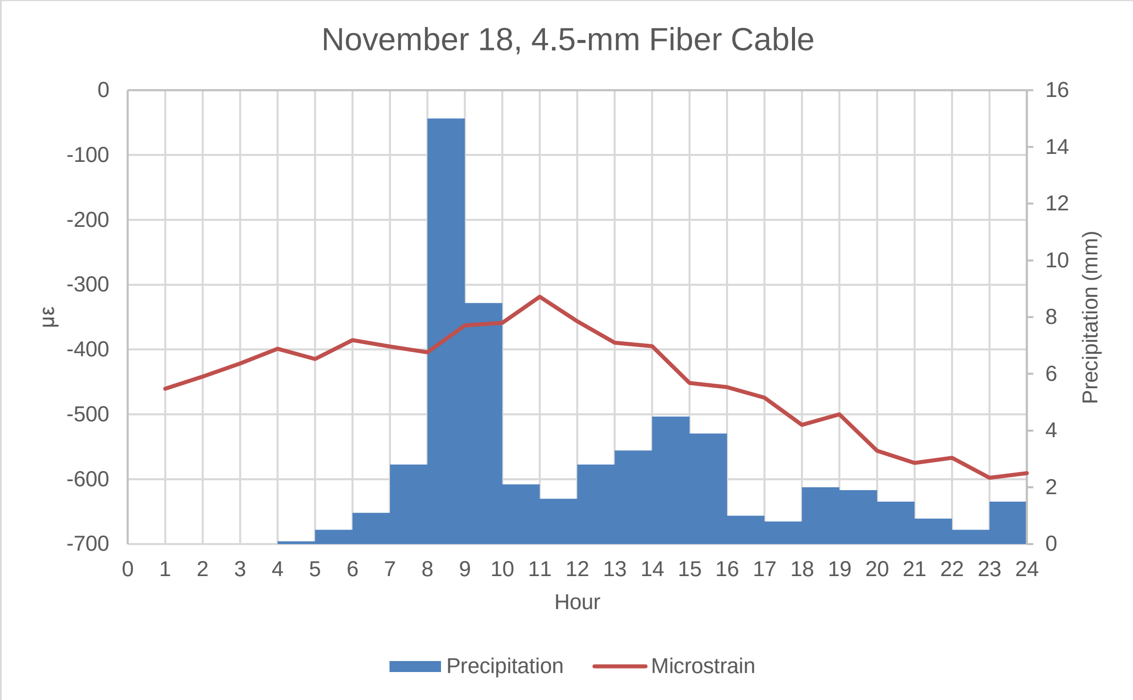

Figure 108. Hourly relation of με vs. precipitation results with 4.5-mm cable for SP 5 on November 18 (BH 15-16)

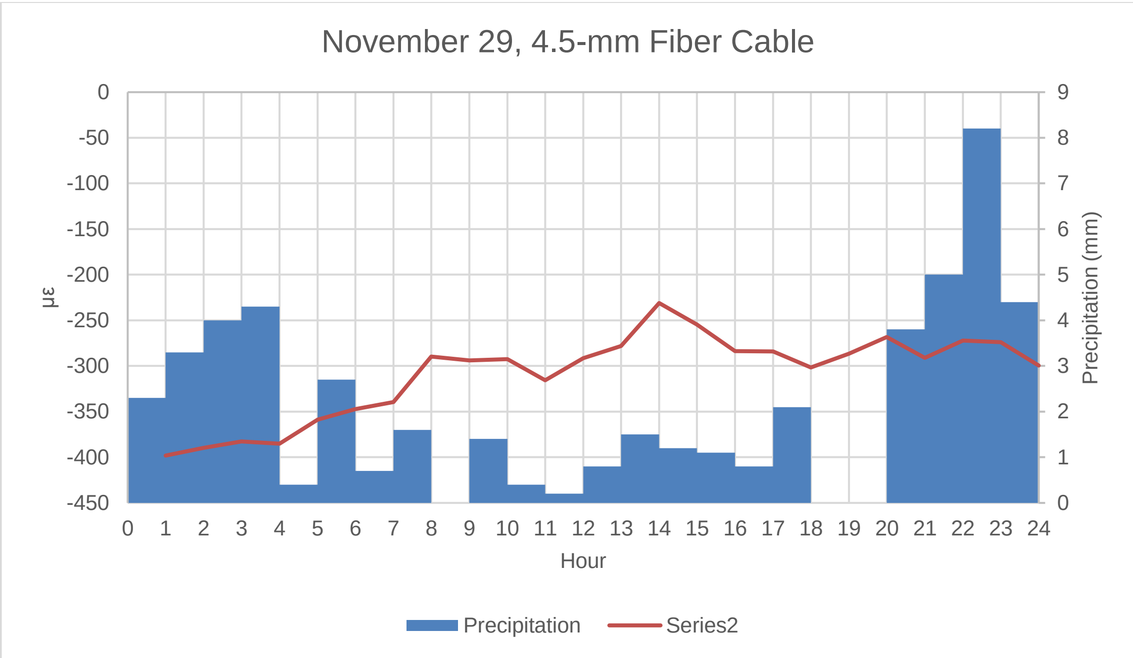

Figure 109. Hourly relation of με vs. precipitation results with 4.5-mm cable for SP 5 on November 29 (BH 15-16)

Figures 110 and 111 represent the cumulative με vs. precipitation relationship for SP 5 of the 4.5-mm cable. In line with the results obtained, cumulative fiber

optic measurements reached a με value of 10328.10 with 56.3 mm rainfall on November 18. After 50.2 mm of rainfall on November 29, fiber optic measurements reached up to 7408.66 με value.

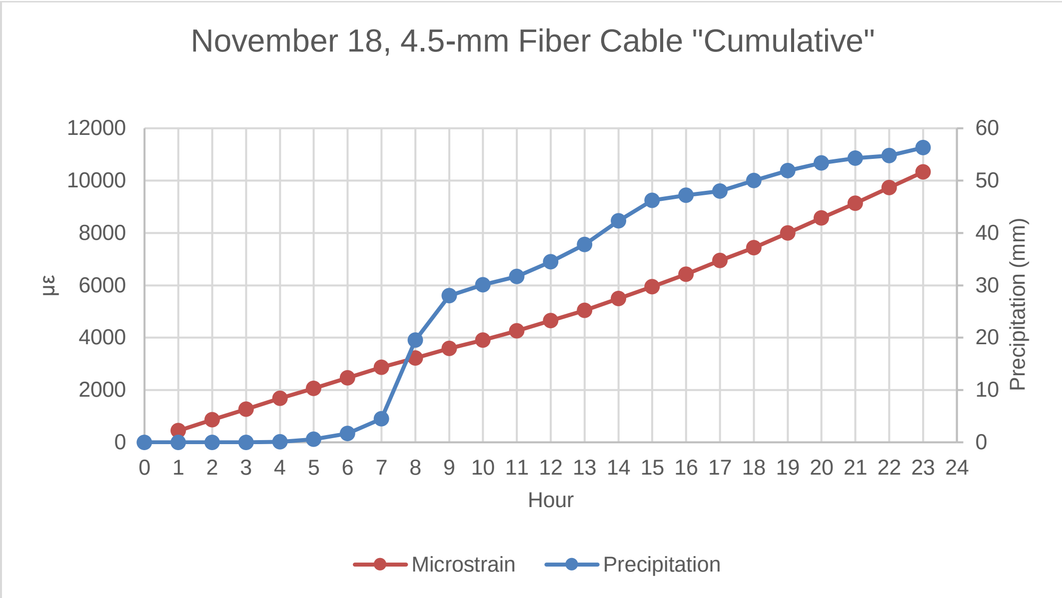

Figure 110. Hourly relation of cumulative με vs. precipitation results with 4.5-mm cable for SP 5 on November 18 (BH 15-16)

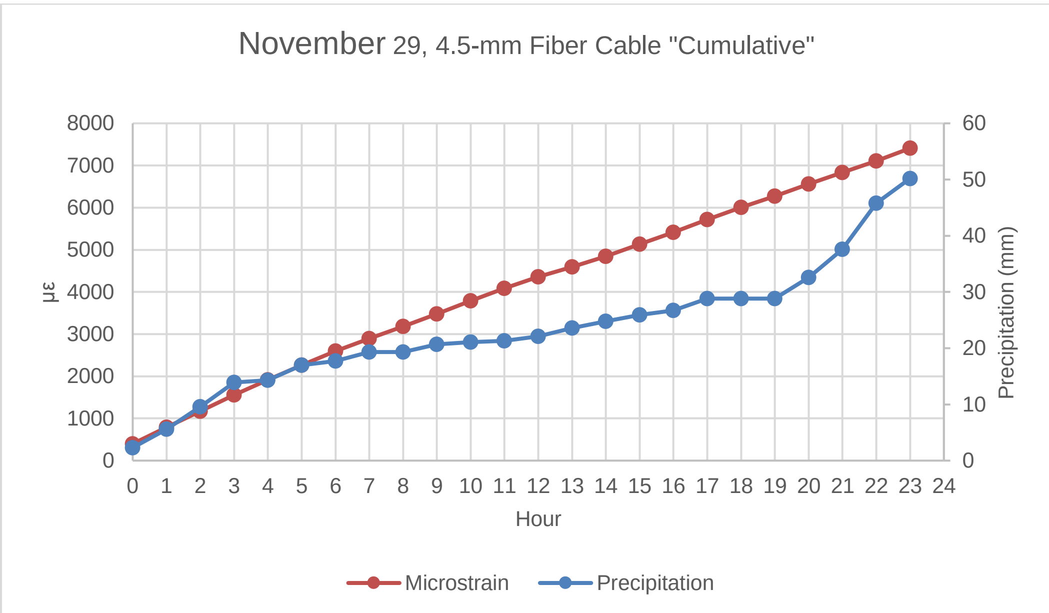

Figure 111. Hourly relation of cumulative με vs. precipitation results with 4.5-mm cable for SP 5 on November 18 (BH 15-16)

Figure 112 illustrates the relationship between weekly precipitation levels and micro-strain (με) values at SP 5, the most active point, covering the period from November 2 to December 21. The graph reveals that SP 5 recorded a micro-strain of -550 με at the beginning of the month. A significant increase in strain with subsequent rainfall resulted in a value of around -300 με.

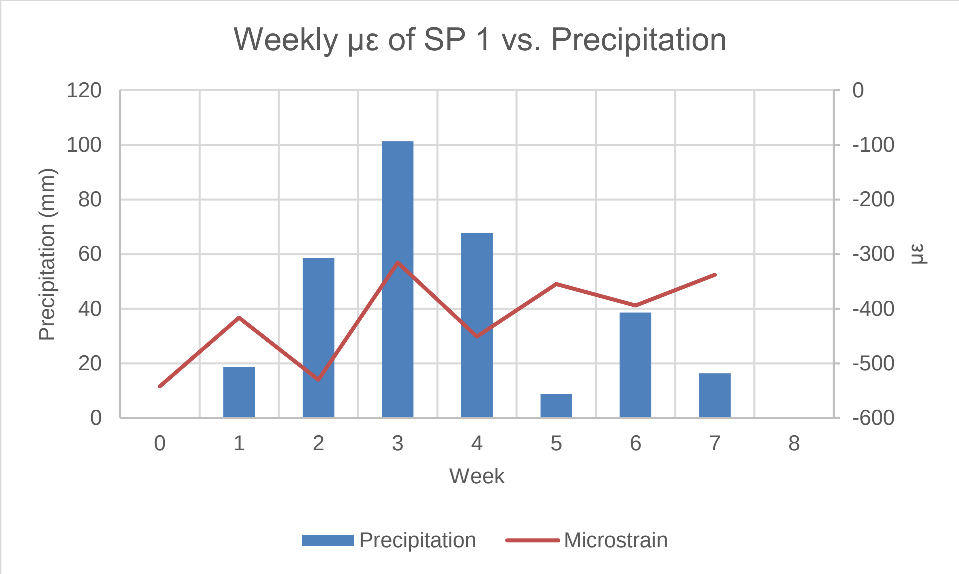

Figure 112. Weekly relation of με vs. precipitation results with 4.5-mm cable for SP 5 during the monitoring (BH 15-16)

7.4.3. Summary of the Comprehensive Analysis of με vs. Precipitation Measurements Across the Full Length of the Monitoring Cable

Slope behaviors have been observed over an extended period through continuous monitoring. The effects of daily rainfall on fiber optic cables were systematically evaluated, leading to the generation of comparative graphs for two different cables. These graphs, covering a 7-week observation period, effectively illustrated the performance and variations at the SPs of each cable under diverse environmental conditions. In the context of this thesis, an initial analysis was conducted on the November dataset to ascertain the SPs in section 7.3. It is imperative to undertake a several-week monitoring period to identify SPs effectively. A salient advantage of BOTDA and DSTS lies in their capability for sensing along the cable's length. This section examines strain variations attributable to precipitation along the entire cable length under surveillance. Figure 113 represents the weekly precipitation received by the monitoring area for 7 weeks. The precipitation data, segmented every week, clearly demonstrates that the province of Yalova experienced heavy rainfall during November, particularly within the third and fourth weeks. In contrast, the subsequent month of December was characterized by comparatively less precipitation in the region.

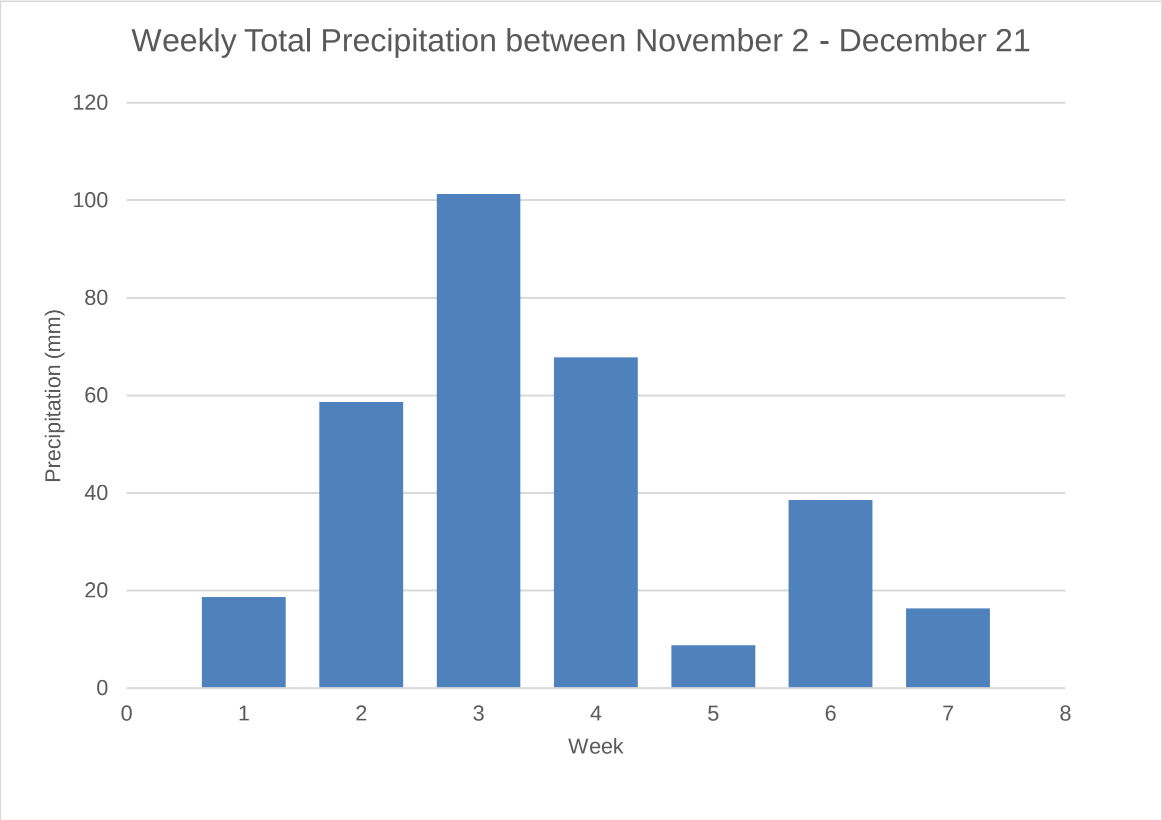

Figure 113. Total weekly precipitation from November 2 to December 21

Figure 114 delineates the με measurements with the 3-mm fiber cable, encompassing seven weeks. The 3-mm cable, noisy for various reasons, had high με values, especially on 23.11.2023 and 07.12.2023. This issue is associated with heavy rainfall in the third and fourth week.

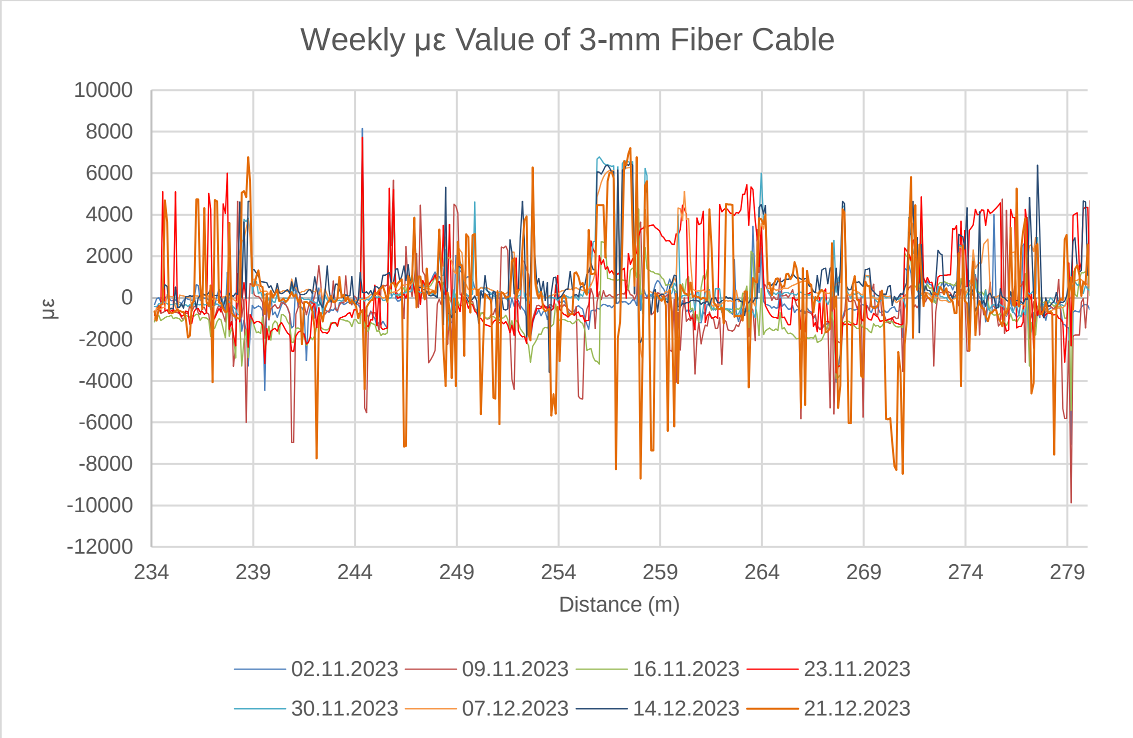

Figure 114. Weekly με data with 3-mm fiber optic cable

Figure 115 illustrates the με profile of the 4.5-mm diameter cable measured for the seven weeks. This cable distinctly exhibits the impact of rainfall on slopes. Notably, in the segment corresponding to SP 3, located at 146 meters, a marked increase in strain was observed during the monitoring period. The pronounced strain spikes between November 16 and 23 align precisely with the periods of heavy rainfall in those weeks. Additionally, the modest increases in strain observed in both cables during December have been attributed to the lower precipitation levels experienced that month.

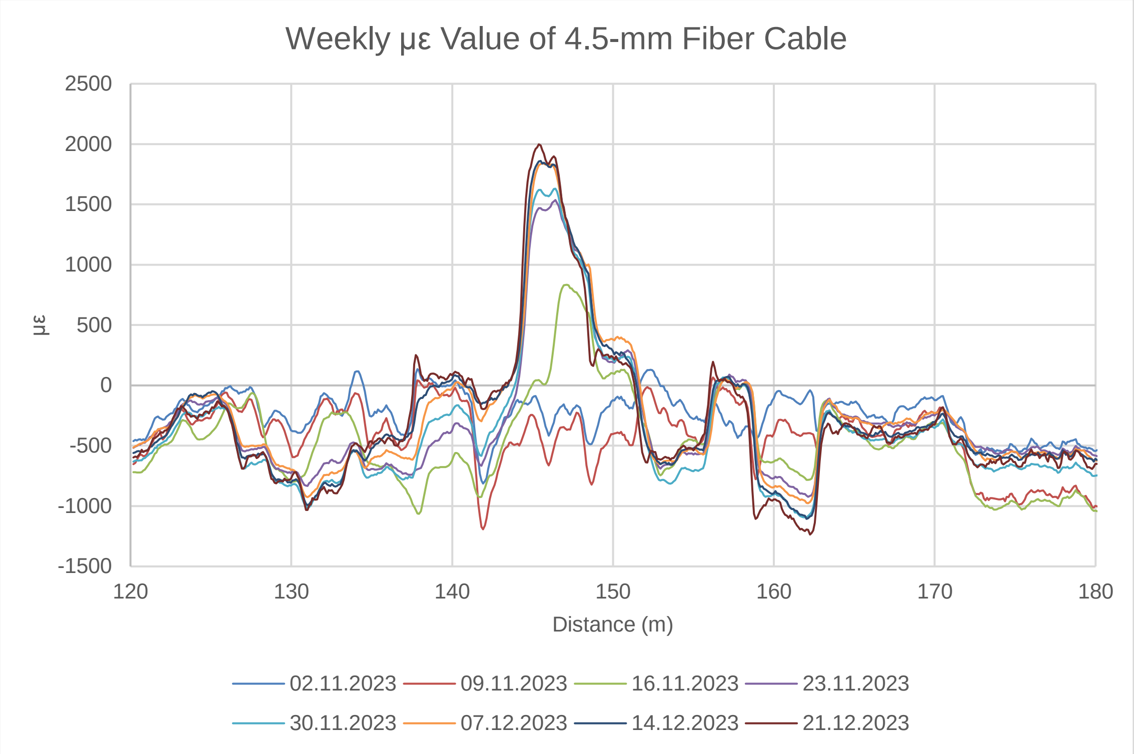

Figure 115. Weekly με data with 4.5-mm fiber optic cable

Based on the observations, it is evident that precipitation significantly affects movements in slopes, which in turn causes strain within fiber optic cables. The relation between heavy rainfall and increased strain readings, as observed in the 3-mm diameter cable, particularly at SPs (i.e., SP 3), underscores this interaction. The temporal alignment of strain peaks with intense rainfall events, especially noted in late November, demonstrates a clear causal relationship. This strain, induced by partial saturation due to infiltration and consequent soil expansion or slope instability due to surcharge from the rear of the head of the slope, highlights the sensitivity of fiber optics in detecting mass movements. Consequently, these findings underscore the critical role of fiber optic monitoring in assessing and predicting slope stability in response to varying weather conditions, particularly precipitation.

7.5. Investigation of Earthquake-Induced Stress Changes

Seismic activity is a crucial triggering mechanism that affects and initiates landslides. Landslides occur due to slope failure, especially when the FS values are low, influenced by this triggering mechanism. Employing fiber optic monitoring makes detecting subtle changes in slope conditions and ground movement possible, thereby enhancing early warning systems. Real-time monitoring using fiber optic technology is essential for better prediction, timely mitigation, and effective management of landslide hazards.

During this period, four earthquakes with a magnitude of more than Mw 3.5 occurred in the Marmara Region, 2 of which were very close to the monitoring area and Mw of 5.1 and 4.1:

1. 26/10/2023 20:18:24, Marmara Sea - [depth: 13.22 km] Tekirdağ Mw: 3.6
2. 07/11/2023 23:05:48, Marmara Sea - [depth: 03.10 km] Balıkesir Mw: 4.1
3. 04/12/2023 10:42:20, Marmara Sea - [depth: 04.73 km] Bursa Mw: 5.1
4. 17/12/2023 23:53:52, Marmara Sea - [depth: 08.52 km] Yalova Mw: 4.1

Although there is not enough data, the frequency of seismic activity in the region in a short period implies that the seismic activity of the region is high and confirms the suitability of Yalova as the monitoring area.

The October 26, Tekirdağ Earthquake's recorded acceleration time history data are shown in Figure 116. This event is relatively far from the monitoring area (approximately 160 km), and the maximum PGA value from the accelerometer was measured as 3.64×10^{-5} g in the E-W direction.

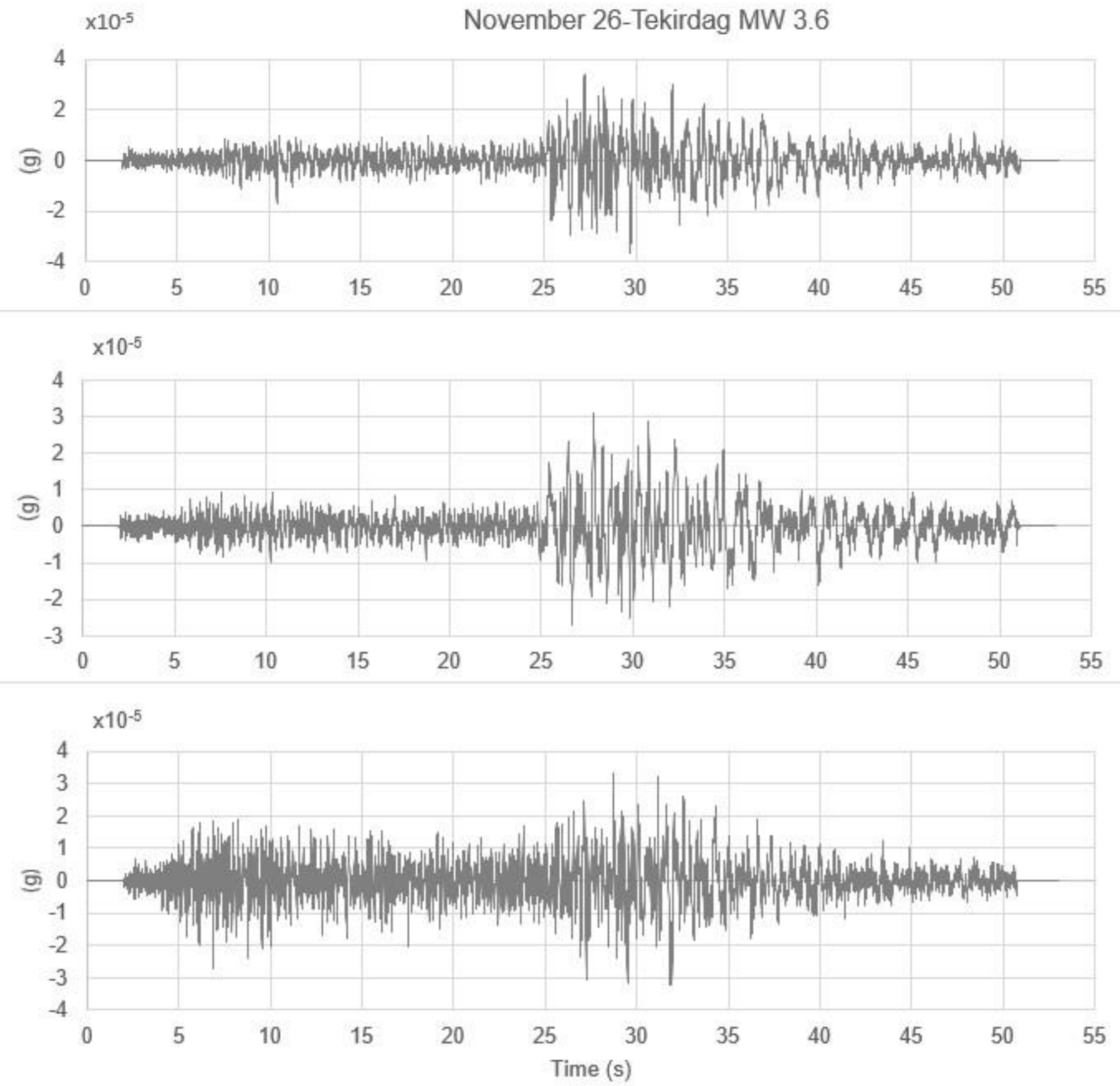

Figure 116. Time history graphs of the strong ground motion records on October 26 during the Tekirdag Earthquake (E-W, N-S, and U-D, respectively)

The strain data of each fiber optic cable caused by this earthquake are shown in Figures 117 and 118. These figures clearly show strain variations in both cables. This earthquake had a PGA of -3.64 x 10^{-5} g:

- 3-mm fiber cable showed a maximum change at 259.27 m, giving a με difference of 8997.63 με. There was an average variation of 919.48 με along the entire cable.
- 4.5-mm fiber cable showed a maximum change at 162.75 m, giving a με difference of 128.18 με. There was an average variation of 37.37 με along the entire cable.

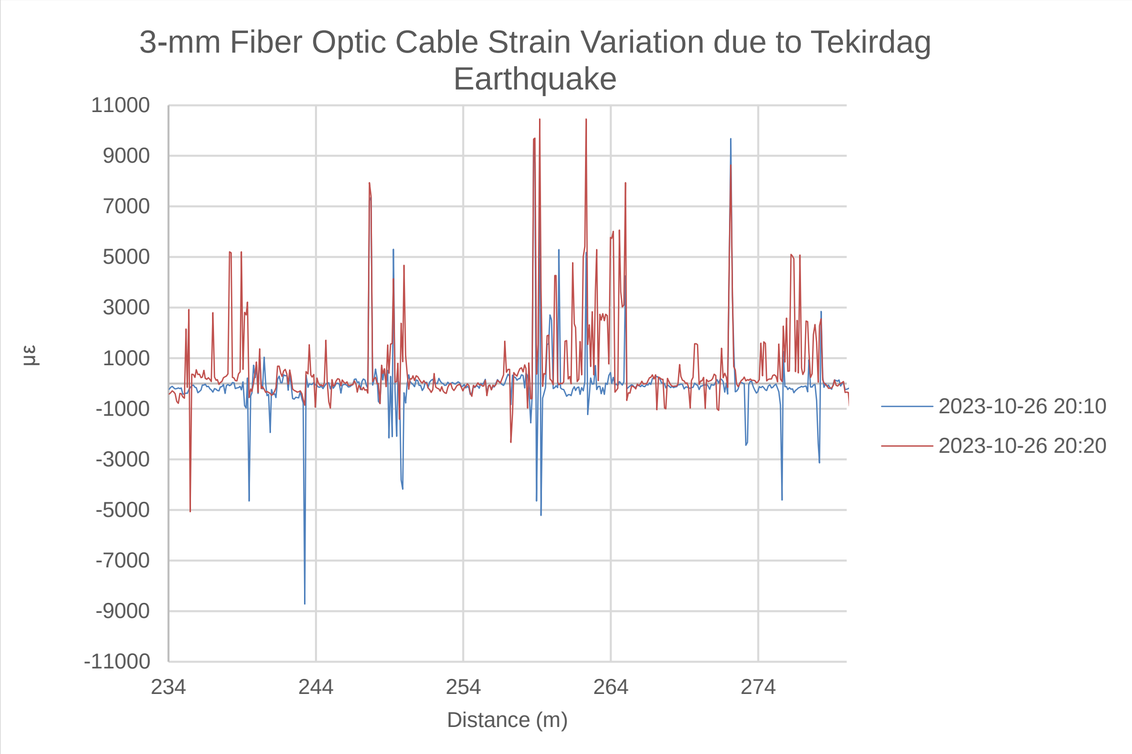

Figure 117. The variation of the strain data on 3-mm fiber optic cable during Tekirdag Earthquake

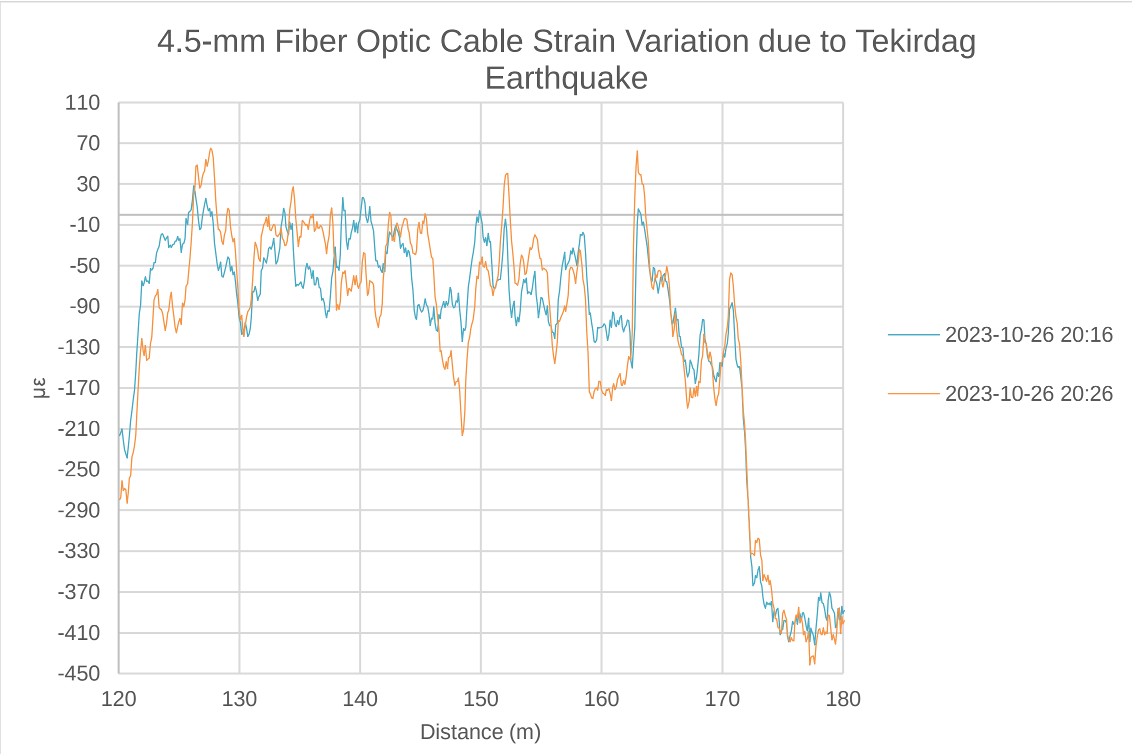

Figure 118. The variation of the strain data on 4.5-mm fiber optic cable during Tekirdag Earthquake

The November 7, Balıkesir Earthquake's recorded acceleration time history data used in the study are shown in Figure 119. This event is relatively far from the monitoring area (approximately 145 km), and the PGA value from the accelerometer was measured as 1.89 x 10^{-4} g in the N-S direction.

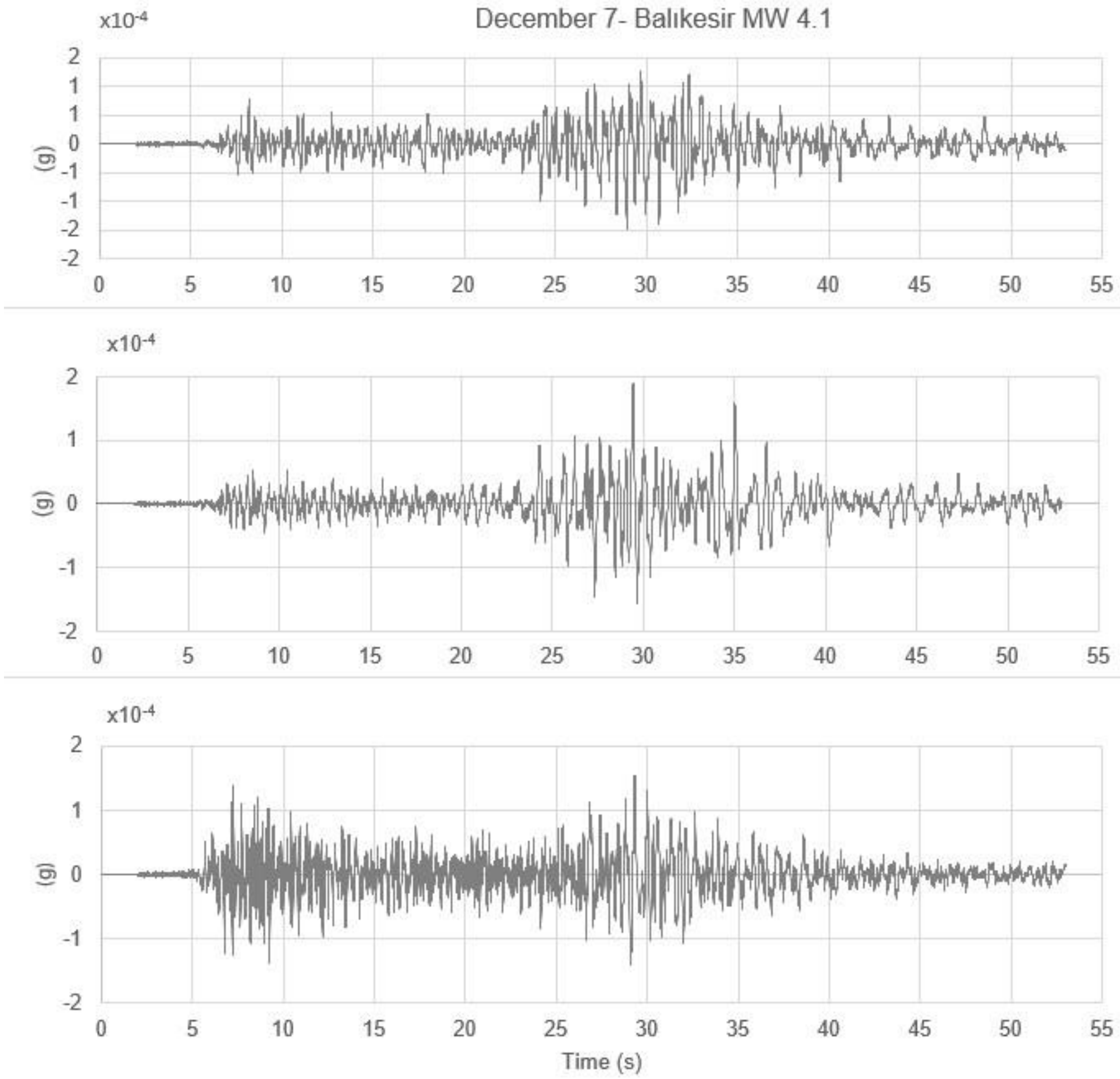

Figure 119. Time history graphs of the strong ground motion records on November 7 during the Balıkesir Earthquake (E-W, N-S, and U-D, respectively)

The strain data of each fiber optic cable caused by this earthquake are shown in Figures 120 and 121. These figures clearly show the strain variations in both cables. This earthquake had a PGA of 1.89 x 10^{-4} g:

- 3-mm fiber cable showed a maximum change at 238.95 m, giving a με difference of 10265.55 με. There was an average variation of 2847.54 με along the entire cable.
- 4.5-mm fiber cable showed a maximum change at 154.89 m, giving a με difference of 179.26 με. There was an average variation of 59.89 με along the entire cable.
-

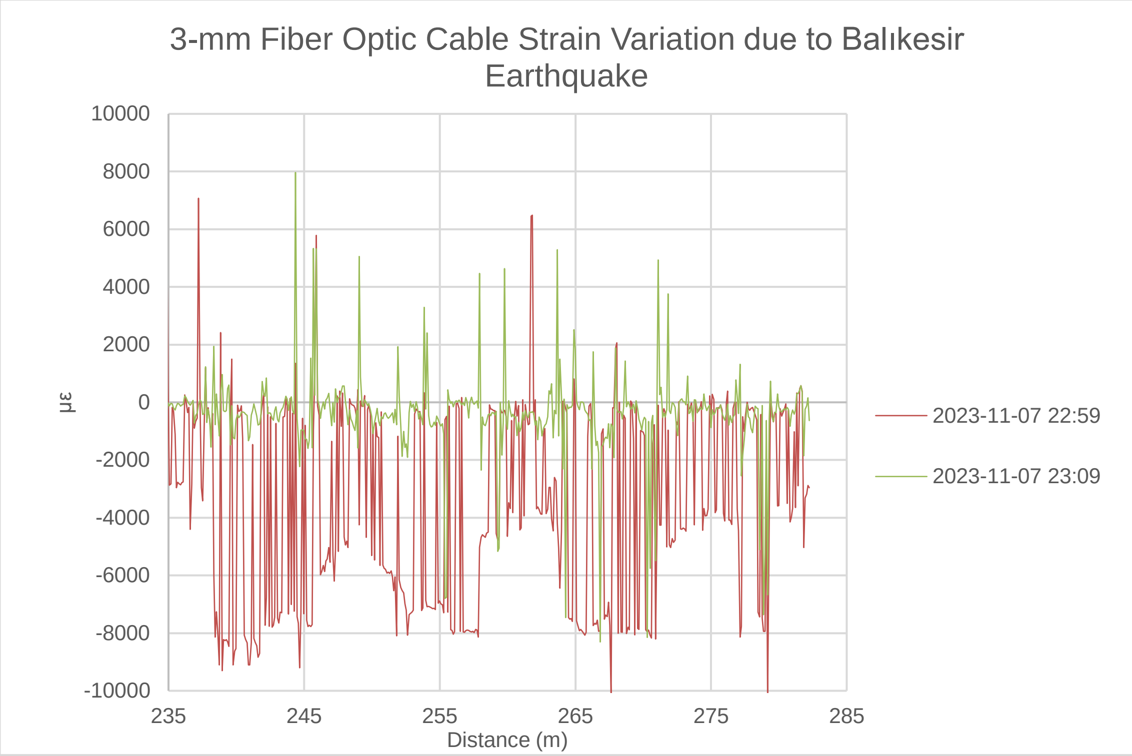

Figure 120. The strain variation along 3-mm fiber optic cable during the Balıkesir Earthquake

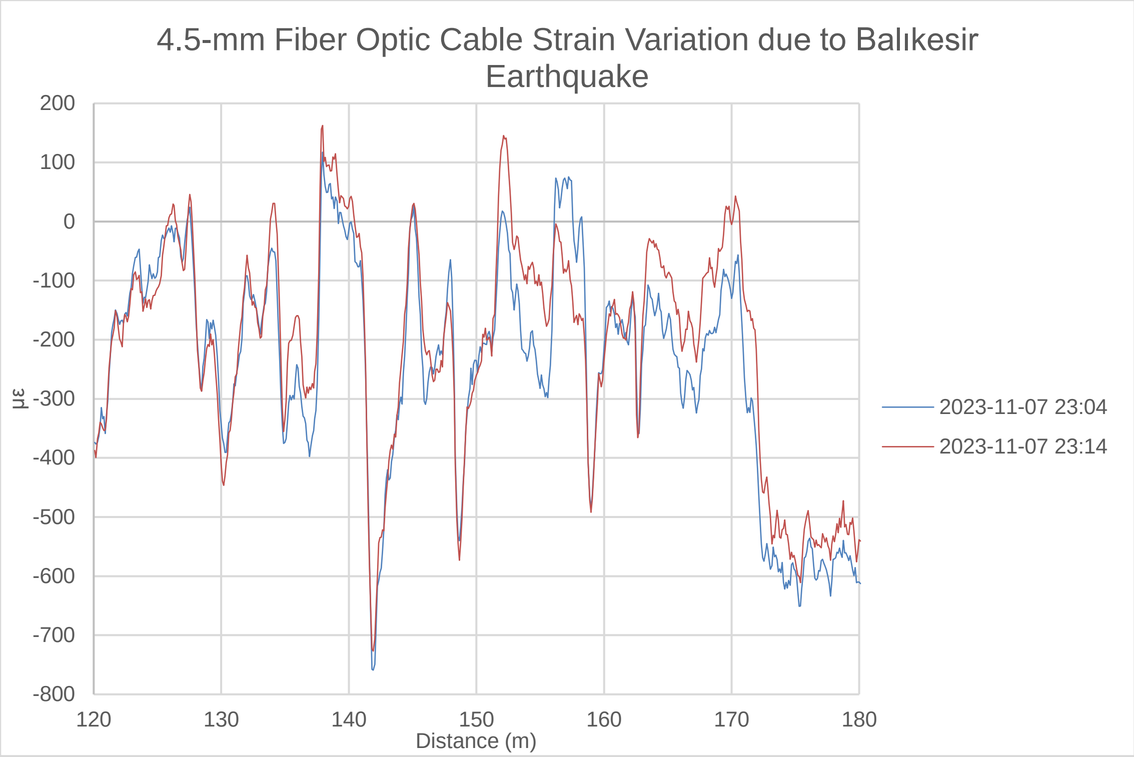

Figure 121. The strain variation along 4.5-mm fiber optic cable during Balıkesir Earthquake

The December 4, Bursa Earthquake's recorded acceleration time history data used in the study are shown in Figure 122. This event is relatively far from the monitoring area (approximately 40 km), and the PGA value from the accelerometer was measured as 4.98 x 10^{-3} g in the N-S direction.

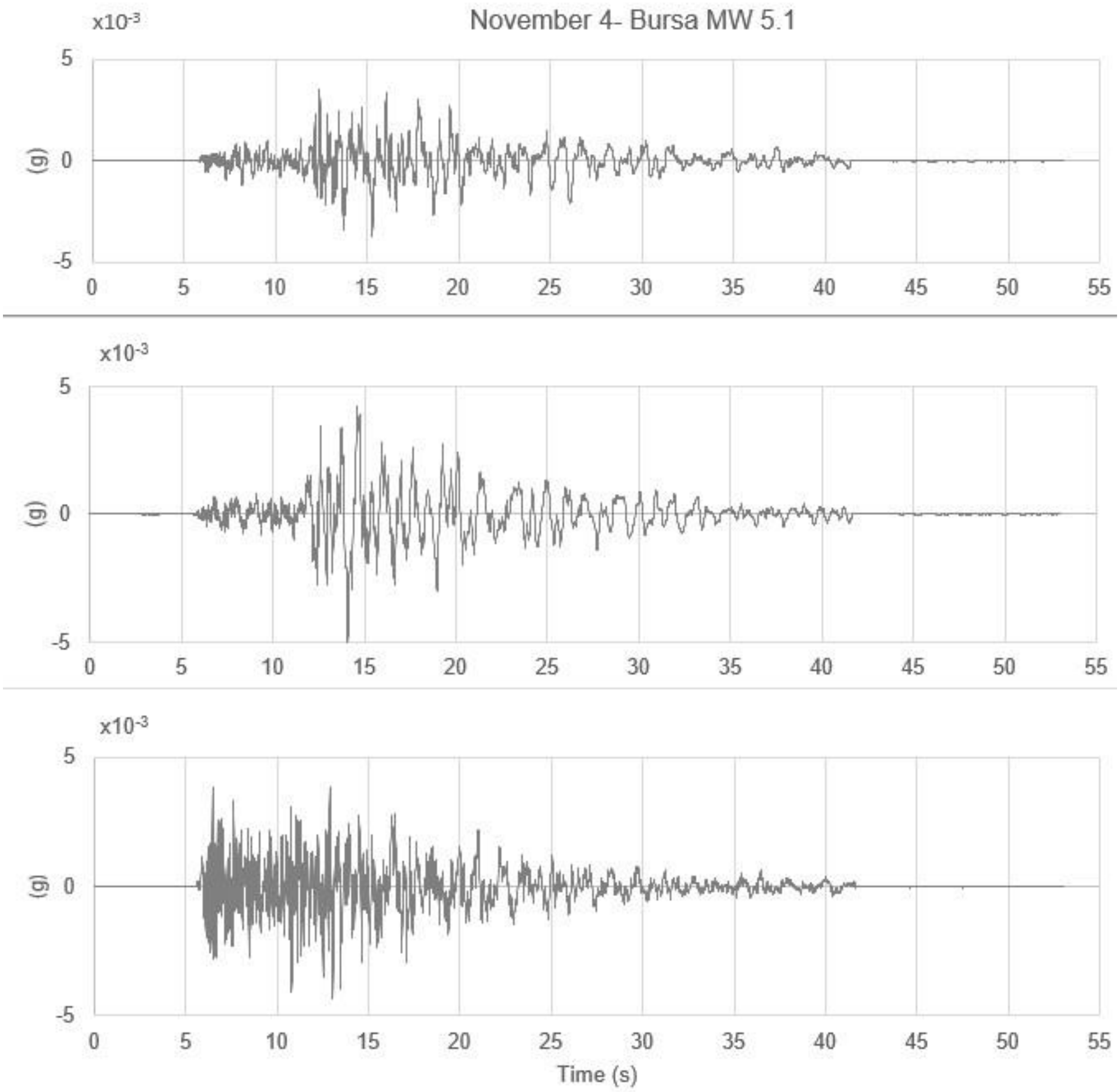

Figure 122. Time history graphs of the strong ground motion records on December 4 during the Bursa Earthquake (E-W, N-S, and U-D, respectively)

The strain data of each fiber optic cable caused by this earthquake are shown in Figures 123 and 124. These figures clearly show strain variations in both cables. This earthquake had a PGA of -4.98 x 10^{-3} g:

- 3-mm fiber cable showed a maximum change at 255.80 m, giving a με difference of 11040.31 με. There was an average variation of 1232.27 με along the entire cable.
- 4.5-mm fiber cable showed a maximum change at 172.54 m, giving a με difference of 137.63 με. There was an average variation of 43.72 με along the entire cable.

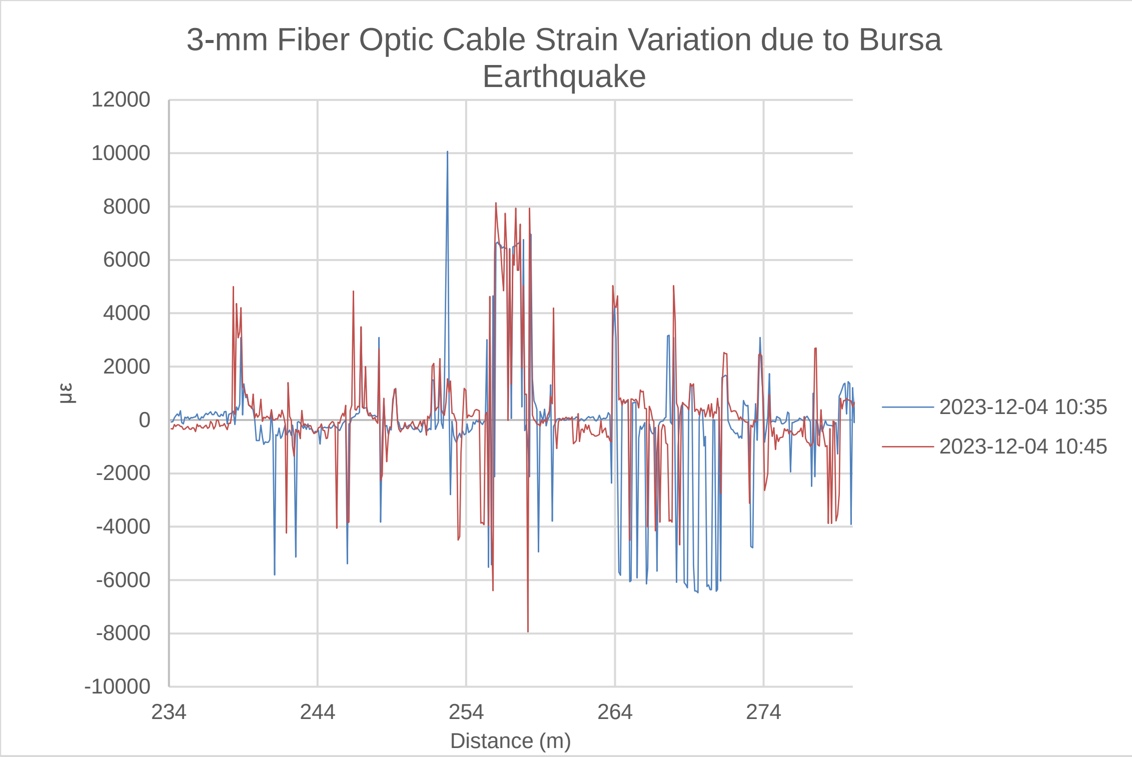

Figure 123. The strain variation along 3-mm fiber optic cable during the Bursa Earthquake

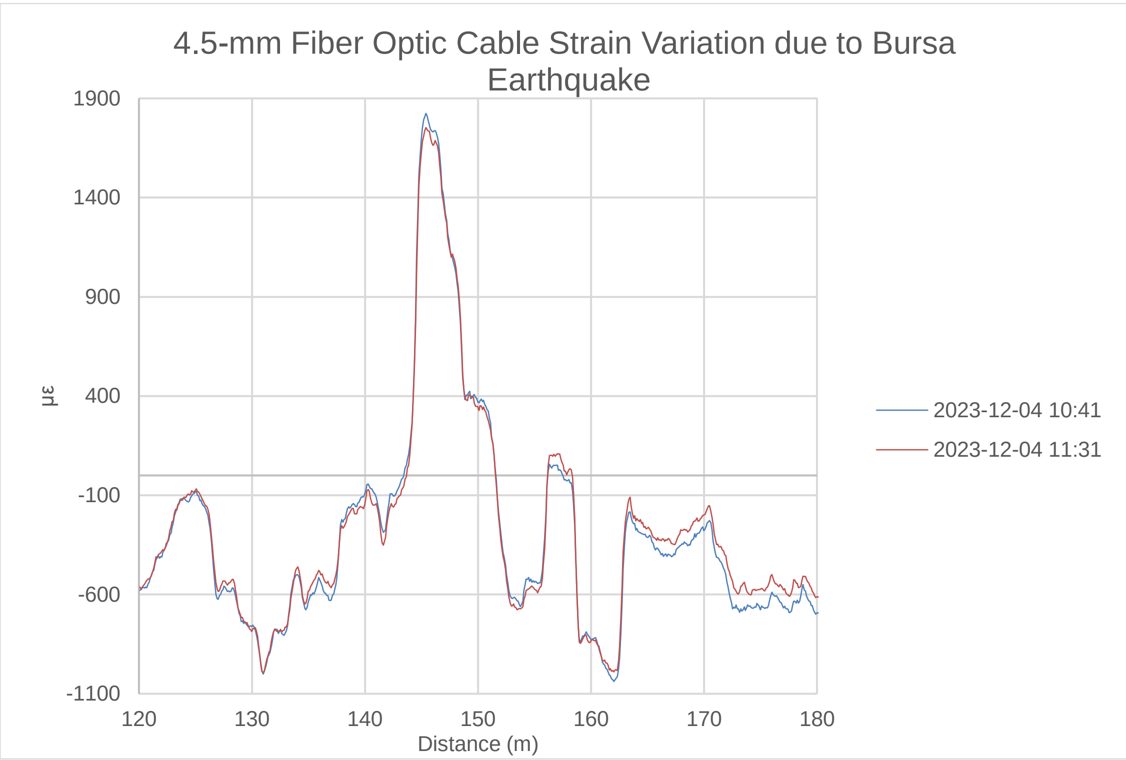

Figure 124. The strain variation along 4.5-mm fiber optic cable during the Bursa Earthquake

The December 4, Yalova Earthquake's recorded acceleration time history data used in the study are shown in Figure 125. This earthquake is close to the monitoring area (approximately 11 km), and the PGA value from the accelerometer was measured as 3.11×10^{-3} g in the E-W direction.

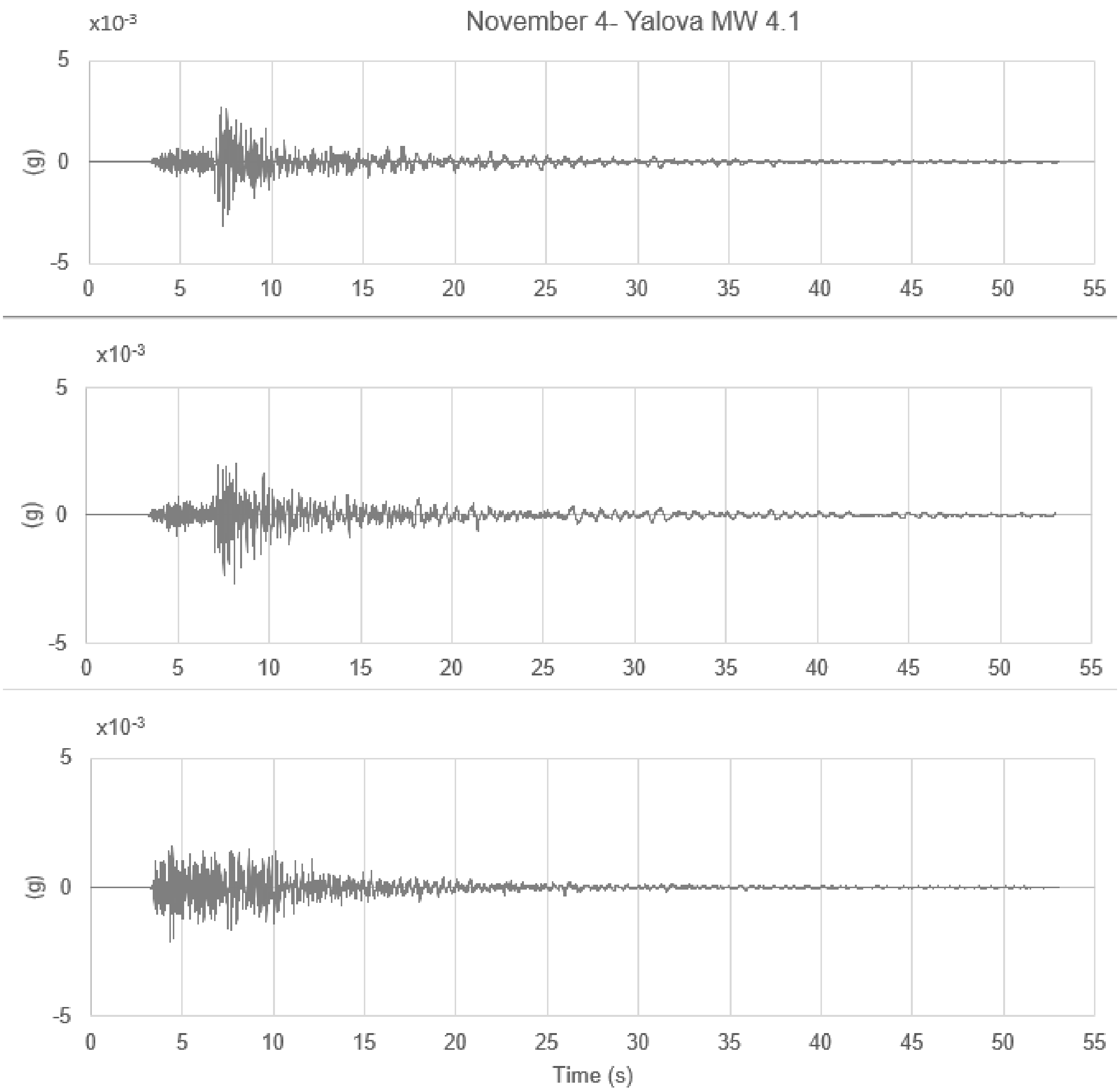

Figure 125 Time history graphs of the strong ground motion records on December 4 during the Yalova Earthquake (E-W, N-S, and U-D, respectively)

The strain data of each fiber optic cable caused by this earthquake are shown in Figures 126 and 127. These figures clearly show strain variations in both cables. This earthquake had a PGA of -3.11×10^{-3} g:

- 3-mm fiber cable showed a maximum change at 240.79 m, giving a με difference of 7418.59 με. There was an average variation of 532.27 με along the entire cable.

  4.5-mm fiber cable showed a maximum change at 144.48 m, giving a με difference of 65.95 με. There was an average variation of 22.28 με along the entire cable.

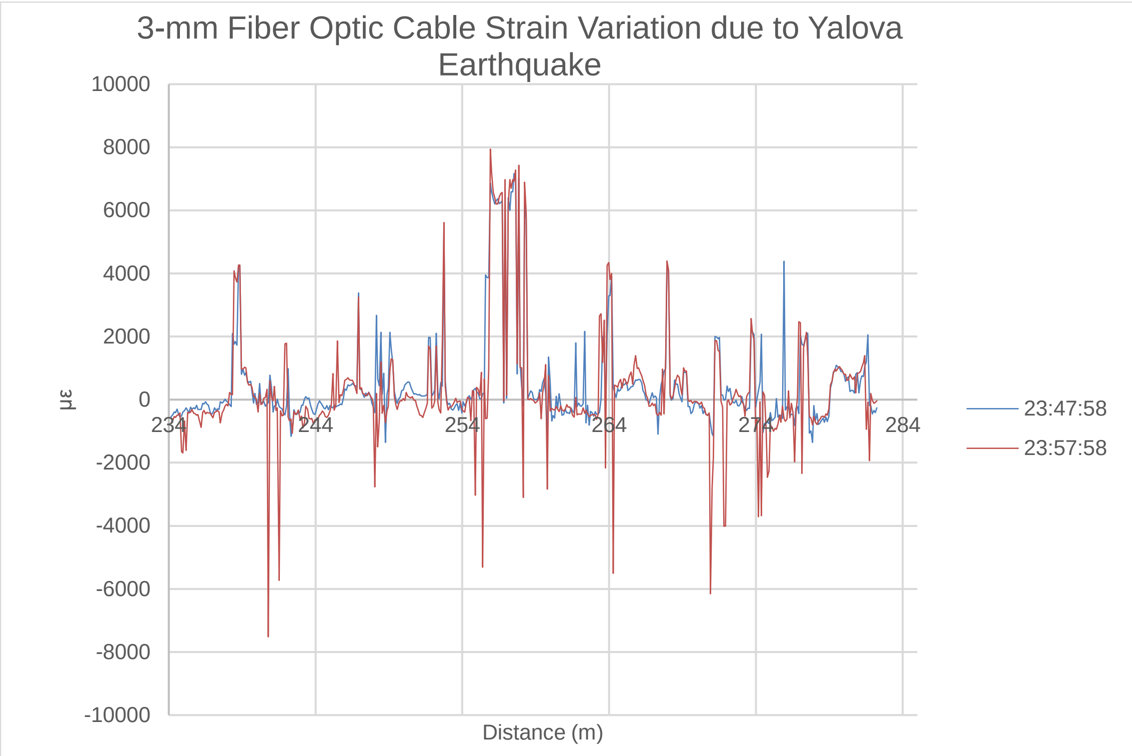

Figure 126. The strain variation along 3-mm fiber optic cable during the Yalova Earthquake

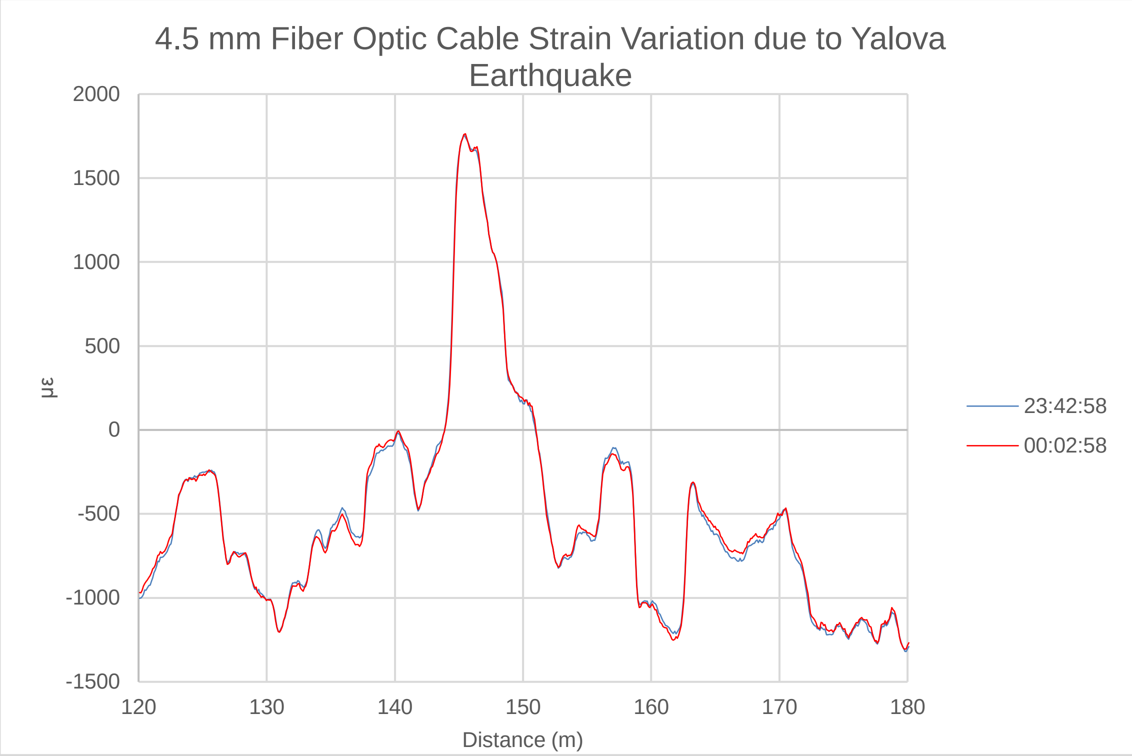

Figure 127. The strain variation along 4.5-mm fiber optic cable during the Yalova Earthquake

7.6. Overall Evaluation

The comprehensive evaluation of the data gathered in this study reveals a consistent and significant correlation between precipitation vs. µε values and seismic activity (acceleration) vs. strain µε values in fiber optic cables. This correlation is evident in the detailed analysis of the strain measurements at various points along the cable.

Initially, the analysis of the µε data was performed daily, proving the adequacy of the instantaneous response rates of the fiber cables. After, the analysis of the µε data demonstrated a clear relationship with weekly precipitation patterns. For instance, at the most active point SP 3, the strain values exhibited a notable shift from -2000 - 7000 µε on 3-mm fiber cable and -500 - 2000 µε on 4.5-mm fiber cable in response to increasing rainfall. This trend was not individual; similar patterns were observed at other strain points along the cable, reinforcing that precipitation significantly influences the strain within the fiber optic cables. The long-term effect of precipitation became more evident by analyzing the 4.5 mm cable in this study.

Additionally, the study explored the impact of seismic events on strain measurements. The data revealed that during periods of seismic activity, there was a discernible increase in strain values, indicative of the cables' sensitivity to ground movements caused by earthquakes. The structure of the 3-mm cable facilitated a more pronounced observation of seismic effects, as indicated in the seismic-effect evaluations. While the 4.5-mm fiber cable also exhibited a consistent shift, its strain variations were less than those of the 3-mm cable. Nevertheless, both cable types successfully captured the seismic impact.

7.6.1. Comparison of Field and Laboratory Study Results

The laboratory studies were highlighted as the foundational work for this research. Cumulative data was employed to assess the laboratory results. These assessments are presented in Figure 128. These results determined that 1.0 mm physical deformation with a 3 mm cable corresponds to the range of 11000-20000 με (Demir, 2023).

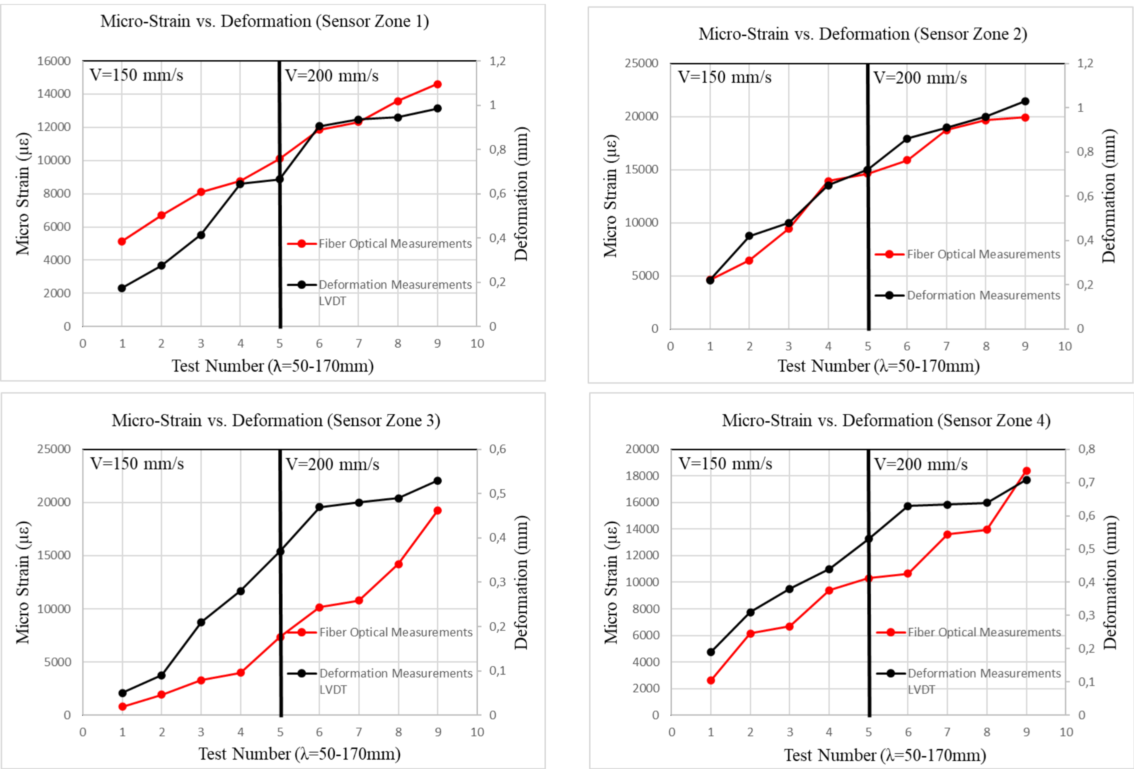

Figure 128. Laboratory test results (Demir, 2023)

Figure 129 displays the cumulative με values recorded from the 3-mm cable at SP 3, identified as the most active point within the monitoring area, as part of the field study. Upon detailed examination of these values, it is observed that they collectively amount to a total of 28561.5 με. According to previous studies, this result corresponds to a deformation of approximately 2.0-2.5 mm.

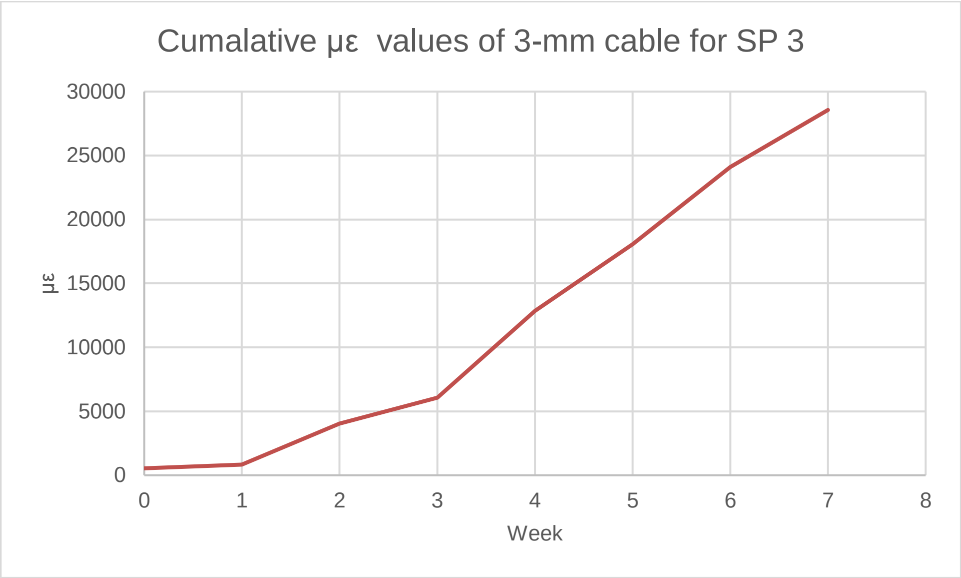

Figure 129. The cumulative με values recorded from the 3-mm cable at SP 3

Figure 130 displays the cumulative με values recorded from the 4.5-mm cable at SP 3. The cumulative με value of 9710.69 recorded at Strain Point 3 (SP 3) of the 4.5-mm cable indicates that a 1 mm deformation in this cable type corresponds to a με range of approximately 3000 to 5000. These findings are thought to be consistent with the results obtained from laboratory studies. However, inclinometer and image processing studies to be carried out in the field with the TÜBİTAK project, which is still being verified, will fully confirm these results.

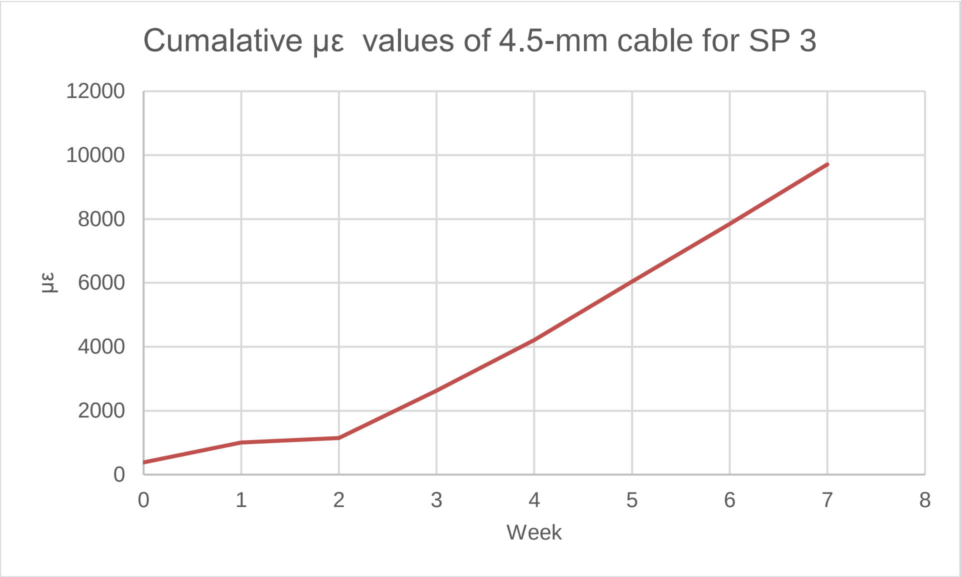

Figure 130. The cumulative με values recorded from the 4.5-mm cable at SP 3

8. CONCLUSIONS

In recent years, the advancement of monitoring technologies has played a pivotal role in enhancing our understanding and management of landslide hazards and risks. These technologies have revolutionized analysis and response to landslide hazards, particularly in regions like Türkiye, where the topography and climatic conditions make certain areas highly susceptible to such events. Monitoring landslides involves a range of techniques, each offering unique insights into the slope stability and potential triggers of landslides. Among these methods, in-situ monitoring tools like inclinometers and extensometers have been used extensively to measure subsurface movements and strain in landslide-prone areas. Airborne methods, including satellite imagery and aerial photography, provide a broad overview of the affected areas, helping to identify new landslides and monitor changes over time. Ground-based LIDAR (Light Detection and Ranging) offers high-resolution, three-dimensional images of the terrain, enabling precise ground deformation measurements. Recent advancements have incorporated more sophisticated technologies like optical fiber systems, which offer several advantages over these methods. Fiber optic systems are susceptible to strain and temperature changes, capable of real-time data transmission, and resist electromagnetic disturbances. Their compactness, portability, and economic efficiency make them suitable for continuous monitoring in diverse terrain.

This thesis focused on the critical issue of landslide hazard and risk assessment and monitoring in Türkiye, particularly in Yalova Province, highlighting the devastating socioeconomic impacts of landslides and emphasizing the need for advanced, real-time early warning systems. The unique geographical and seismic characteristics of Türkiye, especially in areas like Yalova, make it highly susceptible to landslides triggered by earthquakes and heavy rainfall. Integrating light-based fiber optic methods in landslide monitoring represents a significant advancement in this field. These methods, characterized by their high-speed data transmission, sensitivity to environmental changes, and economic efficiency, offer a promising solution for timely landslide detection and prevention.

The successful laboratory testing of fiber optic methods and deploying these techniques in Yalova's landslide-prone area mark a pivotal step toward enhancing the country's disaster readiness. The BOTDA-based fiber optic sensing method, in particular, has proven effective in real-time monitoring, providing valuable data that can inform timely interventions to mitigate landslide risks. BOTDA's ability to measure stress and temperature changes along the length of an optical fiber and provide a detailed and continuous profile of ground motions has been demonstrated over the monitoring period. This feature is particularly advantageous for landslide monitoring, as it detects subtle deformations that precede a landslide, thereby enabling timely warnings.

In the initial phases of the study, the monitoring area was identified as landslide-sensitive through site investigations analysis using Limit Equilibrium Methods (LEM), thereby confirming its susceptibility to landslides. Subsequent actions included channel drilling 1-meter boreholes to prepare the selected area for installing fiber optic cables. These cables were installed, with both ends connected to the BOTDA device. Following a two-week Pre-Monitoring Testing phase, the system was deemed ready for monitoring, leading to the commencement of data acquisition. Then, the incoming data was processed and transformed into meaningful outcomes using suitable software.

The outcomes of this research involved monitoring and processing the deformations (strains) of these cables in the monitoring area, which were subjected to seismic events and rainfall, over a period of 50 days between 02.11.2023 and 21.12.2023. Notably, at the most active point of the monitoring site, the strain values demonstrated significant variations, exhibiting a range from -2000 to 7000 με in the 3 mm fiber cable and from -500 to 2000 με in the 4.5 mm fiber cable. Furthermore, following a comprehensive cumulative analysis, it was identified that the deformation within the monitoring area amounts to approximately 2-2.5 mm, as determined by the results of laboratory studies. This research clearly illustrates that incorporating fiber optic technologies in landslide monitoring significantly enhances the precision and promptness of risk evaluation. It marks a transition towards more sustainable and resilient practices in disaster management.

The context of the thesis comprehensively examined the significant and rapid impact of seismic activities as triggering factors for landslides. The Yalova province and its neighboring, known for high seismic activity, recorded four earthquakes during the monitoring period. Notably, the Bursa earthquake on December 4, with a magnitude of 5.1 MW, recorded the highest acceleration of -4.98 x 10^-3 g in the time-history analysis from the study area. This earthquake has resulted in an average variation of 1200 με along the 3-mm fiber cable and approximately 45 με in the 4.5 mm cable.

The fiber optic monitoring method has proven effective in assessing precipitation and seismic impacts. A comprehensive analysis has revealed that the 3-mm fiber optic cable exhibits high sensitivity to instant responses such as vibrations, making seismic activity effects more pronounced in this cable. Conversely, the 4.5-mm fiber optic cable, equipped with a more robust protective cover, demonstrated a capacity to dampen vibrations. This attribute renders it more suitable for long-term observation of precipitation effects on landslide movements. However, it is essential to note that monitoring mass movements induced by both earthquakes and precipitation has been effectively executed using both cable types. The case study of geotechnical monitoring of a landslide-prone area in the monitoring area in Yalova province with the BOTDA method showed that this method could turn into an early warning system with practical and correct use.

In conclusion, this thesis contributes to the growing knowledge in disaster management and geotechnical engineering. It offers a practical framework for applying light-based fiber optic technologies in landslide monitoring, paving the way for more resilient communities facing natural disasters.

9. FUTURE STUDY AND RECOMMENDATIONS

As a result of this thesis, it is observed that landslides triggered by rainfall and earthquakes can be monitored with fiber optic systems. However, verifying them with a diverse control mechanism is also essential. Studies within the scope of the project, which are not covered by this thesis, include the detection of surface deformations by image processing and remote sensing and the installation of an inclinometer by boring into the sliding surface. By this way, different verification processes will be performed to verify the results of the fiber optic system. First, the spatial deformation data determined by the remote sensing method will be verified with the strain data recorded by the system installed in this thesis. The other is to compare the strain data obtained from the fiber optic cables placed in the inclinometer boring with the deformation measurements, and verification will be performed.

Several key areas are available for future focus in enhancing landslide monitoring and risk management, mainly through fiber optic sensing. Firstly, the large-scale implementation of fiber optic systems across varied geographic areas is crucial. This expanded application will assess the technology's flexibility and adaptability to different environmental conditions and landslide types. Alongside this, promoting interdisciplinary collaboration is essential. Forming partnerships among geotechnical engineers, civil engineers, geological engineers, disaster management experts, computer engineers, and software technology developers is vital for creating more advanced, optimized solutions for landslide monitoring. Increasing public and local authority awareness and education regarding landslide risks and the advantages of sophisticated monitoring technologies is also essential. Moreover, combining systems with other technologies like remote sensing and ground-based radar could lead to more comprehensive monitoring systems. Advocating for policy development and regulatory support is key to integrating fiber optic monitoring into disaster management strategies. Additionally, using machine learning and predictive analytics with fiber optic data can greatly improve the accuracy and timing of landslide predictions, marking a proactive approach in disaster management.

REFERENCES

Abbas, J. M., & Mutiny, Z. A. (2018). Slope stability analysis for earth dams using (geo-slope/w). *Diyala Journal of Engineering Sciences*, 70-81.

About Yalova - Urban Guide. (n.d.). Retrieved from YTSo.org.tr.: https://www.ytso.org.tr/en/urban-guide/about-yalova

Abraham, M., Satyam, N., Pradhan, B., & Alamri, A. (2020). IoT-based geotechnical monitoring of unstable slopes for landslide early warning in the Darjeeling Himalayas. *Sensors*, p. 2611.

Agam, M., Hashim, M., Murad, M., & Zabidi, H. (2016). Slope Sensitivity Analysis Using Spencer's Method in Comparison with General Limit Equilibrium Method. *Procedia Chemistry*, 651-658.

Agrawal, G. (2012). *Fiber-optic communication systems.*

Agrawal, G. (2012). Fiber-optic communication systems. *John Wiley & Sons.*

Akgün, A., & Bulut, F. (2007). GIS-based landslide susceptibility for Arsin-Yomra (Trabzon, North Turkey) region. *Environmental geology*, 1377-1387.

Al-Azzawi, A. (2007). *Fiber Optics Principles and Practices.* Taylor & Francis Group: Boca Raton.

Alparslan, E. (2011). Landslide susceptibility mapping in Yalova, Turkey, by remote sensing and GIS. *Environmental & Engineering Geoscience*, 255-265.

Al-Rawabdeh, A., Moussa, A., Foroutan, M., El-Sheimy, N., & Habib, A. (2017). Time series UAV image-based point clouds for landslide progression evaluation applications. *Sensors*, p. 2378.

Altuğ, G. (2007). Fiber Optik Grating Sensörler. *Yüksek Lisans Tezi, Gazi Üniversitesi.*

Ambraseys, N., & Finkel, C. (1991). Long-term seismicity of Istanbul and of the Marmara Sea region. *Engin. Seis. Earthq. Engin. Report, 91/8, Imperial College*.

Arslan Kelam, A., Akgün, H., & Koçkar, M. K. (2022). Application of an optical fber-based system for mass movement. *Environmental Earth Sciences*, 81.

Arslan Kelam, A., Kelam, M. A., Eker, A. M., Akgün, H., & Koçkar, M. K. (2015). Optical Fiber Technology to Monitor Slope Movement. *Engineering Geology for Society and Territory - Volume 2*, 1425-1429.

Arslan Kelam, A., Koçkar, M. K., & Akgün, H. (2016). Utilization of Optical Fiber System for Mass Movement Monitoring. *DISASTER SCIENCE AND ENGINEERING*, 19-24.

Azmoon, B., Biniyaz, A., Liu, Z., & Sun, Y. (2021). Image-Data-Driven Slope Stability Analysis for Preventing Landslides Using Deep Learning. *IEEE Access*, pp. 150623-150636.

Bai, B., Yuan, W., & Li, X. (2014). A new double reduction method for slope stability analysis. *Journal of Central South University*, 1158-1164.

Bai, G., Hou, Y., Wan, B., An, N., Yan, Y., Tang, Z., . . . Sun, D. (2022). Performance Evaluation and Engineering Verification of Machine Learning Based Prediction Models for Slope Stability. *Applied Sciences*, p. 7890.

Barnoski, M., & Jensen, S. (1976). Fiber waveguides: a novel technique for investigating attenuation characteristics. *Applied optics*.

Bishop, A. (1955). The use of the slip circle in the stability analysis of slopes. *Geotechnique*.

Braunfelds, J., Spolitis, S., Porins, J., & Bobrovs, V. (2020). Fiber Bragg Grating Sensors Integration in Fiber Optical Systems. In S. W. Harun, *Application of Optical Fiber in Engineering.*

C Bidisha, P. S. (2017). Two-dimensional slope stability analysis by plaxis-2d. *Journal for Research in Applied Science*, 871-877.

Cala, M., Jakobczykİ, J., & Cyran, K. (2016). INCLINOMETER MONITORING SYSTEM FOR STABILITY ANALYSIS:THE WESTERN SLOPE OF THE BEŁCHATÓW FIELD CASE STUDY. *Studia Geotechnica et Mechanica*.

Carlino, S., Mirabile, M., Troise, C., Sacchi, M., Zeni, L., Minardo, A., . . . Natale, G. D. (2016). Distributed-Temperature-Sensing Using Optical Methods: A First Application in the Offshore Area of Campi Flegrei Caldera (Southern Italy) for Volcano Monitoring. *Remote Sensing*, 674.

Casagli, N., Intrieri, E., Tofani, V., Gigli, G., & Raspini, F. (2023). Landslide detection, monitoring and prediction with remote-sensing techniques. *nature reviews earth & environment*, 51-64.

Chang, Z., Du, Z., Zhang, F., Huang, F., Chen, J., Li, W., & Guo, Z. (2020). Landslide Susceptibility Prediction Based on Remote Sensing Images and GIS: Comparisons of Supervised and Unsupervised Machine Learning Models. *Remote Sensing*, 502.

Choi, T. D. (2008). Slope inclinometers for landslides. *Landslides*, 339-350.

Corominas, J., Moya, J., Ledesma, A., Lloret, A., & Gili, J. A. (2005). Prediction of ground displacements and velocities. *Landslides*, 83-96.

Corominas, J., Moya, J., Lloret, A., Gili, J., Angeli, M., & Pasuto, A. (1999). Measurement of landslide displacements using. *Engineering Geology*, 149-166.

Deliveris, A. V., Theocharis, A. I., Koukouzas, N. C., & Zevgolis, I. E. (2022). Numerical Slope Stability Analysis of Deep Excavations Under Rainfall Infiltration. *Geotechnical and Geological Engineering*, pp. 4023–4039.

Demir, C. (2023). Laboratory testing of effects caused by landslides triggered by earthquakes through utilizing fiber optic methods, Master Thesis. *Hacettepe Üniversitesi Fen Bilimleri Enstitüsü*.

Dewedree, S., & Jusoh, S. (2019). Slope stability analysis under different soil nailing parameters using the SLOPE/W software. *In Journal of Physics: Conference Series*, 012008.

Dhanagopal, R., & Muthukumar, B. (2021). A model for low power, high speed and energy efficient early landslide detection system using IoT. *Wireless Personal Communications*, pp. 2713-2728.

Dongping, D., Liang, L., & Lian-heng, Z. (2017). Limit-Equilibrium Method for Reinforced Slope Stability and Optimum Design of Antislide Micropile Parameters. *International Journal of Geomechanics*, 06016019.

Dunnicliff, J. (1993). *Geotechnical instrumentation for monitoring field performance.* John Wiley & Sons.

Erzin, Y., & Çetin, T. (2013). The prediction of the critical factor of safety of homogeneous finite slopes using neural networks and multiple regressions. *Computers & Geosciences*, 305-313.

Fang, Z., Chin, K., Qu, R., & Cai, H. (2012). *Fundamentals of optical fiber sensors.* New Jersey: John Wiley & Sons, Inc.

Fellenius, W. (1936). Calculation of the stability of earth dams. *2nd. Congr. Large Dams*, (pp. 455-463).

Fenta, M., Potter, D., & Szanyi, J. (2021). Fibre optic methods of prospecting: A comprehensive and modern branch of geophysics. *Surveys in Geophysics*, 551-584.

Firincioglu, B. S., & Ercanoglu, M. (2021). Insights and perspectives into the limit equilibrium method from 2D and 3D analyses. *Engineering Geology*, 105968.

Giordan, D., Manconi, A., Allasia, P., & Bertolo, D. (2015). Brief Communication: On the rapid and efficient monitoring results dissemination in landslide emergency scenarios: the Mont de La Saxe case study. *Natural Hazards and Earth System Sciences*, pp. 2009-2017.

Gökçe, O., Özden, Ş., & Demir, A. (2008). Türkiye'de afetlerin mekansal ve istatistiksel dağılımı afet bilgileri envanteri. *Bayındırlık ve İskan Bakanlığı Afet İşleri Genel Müdürlüğü*.

Gupta, S. C. (2018). *Textbook on optical fiber communication and its applications (3rd Edition).* PHI Learning Pvt. Ltd.

Hakim, W., Ramli, A., Basarudin, H., Abu, M., & Ahmad, I. (2020). WSN and IoT based landslide monitoring system. *Test Engineering and Management*, pp. 10926-10932.

Halley, P. (1987). *Fibre optic systems.* United Kingdom: John Wiley & Sons.

Han, H., Shi, B., Zhang, L., Zheng, X., Sun, M., Jinghong, & Wei, G. (2023). Comprehensive error equation for fiber optic inclinometer. *IEEE Sensors Journal*.

Hartog, A. (2017). *An introduction to distributed optical fibre sensors.* CRC press.

Intrieri, E., Gigli, G., & Francesco Mugnai Riccardo Fanti, N. C. (n.d.).

Intrieri, E., Gigli, G., Mugnai, F., Fanti, R., & Casagli, N. (2012). Design and implementation of a landslide early warning system. *Engineering Geology*, 124-136.

IPCC. (2012). Summary for Policymakers. In: Managing the Risks of Extreme Events and Disasters to Advance Climate Change Adaptation. *[Field, C.B., V. Barros, T.F. Stocker, D. Qin, D.J. Dokken, K.L. Ebi, M.D. Mastrandrea, K.J. Mach, G.-K. Plattner, S.K. Allen, M. Tignor and P.M. Midgley (eds.)]. A Special Report of Working Groups I and II ofthe Intergovernmental Panel on Climate Change*. Cambridge University Press,: Cambridge, UK, and New York, NY, USA, pp 3-21.

Janbu. (n.d.). Retrieved from Fine Software: https://www.finesoftware.eu/help/geo5/en/janbu-01/

Janbu, N. (1973). Slope Stability Computations. *Publication of: Wiley (John) and Sons, Incorporated*, 47-86.

Johnson, S., Haneberg, W., Bryson, L., & Crawford, M. (2023). Measuring ground surface elevation changes in a slow-moving colluvial landslide using combinations of regional airborne lidar, UAV lidar and UAV photogrammetric surveys . *Quarterly Journal of Engineering Geology and Hydrogeology*.

Kamal, A., Hossain, F., Rahman, M., Ahmed, B., & Sammonds, P. (2022). Geological and soil engineering properties of shallow landslides occurring in the Kutupalong Rohingya Camp in Cox’s Bazar, Bangladesh. *Landslides*, pp. 465–478.

Kendir, O. (2010). *Yalova il merkezinde alüvyon çökellerin mühendislik özellikleri (yüksek lisans tezi).* YÖKtez (282675).

Khan, M. I., & Wang, S. (2021). Slope Stability Analysis to Correlate Shear Strength with Slope. *Applied Sciences*, p. 4568.

Kogure, T., & Okuda, Y. (2018). Monitoring the Vertical Distribution of Rainfall-Induced Strain Changes in a Landslide Measured by Distributed Fiber Optic Sensing With Rayleigh Backscattering. *Geophysical Research Letters*, 4033-4040.

Kwon, I.-B., & Choi, K.-S. (2012). Fiber optic sensors and their applications on structural health monitoring in South Korea. *OFS2012 22nd International Conference on Optical Fiber Sensor* (pp. 130-137). Beijing: SPIE.

Li, F., Du, Y., Zhang, W., B Sun, & Li, F. (2012). Monitoring system for a high steep slope based on optical fiber sensing technology. *Advanced Sensor Systems and Applications V*, 78-83.

Liu, B., Zhang, D., & Xi, P. (2017). Mechanical behaviors of SD and CFA piles using BOTDA-based fiber optic sensor system: A comparative field test study. *Measurement*, 253-262.

Liu, S., Shao, L., & Li, H. (2015). Slope stability analysis using the limit equilibrium method and two finite element methods. *Computers and Geotechnics*, 291-298.

Liu, X., Chen, X., Su, M., Zhang, S., & Lu, D. (2021). Stability analysis of a weathered-basalt soil slope using the double strength reduction method. *Advances in Civil Engineering*, pp. 1-12.

Liu, Y., Dai, Z., Zhang, X., Peng, Z., Li, J., Ou, Z., & Liu, Y. (2010). Optical fiber sensors for landslide monitoring. *Semiconductor Lasers and Applications IV,*, 41-46.

Lu, P., & Rosenbaum, M. (2003). Artificial neural networks and grey systems for the prediction of slope stability. *Natural Hazards*, 383-398.

Lubkowski, A., Chapman, T., & Free, M. (2022). Identification of geohazards for the rehabilitation plan of Yalova Turkey. *12th European Conference on Earthquake Engineering* (p. 618). London: Elsevier Science Ltd.

Lumens, P. (2014). Fibre-optic sensing for application in oil and gas wells.

Macciotta, R., & Hendry, M. T. (2021). Remote Sensing Applications for Landslide Monitoring and Investigation in Western Canada. *Remote Sensing*, 366.

Mahmood, N., Aude, S., Abdullah, H., & Sulaiman, S. (2022). Analysis of Slope Stability and Soil Liquefaction of Zoned Earth Dams Using Numerical Modeling. *International Journal of Design & Nature and Ecodynamics*, pp. 557-562.

Marin, R., Mattos, Á., & Fernández-Escobar, C. (2022). Understanding the sensitivity to the soil properties and rainfall conditions of two physically-based slope stability models. *Boletín de Geología*, pp. 93-109.

Measures, R. M. (2001). *Structural Monitoring With Fiber Optic Technology.* Academic Press, USA.

Minardo, A., Catalano, E., Coscetta, A., Zeni, G., Maio, C. D., Vassallo, R., . . . Zeni, L. (2021). Long-Term Monitoring of a Tunnel in a Landslide Prone Area by Brillouin-Based Distributed Optical Fiber Sensors. *Sensors*, 7032.

Moayedi, H., Bui, D. T., Gör, M., Pradhan, B., & Jaafari, A. (2019). The Feasibility of Three Prediction Techniques of the Artificial Neural Network, Adaptive Neuro-Fuzzy Inference System, and Hybrid Particle Swarm Optimization for Assessing the Safety Factor of Cohesive Slopes. *International Journal of Geo-Informatiın*.

Mohammed, Z. F., & Fatth, A. Y. (2013). *Digital Signal Processing for Cancellation of Fiber Optic Impairments: Design and Simulation Using OptiSystem and Matlab.* Germany: Lambert Academic Publishing.

Mora, O., Lenzano, M., Toth, C., Grejner-Brzezinska, D., & Fayne, J. (2018). Landslide change detection based on multi-temporal Airborne LiDAR-derived DEMs. *Geosciences*, 23.

Morgenstern, N., & Price, V. (1965). The analysis of the stability of general slip surfaces. *Geotechnique*, 79-93.

Morgenstern, N., & Price, V. (1967). A numerical method for solving the equations of stability of general slip surfaces. *The Computer Journal*, 388-393.

Muanenda, Y., Oton, C., & Pasquale, F. D. (2019). Application of Raman and Brillouin scattering phenomena in distributed optical fiber sensing. *Frontiers in Physics*, 155.

Niu, X., Ma, J., Wang, Y., Zhang, J., Chen, H., & Tang, H. (2021). A Novel Decomposition-Ensemble Learning Model Based on Ensemble Empirical Mode Decomposition and Recurrent Neural Network for Landslide Displacement Prediction. *Applied Sciences*, p. 4684.

NJ Lindsey, E. M.-F. (2017). Fiber-optic network observations of earthquake wavefields. *Geophysical Research Letters*.

Ohno, H., Naruse, H., Kihara, M., & Shimada, A. (2001). Industrial applications of the BOTDR optical fiber strain sensor. *Optical fiber technology*, 45-64.

Okalp, K., & Akgün, H. (2016). National level landslide susceptibility assessment of Turkey utilizing public domain dataset. *Environmental Earth Sciences*, 1-21.

Oleksander Trofymchuk, Kaliukh, I., & Klymenkov, O. (2017). TXT-tool 2.380-1.1: Monitoring and Early Warning System of the Building Constructions of the Livadia Palace, Ukraine. *Landslide Dynamics: ISDR-ICL Landslide Interactive Teaching Tools*, 491-508.

Omar, R., Baharuddin, I., Taha, H., Roslan, R., H, N., & M, M. (2018). Slope stability analysis of granitic residual soil using Slope/W, resistivity and seismic. *International Journal of Engineering and Technology*, pp. 172-176.

Pami, S. N., Ismail, N. N., & Ramli, A. B. (2021). Comparison on Factor of Safety using Different Method of Analysis for Slope. *Journal of Applied Engineering Design and Simulation* , 52-58.

Pei, H., Cui, P., Yin, J., Zhu, H., Chen, X., Pei, L., & Xu, D. (2011). Monitoring and warning of landslides and debris flows using an optical fiber sensor technology. *Journal of Mountain Science*, 728-738.

Pei, H., Cui, P., Yin, J., Zhu, H., Chen, X., Pei, L., & Xu, D. (2011). Monitoring and warning of landslides and debris flows using an optical fiber sensor technology. *Journal of Mountain Science*, 728-738.

Powers, J. (1997). *Introduction to Fiber Optic Systems (second ed.) .* McGraw-Hill Professional.

Qu, T., Lu, P., Liu, C., Wu, H., Shao, X., Wan, H., . . . Li, R. (2016). Hybrid-SAR technique: Joint analysis using phase-based and amplitude-based methods for the Xishancun giant landslide monitoring. *Remote Sensing*, p. 874.

Ray, A., Kumar, V., Kumar, A., Rai, R., Khandelwal, M., & Singh, T. N. (2020). Stability prediction of Himalayan residual soil slope using artificial neural network. *Natural Hazards volume*, 3523-3540.

Rørstadbotnen, R. A., Dong, H., Landrø, M., Duffaut, K., Growe, K., Kakhkhorov, U., . . . Jacobsen, J. (2023). Quick clay monitoring using distributed acoustic sensing: A case study from Rissa, Norway. *GEOPHYSICS*, 1-64.

Sakellariou, M., & Ferentinou, M. (2005). A study of slope stability prediction using neural networks. *Geotechnical & Geological Engineering*, 419-445.

Salih, A. G. (2021). Stability Analysis of Residual Soil Slope Model by Numerical Modeling Using FEM Against LEM. *IOP Conference Series: Earth and Environmental Science. Vol. 856. No. 1. IOP Publishing* (p. 012046). IOP Publishing.

Sarkar, S., & Chakraborty, M. (2021). Stability analysis for two-layered slopes by using the strength reduction method. *International Journal of Geo-Engineering*.

Savvaidis, P. (2003). Existing landslide monitoring systems and techniques. *From Stars to Earth and Culture*, 242-258.

Schuster, R. L., & Highland, L. M. (2001). *U.S. Geological Survey Open-File Report 01-0276 .* U.S.A.: U.S. Geological Survey.

Shafna, P., & Anjana, T. (2021). Generalized Three-Dimensional Slope Stability Analysis of Soil Using Plaxis 3D. *Proceedings of the Indian Geotechnical Conference 2019*, (pp. 745-752). Springer Singapore.

Shepheard, C., Vardanega, P., Holcombe, E., Hen-Jones, R., & De Luca, F. (2019). Minding the geotechnical data gap: appraisal of the variability of key. *Bulletin of Engineering Geology and the Environment*, pp. 4851-4864.

Shiferaw, H. M. (2021). Study on the influence of slope height and angle on the factor of safety and shape of failure of slopes based on strength reduction method of analysis. *Beni-Suef University Journal of Basic and Applied Sciences volume*, 10.

Shirley, J. (1951). An early experimental determination of Snell's law. *American Journal of Physics*, 507-508.

Song, F., Chen, R., Ma, L., & Zhao, J. (2018). Stability analysis of reinforced slope based on limit equilibrium method. *Tehnički vjesnik*, 224-229.

Sruthy, M., Anjana, R., Archana, R., Dhanya, V., & Hridya, A. (2020). IoT based landslide detection and monitoring system. *Int J Res Eng Sci Manag*, pp. 596-9.

Stark, T. D., & Choi, H. (2008). Slope inclinometers for landslides. *Landslides*, 339-350.

Supper, R., Römer, A., Jochum, B., Bieber, G., & Jaritz, W. (2008). A complex geo-scientific strategy for landslide hazard mitigation – from airborne mapping to ground monitoring. *Advances in Geosciences*, pp. 195–200.

Thevenaz, L. (2011). *Advanced fiber optics: concepts and technology.* EPFL press.

Thyagarajan, K. S., & Ghatak, A. (2007). *Fiber Optic Essentials.* Wiley-IEEE Press.

Tia, Y., P. L., Wilkinson, J., Schroeder, G., Sutton, S., & Swingler, S. (2005). An improved optically based PD detection system for continuous on-line monitoring of HV cables. *IEEE transactions on dielectrics and electrical insulation*, 1222-1234.

Tripathi, S., Kumar, A., Marin, E., & Meunier, J. (2010). Single-multi-single mode structure based band pass/stop fiber optic filter with tunable bandwidth. *Journal of Lightwave Technology*, 3535-3541.

Turkey Earthquake Hazard Maps Interactive Web Application. (2018). Retrieved from https://tdth.afad.gov.tr/

(2018). *Türkiye Building Earthquake Code.* Ankara: Disaster and Emergency Management Presidency.

UNESCO. (2015). *Light-based technologies: sustainable solutions for the future*. Retrieved from https://www.unesco.org/en/articles/light-based-technologies-sustainable-solutions-future

Varnes, D. (1978). Slope movement types and processes. *Special report*, pp. 11-33.

Wang, B., Li, K., Shi, B., & Wei, G. (2008). Test on application of distributed fiber optic sensing technique into soil slope monitoring. *Landslides*, 61-68.

Wei, Y., Jiaxin, L., Zonghong, L., Wei, W., & Xiaoyun, S. (2020). A strength reduction method based on the Generalized Hoek-Brown (GHB) criterion for rock slope stability analysis. *Computers and Geotechnics*, 103240.

Whiteley, J., J. C., Uhlemann, S., Boyd, J., Cimpoiasu, M., Holmes, J., . . . Kendall, J. (2020). Landslide monitoring using seismic refraction tomography – The importance of incorporating topographic variations. *Engineering Geology*.

Wu, T., Liu, G., Fu, S., & Xing, F. (2020). Recent progress of fiber-optic sensors for the structural health monitoring of civil infrastructure. *Sensors*, 4517.

Xiaofei, Z., Wenjie, H., Qing, Z., Yanxin, S., Xianwei, M., & Yongwen, H. (2011). Development of optical fiber strain monitoring system based on BOTDR. *IEEE 2011 10th International Conference on Electronic Measurement & Instruments* (pp. 38-41). IEEE.

Xu, Q., Guo, C., Dong, X., Li, W., Lu, H., Fu, H., & Liu, X. (2021). Mapping and characterizing displacements of landslides with InSAR and airborne

LiDAR technologies: A case study of danba county, southwest China. *Remote Sensing*, 4234.

Yalova. (n.d.). Retrieved from Wikipedia: https://en.wikipedia.org/wiki/Yalova

Yalova Annual Weather Averages. (n.d.). Retrieved from WorldWeatherOnline.com. : https://www.worldweatheronline.com/yalova-weather-averages/yalova/tr.aspx

Yalova Climate, Weather By Month, Average Temperature (Turkey. (n.d.). Retrieved from WeatherSpark: https://weatherspark.com/y/96001/Average-Weather-in-Yalova-Turkey-Year-Round

(2022). *Yalova İl Afet Risk Azaltma Planı.* Yalova: T.C. Yalova Valiliği İl Afet ve Acil Durum Müdürlüğü.

Yalova, TR Climate Zone, Monthly Weather Averages and Historical Data. (n.d.). Retrieved from WeatherandClimate.com.: https://weatherandclimate.com/turkey/yalova

Yalova, Turkey - Climate. (n.d.). Retrieved from Weather-Atlas.com: https://www.weather-atlas.com/en/turkey/yalova-climate

Yan, E., & K Song, H. L. (n.d.).

Yan, E., Song, K., & Li, H. (2010). Applicability of time domain reflectometry for Yuhuangge landslide monitoring. *Journal ofr Earth Sciences, vol 21, no.6*, 856-860.

Yer Bilimleri Görüntüleyici. (2021). Retrieved from Yer Bilimleri MTA: http://yerbilimleri.mta.gov.tr/anasayfa.aspx

Yin, Y., Wang, H., Gao, Y., & Li, X. (2010). Real-time monitoring and early warning of landslides at relocated Wushan Town, the Three Gorges Reservoir, China. *Landslides*, 339-349.

Yu, Z., Li, B., & Huang, C. (2018). Research on limit equilibrium method of three-dimensional slope stability. *Archive of Applied Mechanics*, 1175-1186.

Zeni, L., Picarelli, L., Avolio, B., Coscetta, A., Papa, R., Zeni, G., . . . Minardo, A. (2015). Brillouin optical time-domain analysis for geotechnical monitoring. *Journal of Rock Mechanics and Geotechnical Engineering*, 458-462.

Zhang, Z., Lu, Y., & Zhao, Y. (2018). Channel capacity of wavelength division multiplexing-based brillouin optical time domain sensors. *IEEE Photonics Journal*, 1-15.

Zhao, M., Yi, X., Zhang, J., & Lin, C. (2021). PPP-BOTDA distributed optical fiber sensing technology and its application to the Baishuihe landslide. *Frontiers in Earth Science*, 660918.

Zhong, H., Liu, X., & C Fu, Y. W. (2022). Quasi-distributed temperature sensing using series-integrated fiber Bragg gratings. *In Eighth Symposium on Novel Photoelectronic Detection Technology and Applications Vol. 12169* (pp. 1265-1269). SPIE.

Zhou, T., Zhang, L., Cheng, J., Wang, J., Zhang, X., & Li, M. (2022). ssessing the rainfall in□ltration on FOS via a new NSRM for a case study at high rock slope stability. *Scientific Reports*.

Zhu, C., Alsalman, O., & Huang, J. (2023). Microwave-photonic Vernier effect enabled high-sensitivity fiber Bragg grating sensors for point-wise and quasi-distributed sensing. *Optics Express*, 41996-42014.

Zhu, H.-H., Ho, A. N., Yin, J.-H., Sun, H., & Pei, H.-F. (2012). An optical fibre monitoring system for evaluating the performance of a soil nailed slope. *Smart Structures and Systems*, 393-410.

APPENDICES

APPENDIX A- Boring Logs

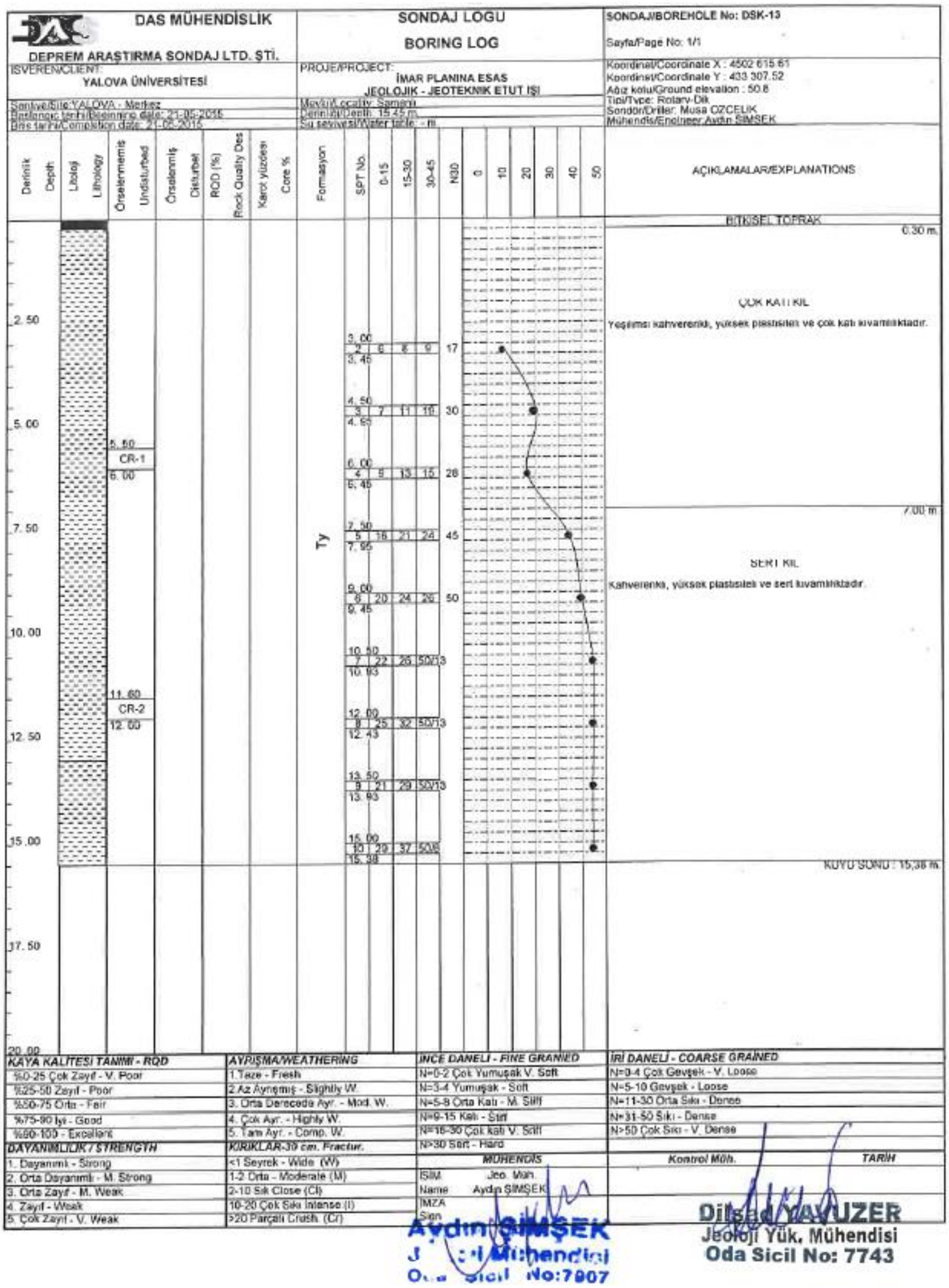

DAS MÜHENDİSLİK
DEPREM ARAŞTIRMA SONDAJ LTD. ŞTİ.

SONDAJ LOGU
BORING LOG

SONDAJ/BOREHOLE No: DSK-14
Sayfa/Page No: 1/1

İŞVEREN/CLIENT: YALOVA ÜNİVERSİTESİ
Şantiye/Site: YALOVA - Merkez
Başlangıç tarihi/Beginning date: 21-05-2015
Bitiş tarihi/Completion date: 21-05-2015

PROJE/PROJECT: İMAR PLANINA ESAS JEOLOJİK - JEOTEKNİK ETÜT İŞİ
Mevki/Locality: Semerli
Derinlik/Depth: 12.27 m
Su seviyesi/Water table: - m

Koordinat/Coordinate X : 4502 590.21
Koordinat/Coordinate Y : 433 190.56
Ağız kotu/Ground elevation : 34.9
Tip/Type: Rotary-Dik
Sondör/Driller: Musa ÖZÇELİK
Mühendis/Engineer: Aydın ŞİMŞEK

Derinlik Depth	Örselenmemiş Undisturbed	Formasyon	SPT No.	0-15	15-30	30-45	N30	AÇIKLAMALAR/EXPLANATIONS
0.00–0.30		Ty						Bitkisel TOPRAK (0.30 m)
1.50–1.95		Ty	1	5	7	9	16	ÇOK KATI KIL – Kahverenkli, yüksek plastisiteli ve çok katı kıvamlılıktadır. (3.00 m)
3.00–3.45		Ty	2	7	10	21	31	SERT KIL – Kahverenkli, yüksek plastisiteli ve sert kıvamlılıktadır.
4.00–4.50	CR-1	Ty						
4.50–4.95		Ty	3	10	16	19	35	
6.00–6.43		Ty	4	22	25	50/13		
7.50–7.93		Ty	5	23	28	50/13		
9.00–9.27		Ty	6	28	50/12			
10.50–10.93		Ty	7	25	36	50/13		
11.60–12.00	CR-2	Ty						
12.00–12.27		Ty	8	29	50/12			KUYU SONU : 12,27 m

Depth scale: 2.50, 5.00, 7.50, 10.00, 12.50, 15.00, 17.50, 20.00

KAYA KALİTESİ TANIMI - RQD	AYRIŞMA/WEATHERING	İNCE DANELİ - FINE GRAINED	İRİ DANELİ - COARSE GRAINED
%0-25 Çok Zayıf - V. Poor	1. Taze - Fresh	N=0-2 Çok Yumuşak V. Soft	N=0-4 Çok Gevşek - V. Loose
%25-50 Zayıf - Poor	2. Az Ayrışmış - Slightly W.	N=3-4 Yumuşak - Soft	N=5-10 Gevşek - Loose
%50-75 Orta - Fair	3. Orta Derecede Ayr. - Mod. W.	N=5-8 Orta Katı - M. Stiff	N=11-30 Orta Sıkı - Dense
%75-90 İyi - Good	4. Çok Ayr. - Highly W.	N=9-15 Katı - Stiff	N=31-50 Sıkı - Dense
%90-100 - Excellent	5. Tam Ayr. - Comp. W.	N=16-30 Çok katı V. Stiff	N>50 Çok Sıkı - V. Dense
DAYANIMLILIK / STRENGTH	**KIRIKLAR-30 cm. Fractur.**	N>30 Sert - Hard	
1. Dayanımlı - Strong	<1 Seyrek - Wide (W)	**MÜHENDİS**	**Kontrol Müh.** / **TARİH**
2. Orta Dayanımlı - M. Strong	1-2 Orta - Moderate (M)	İSİM Name: Jeo. Müh. Aydın ŞİMŞEK	
3. Orta Zayıf - M. Weak	2-10 Sık Close (Cl)	İMZA Sign	
4. Zayıf - Weak	10-20 Çok Sıkı Intense (I)		
5. Çok Zayıf - V. Weak	>20 Parçalı Crush. (Cr)		

Aydın ŞİMŞEK
Jeoloji Mühendisi
Oda Sicil No:7907

Dilşad YAVUZER
Jeoloji Yük. Mühendisi
Oda Sicil No: 7743

DAS MÜHENDİSLİK DEPREM ARAŞTIRMA SONDAJ LTD. ŞTİ.	SONDAJ LOGU BORING LOG	SONDAJ/BOREHOLE No: DSK-15 Sayfa/Page No: 1/1
İŞVEREN/CLIENT: YALOVA ÜNİVERSİTESİ	PROJE/PROJECT: İMAR PLANINA ESAS JEOLOJİK - JEOTEKNİK ETUT IŞI	Koordinat/Coordinate X : 4502 546.63 Koordinat/Coordinate Y : 433 472.59 Ağız kotu/Ground elevation : 73.8
Şantiye/Site: YALOVA - Merkez Başlangıç tarihi/Beginning date: 22-05-2015 Bitiş tarihi/Completion date: 22-05-2015	Mevki/Locality: Samanlı Derinliği/Depth: 12.40 m. Su seviyesi/Water table: - m.	Tip/Type: Rotary-Dik Sondör/Driller: Musa ÖZÇELİK Mühendis/Engineer: Aydın ŞİMŞEK

Derinlik Depth	Litoloji Lithology	Örselenmemiş Undisturbed	Örselenmiş Disturbed	RQD (%) Rock Quality Des	Karot yüzdesi Core %	Formasyon	SPT No.	0-15	15-30	30-45	N30
2.50						Ty	1 (1.50 – 1.95)	5	6	6	12
							2 (3.00 – 3.45)	7	8	8	16
5.00							3 (4.50 – 4.95)	7	7	12	19
		5.70 CR-1 6.00					4 (6.00 – 6.34)	17	24	50/4	
7.50							5 (7.50 – 7.93)	21	29	50/13	
							6 (9.00 – 9.43)	31	40	50/13	
10.00							7 (10.50 – 10.92)	30	38	50/12	
12.50							8 (12.00 – 12.40)	32	41	50/10	
15.00											
17.50											
20.00											

N30: 0 10 20 30 40 50

AÇIKLAMALAR/EXPLANATIONS

Bitkisel TOPRAK — 0.30 m.

KATI - ÇOK KATI KİL

Koyu kahverenkli, orta plastisiteli ve katı - çok katı kıvamlıdır.

5.00 m.

SERT KİL

Kahverenkli, yüksek plastisiteli ve sert kıvamlıdır.

KUYU SONU : 12,40m.

KAYA KALİTESİ TANIMI - RQD	AYRIŞMA/WEATHERING	İNCE DANELİ - FINE GRANIED	İRİ DANELİ - COARSE GRAINED
%0-25 Çok Zayıf - V. Poor	1. Taze - Fresh	N=0-2 Çok Yumuşak V. Soft	N=0-4 Çok Gevşek - V. Loose
%25-50 Zayıf - Poor	2. Az Ayrışmış - Slightly W.	N=3-4 Yumuşak - Soft	N=5-10 Gevşek - Loose
%50-75 Orta - Fair	3. Orta Derecede Ayr. - Mod. W.	N=5-8 Orta Katı - M. Stiff	N=11-30 Orta Sıkı - Dense
%75-90 İyi - Good	4. Çok Ayr. - Highly W.	N=9-15 Katı - Stiff	N=31-50 Sıkı - Dense
%90-100 - Excellent	5. Tam Ayr. - Comp. W.	N=16-30 Çok katı V. Stiff	N>50 Çok Sıkı - V. Dense
DAYANIMLILIK / STRENGTH	**KIRIKLAR-30 cm. Fractur.**	N>30 Sert - Hard	
1. Dayanımlı - Strong	<1 Seyrek - Wide (W)	**MÜHENDİS**	**Kontrol Müh.** **TARİH**
2. Orta Dayanımlı - M. Strong	1-2 Orta - Moderate (M)	İSİM Name: Jeo. Müh. Aydın ŞİMŞEK	
3. Orta Zayıf - M. Weak	2-10 Sık Close (Cl)		
4. Zayıf - Weak	10-20 Çok Sıkı Intense (I)	İMZA Sign	
5. Çok Zayıf - V. Weak	>20 Parçalı Crush. (Cr)		

Aydın ŞİMŞEK
J[illegible] Mühendisi
Oda Sicil No:7907

Dilşad [illegible]
Jeoloji Yük. Mühendisi
Oda Sicil No: 7743

DAS MÜHENDİSLİK DEPREM ARAŞTIRMA SONDAJ LTD. ŞTİ.	SONDAJ LOGU BORING LOG	SONDAJ/BOREHOLE No: DSK-42 Sayfa/Page No: 1/1
İŞVEREN/CLIENT: YALOVA ÜNİVERSİTESİ	PROJE/PROJECT: İMAR PLANINA ESAS JEOLOJİK - JEOTEKNİK ETUT İŞİ	Koordinat/Coordinate X : 4502 612.09 Koordinat/Coordinate Y : 434 190.06 Ağız kotu/Ground elevation : 40
Saha/Site: YALOVA - Merkez	Mevki/Locality: Samanlı	Tip/Type: Rotary-Dik
Başlangıç tarihi/Beginning date: 02-07-2015	Derinlik/Depth: 15.45 m.	Sondör/Driller: Halil DALYAN
Bitiş tarihi/Completion date: 02-07-2015	Su seviyesi/Water table: - m.	Mühendis/Engineer: Aydın ŞİMŞEK

Derinlik Depth	Litoloji Lithology	Örselenmemiş Undisturbed	Örselenmiş Disturbed	RQD (%) Rock Quality Des.	Karot yüzdesi Core %	Formasyon	SPT No.	0-15	15-30	30-45	N30	AÇIKLAMALAR/EXPLANATIONS
0.00–0.30						Ty						BİTKİSEL TOPRAK (0.30 m.)
2.50–3.00		2.50 UD-1 3.00				Ty						SERT KİL Yeşilimsi kahverenkli, orta - yüksek plastisiteli ve sert kıvamlıdır.
3.00–3.45						Ty	2	12	14	18	32	
4.50–4.95						Ty	3	15	16	18	37	
6.00–6.45						Ty	4	19	20	22	42	
7.50–7.95						Ty	5	21	24	27	>50	
9.00–9.45						Ty	6	23	28	32	>50	
10.50–10.95						Ty	7	25	32	35	>50	(12.00 m.)
12.00–12.45						Ty	8	30	35	37	>50	SERT KİL Mavi - yeşil renkli, yüksek plastisiteli ve sert kıvamlıdır.
15.00–15.45						Ty	10	31	34	36	>50	KUYU SONU : 15,45 m.

Depth scale: 2.50, 5.00, 7.50, 10.00, 12.50, 15.00, 17.50, 20.00

KAYA KALİTESİ TANIMI - RQD	AYRIŞMA/WEATHERING	İNCE DANELİ - FINE GRAINED	İRİ DANELİ - COARSE GRAINED
%0-25 Çok Zayıf - V. Poor	1. Taze - Fresh	N=0-2 Çok Yumuşak V. Soft	N=0-4 Çok Gevşek - V. Loose
%25-50 Zayıf - Poor	2. Az Ayrışmış - Slightly W.	N=3-4 Yumuşak - Soft	N=5-10 Gevşek - Loose
%50-75 Orta - Fair	3. Orta Derecede Ayr. - Mod. W.	N=5-8 Orta Katı - M. Stiff	N=11-30 Orta Sıkı - Dense
%75-90 İyi - Good	4. Çok Ayr. - Highly W.	N=9-15 Katı - Stiff	N=31-50 Sıkı - Dense
%90-100 - Excellent	5. Tam Ayr. - Comp. W.	N=16-30 Çok katı V. Stiff	N>50 Çok Sıkı - V. Dense
DAYANIMLILIK / STRENGTH	KIRIKLAR-30 cm. Fractur.	N>30 Sert - Hard	
1. Dayanımlı - Strong	<1 Seyrek - Wide (W)	MÜHENDİS	Kontrol Müh. / TARİH
2. Orta Dayanımlı - M. Strong	1-2 Orta - Moderate (M)	İSİM Name: Jeo. Müh. Aydın ŞİMŞEK	
3. Orta Zayıf - M. Weak	2-10 Sık Close (Cl)		
4. Zayıf - Weak	10-20 Çok Sıkı Intense (I)		
5. Çok Zayıf - V. Weak	>20 Parçalı Crush. (Cr)	Sign	

Aydın ŞİMŞEK
Jeoloji Mühendisi
Oda Sicil No:7907

Dilşad YAVUZER
Jeoloji Yük. Mühendisi
Oda Sicil No: 7743

APPENDIX B- Precipitation Data of Yalova Province in November and December,

Table B1. Hourly precipitation data on November from MGM station Yalova/17119

Hourly Total Precipitation (mm=kg÷m²) OMGi																								
Day/Time	**0**	**1**	**2**	**3**	**4**	**5**	**6**	**7**	**8**	**9**	**10**	**11**	**12**	**13**	**14**	**15**	**16**	**17**	**18**	**19**	**20**	**21**	**22**	**23**
1	0	0	0	0	0	0	0	0	0	0	0	0	0	0	0	0	0	0	0	0	0	0	0	0
2	0	0	0	0	0	0	0	0	0	0	0	1.7	2.1	2.1	4.6	2.5	0	0.1	0	0.2	0	0	0	0
3	0	0	0	0	0	0	0	0	0	0	0	0	0	0	0	0	0	0	0	0	0	0	0	0
4	0	0	0	0	0	0	0	0	0	0	0	0	0	0	0	0	0	0	0	0	0	2.6	2	0.8
5	0	0	0	0	0	0	0	0	0	0	0	0	0	0	0	0	0	0	0	0	0	0	0	0
6	0	0	0	0	0	0	0	0	0	0	0	0	0	0	0	0	0	0	0	0	0	0	0	0
7	0	0	0	0	0	0	0	0	0	0	0	0	0	0	0	0	0	0	0	0	0	0	0	0
8	0	0	0	0	0	0	0	0	0	0	0	0	0	0	0	0	0	0	0	0	0	0	0	0
9	0	0.5	0.4	0.3	5.6	0.9	0.2	0.8	0.1	0.1	0	0	0	0	0	0	0	0	0	0	0	0	0	0
10	0	0	0	0	0	0	0	0	0	0	0	0	0	0	0	0	0	0	0	0	0	0	0	0
11	0	0	0	0	0	0	0	0	0	0	0	3.4	0.6	1.9	5.4	3.4	0	0	0	0	2.2	4.9	0.2	1.5
12	0.3	0	0	0	0	0	0	0	0	0	0	0	0	0	0	0	0	1.3	0	0	0	0	0	0
13	0	0	0	0.1	0	0	0	0	0	1	1.1	1.2	1.6	1.5	14.4	1.2	0.3	0.6	0	0	0	0	0	0
14	0	0	0	0	0	0	0	0	0	0	0	0	0	0	0	0	0	0	0	0	0	0	0	0
15	0	0	0	0	0	0	0	0	0	0	0	0	0	0	0	0	0	0	0	0	0	0	0	1.6
16	2.2	3.7	5.9	2.4	2.5	2.3	2.9	0	0	0	0	0	0	0	0	0	0	0	0	0	0	0	0	0
17	0	0	0	0	0	0	0	0	0	0	0	0	0	0	0	0	0	0	0	0	0	0	0	0
18	0	0	0	0	0.1	0.5	1.1	2.8	15	8.5	2.1	1.6	2.8	3.3	4.5	3.9	1	0.8	2	1.9	1.5	0.9	0.5	1.5
19	0.7	0	0.3	1.3	2.3	2	1.7	2.4	1.6	1.8	1.6	0.6	0.7	1.1	0.3	0	0	0	0	0	0	0	0	0
20	0	0	0	0	0	0	0	0	0	0	0	0	0	0	0	0	0	0	0	0.2	2.3	1.4	0.1	0
21	0	0	0	0						0	0	0	0	0	0	0	0	0	0	0	0	0	0	0
22	0	0	0	0	0	0	0	0	0	0	0	0	0	0	0	0	0	0	0.3	0.4	0	0	0	0
23	0.2	0	0.6	0.5	1.5	0.8	0.5	0	0	0	0	0	0	0	0	0	0	0	0	0	0	0	0	0
24	0	0	0	0	0	0	0.9	0.1	0	0	0	0	0.4	0	0	0	0	0	0	0	0	0	0	0
25	0	0	0	0	0	0	0	0	0	0	0	0	0	0	0	0	0	0	0	0	0	0	0	0
26	0.5	0.6	3.9	0.4	0.2	0.2	0	0.1	0	0.1	0.2	0	0	0	0	0.5	0	0	0	0	0	0	0	0
27	0	0	0	0	0	0	0	0.2	0.3	0	0	0	0	0	0	0		0	0		0	0	0	0
28	0				0	0	0	0	0	0	0	0	0	0	0.1	0.2	0.2	0.1	0.1	0.4	0	0.8	1.2	1.8
29	2.3	3.3	4	4.3	0.4	2.7	0.7	1.6	0	1.4	0.4	0.2	0.8	1.5	1.2	1.1	0.8	2.1	0	0	3.8	5	8.2	4.4
30	1	0.5	0.2	1	0	0	0	0	0	0	0	0	0	0	0	0	0	0	0	0	0	0	0	0

Table B2. Hourly precipitation data on December from MGM station Yalova/17119

Hourly Total Precipitation (mm=kg÷m^2) OMGi																								
Day/Time	**0**	**1**	**2**	**3**	**4**	**5**	**6**	**7**	**8**	**9**	**10**	**11**	**12**	**13**	**14**	**15**	**16**	**17**	**18**	**19**	**20**	**21**	**22**	**23**
1	0	0	0	0	0	0	0	0	0	0	0		0	0	0	0	0	0	0	0	0	0	0	0
2	0	0	0	0	0	0	0	0	0	0	0	0	0	0	0	0	0	0	0	0	0	0	0	0
3	0	0	0	0	0	0	0	0	0	0	0	0	0	0	0	0	0	0	0	0	0	0	0	0
4	0	0	0	0	0	0.1	0.4	0.3	0	0	1.2	1.6	1.3	0.1	0	0	0	0	0	0	0	0	0	0
5	0	0	0	0	0	0	0	0	0	0	0	0	0	0	0	0	0	0	0	0	0	0	0	0
6	0	0	0	0	0	0	0	0	0	0	0	0	0	0	0	0.2	0.9	0		0	0	0	0	0
7	0	0	0	0	0.1	0	0	0	0	0	0.3	0.8	0.5	0	1.2	0	0	0	0	1.2	3	3.5	2.4	0.5
8	2.2	0.3	0.1	0.5	0.4	0.2	1.4	1.3	1.5	1.1	0.4	0	0	0	0	0	0.4	0	0.3	0.8	0	0.1	0.1	0
9	0.1	0.3	0.8	1.5	0.3	0	0	1.1	0.3	1.1	1.2	1.4	1.5	1.1	1.3	1	0.4	0		0.3	0	0	0	0
10	0	0	0	0	0	0	0	0	0	0	0	0	0	0	0	0	0	0	0	0	0	0	0	0
11	0	0	0.2	0	0	0	0	0	0	0	0	0	0	0	0	0	0	0	0	0	0	0	0	0
12	0	0	0	0	0	0	0	0	0	0	0	0	0	0	0	0	0	0	0	0	0	0	0	0
13	0	0	0	0	0	0	0	0	0	0	0.1	0	0	0	0	0	0	0	0	0	0	0	0	0
14	0	0	0	0	0	0	0	0	0	0	0	0	0	0	0	0	0	0	0	0	0	0	0	0
15	0	0	0	0.1	0.1	0	0	0	0	0	0.1	0.1	0.1	0.1	0.2	0.1	0.3	0.1	0.1	0.4	0.1	0.1	0.1	0.1
16	0.1	0.2	0.4	0.5	0.1	0.1	0.1	1.2	1.4	1.1	1.5	3.5	1.4	0.1	0.2	0	0	0		0.4	0.6	0.7	0.5	0
17	0	0	0	0	0	0	0	0	0	0	0	0	0	0	0	0	0	0	0	0	0	0	0	0
18	0	0	0	0	0	0	0	0	0	0	0	0	0	0	0	0	0	0	0	0	0	0	0	0
19	0	0	0	0																				
20								0	0	0	0	0	0	0	0	0	0	0	0	0	0	0	0	0
21	0	0	0	0	0	0	0	0	0	0	0	0	0	0	0	0	0	0.4	0.9	1.1	0.3	0.3	0.1	0.2
22	0.3	0.1	0	0	0	0	0	0	0	0	0	0	0	0.2	2.1	2.9	0.9	0.4	0					